ABSTRACT

SHESHADRI, PRIYANKA. Characterization of 3D-Bioplotting of ε-Polycaprolactone for Tissue Engineering Applications. (Under the direction of Dr. Rohan A. Shirwaiker).

Tissue engineering is an emerging field which integrates the principles of engineering and life sciences to develop biological substitutes to restore, repair or regenerate defective tissues. One of the approaches in this discipline is the use of three-dimensional matrices or scaffolds to create these substitutes. Scaffolds are designed to be porous and biodegradable, acting as temporary housing for cells which eventually proliferate to form organized tissue systems. Scaffold requirements are stringent and tissue/organ specific and the fabrication method are critical to the clinical success of this approach. Additive Manufacturing (AM) processes provide the ability to engineer and fabricate patient-specific biodegradable scaffolds. Extrusion based AM processes such as 3D-Bioplotting in particular offer flexibility and customizability in terms of achievable scaffold geometries and biomaterials that can be dispensed. In 3D-Bioplotting, scaffolds are constructed by pneumatically extruding biomaterial melts through a nozzle along a tool path governed by an input STL file. Extrusion based AM processes are being widely studied since they can incorporate biomolecules such as cell - hydrogel suspensions.

This thesis investigates the relationship between the material rheology and 3D-Bioplotting process parameters for ε-Polycaprolactone (PCL, MW: 43-50kDa), a biomaterial used in several tissue engineering applications. The main motivation behind this research is to minimize the time taken for scaffold fabrication for 3D-Bioplotting. The focus of the experiments is to establish critical relationships between polymer viscosity, processing parameters (nozzle diameter, extrusion temperature, extrusion pressure, dispensing speed) and resultant characteristics of the fabricated scaffolds (geometry and strength). The effect of these feasible levels of process parameters on scaffold properties were evaluated using a statistical design of experiments (*2 x 3*). PCL scaffolds designed to fit a 24-well plate (14mm diameter, 2mm height) were fabricated with a 0°_90° lay down pattern using two levels of nozzle diameter (300 µm and 400 µm) and three levels of extrusion temperatures (80°C,

90°C and 100°C). One factor analysis of variance and Tukey's test results show that the average scaffold strand width at each extrusion temperature is significantly different ($p < 0.0001$). The peak load and compression modulus of scaffolds fabricated at the different experimental levels also showed an increasing trend with extrusion temperatures – 2654N, 0.5MPa; 2674N, 0.65MPa; 5043N, 0.97MPa respectively for a nozzle diameter 300 µm and 4144N, 0.59MPa; 5488N, 0.79MPa for a nozzle diameter 400 µm. A rheological analysis of PCL (43-50kDa) at chosen extrusion temperatures showed that the average viscosity is significantly different at each temperature level ($p < 0.0001$). The results also showed that PCL exhibits shear-thinning with a flow-index n ranging from 0.69 to 0.71 determined experimentally. These parameters were used to estimate the apparent viscosity of PCL at the nozzle tip during 3D-Bioplotting. The results suggest the sensitivity of the process to material viscosity and that temperature-viscosity behavior of a material can be used to develop a generalized process model to predict scaffold output during 3D-Bioplotting.

Characterization of 3D-Bioplotting of ε-Polycaprolactone for Tissue Engineering Applications

by
Priyanka Sheshadri

A thesis submitted to the Graduate Faculty of
North Carolina State University
in partial fulfillment of the
requirements for the degree of
Master of Science

Industrial Engineering

Raleigh, North Carolina

2014

APPROVED BY:

Dr. Rohan Shirwaiker Committee Chair	Dr. Ola. L. Harrysson Member of Advisory Committee

Dr. Arellano Conseullo
Member of Advisory Committee

DEDICATION

To my parents and my sister, who have always been my source of encouragement, support and strength.

BIOGRAPHY

Priyanka Sheshadri completed her Bachelor's degree in Manufacturing Science and Engineering from BMS College of engineering, Bangalore, India in July 2009. She then joined Cummins India Limited as a part of the Young Managers Development Program for two years. She joined the M. S in Industrial Engineering program at North Carolina State University in Spring 2012. She began working on her master's thesis at the Medical Implants and Tissue Engineering (MITE) lab under the guidance of Dr. Rohan A. Shirwaiker in Summer 2012.

ACKNOWLEDGMENTS

I would like to thank my advisor Dr. Rohan Shirwaiker for his continuous support and guidance. Learning and working with him over the past two years has been inspiring and rewarding. He has been a great mentor and constant source of encouragement.

I would also like to thank Dr. Harvey West for his guidance and assistance in conducting mechanical testing. His enthusiasm and cheerful demeanor was truly inspiring. I would like to thank Dr. Ola Harrysson for his willingness to be on my committee and his insightful comments and guidance. I would also like to thank Dr. Consuello Arellano for being a part of my committee. Her expertise and direction in the statistical analysis conducted in this research has been immensely valuable.

I would like to thank my colleague Zhou Tan for his insightful recommendations and encouragement which has been invaluable in completing this research. I would also like to thank Harshad Srinivasan, Jennifer Godwin and Chinmay Vaidya for their help.

I would like to thank Nikil Kumar for being a constant source of inspiration and support that kept me going through graduate school and my research. I am also grateful to Kishore Krishna, Namita Lokare, Sirat Sikka and for their invaluable support and help.

TABLE OF CONTENTS

LIST OF TABLES

LIST OF FIGURES

LIST OF ACRONMYS

Acronym	Nomenclature
3D	Three dimensional
AM	Additive manufacturing
ANOVA	Analysis of variance
ASTM	American Society of Testing and Materials
CAD	Computer aided drawing
CI	Confidence interval
CL	Confidence limit
DF	Degrees of freedom
ECM	Extracellular matrix
FDA	Food and drug administration
FDM	Fused deposition modeling
FEA	Finite element analysis
FSR	Full scale reading
GAG	Glycosaminoglycans
HA	Hydroxyapatite
HSD	Honest significant difference
ID	Inner diameter
MSC	Mesenchymal stem cells
OD	Outer diameter
OPTN	Organ procurement and transplant network
PCL	Polycaprolactone
PGA	Poly-glycolic acid
PLA	Poly-lactic acid
PLLA	Poly-L-lactic acid
RPM	Rotations per minute
SD	Standard deviation

SEM	Scanning electron microscope
SFF	Solid freeform fabrication
SLA	Stereolithography
SLS	Selective laser sintering
SMC	Spindle multiplier constant
STL	Stereolithographic file
TCP	Tri-Calcium phosphate
TE	Tissue engineering
TEMP	Tissue engineered medical products
TK	Torque constant
UV	Ultraviolet

CHAPTER 1: INTRODUCTION

This chapter gives a brief background of tissue engineering with an introduction to scaffold based tissue engineering. It includes the motivation and objectives behind this research which pertains to scaffold fabrication.

1.1 Background

Tissue Engineering (TE) is a rapidly evolving discipline with synergistic efforts in life sciences and engineering [1]. It has the potential to revolutionize treatment of various diseases and disorders by creating biological substitutes to restore, repair, maintain and improve tissue/organ function. The formal definition proposed during the first TE symposium in 1988 is as follows [2]:

"The application of the principles and methods of engineering and life sciences toward the fundamental understanding of structure-function relationships in normal and pathological mammalian tissue and the development of biological substitutes to restore, maintain, or improve tissue function"

Tissue engineered medical products (TEMPs) can be broadly classified into the following three categories [3]:

1) Cell therapy using genetically modified cells.
2) Tissue inducing products, such as growth factors
3) Hybrid products consisting of a biological component within matrices

The need for such a hybrid and innovative approach can be attributed to the following factors:

1) Organ shortage:

The annual expenditure for patients suffering from organ failure in the health care industry is over $400 billion [3]. The Organ Procurement and Transplant Network (OPTN) statistics up until 2013 (Figure 1 - 1) show an increasing trend in the waiting list for organ transplant

patients [4]. The discrepancy between the number of donors and the number of patients on the waiting list (Table 1 - 1) suggests the need for an alternate approach.

2) Complications associated with donor organs:

Donor organs are occasionally rejected by the host immune system and also run the risk of infections [5]. Implants and other *in vitro* medical devices which are used in lieu of transplants to treat such patients are also associated with similar complications [6].

3) Study models:

Products of TE can also serve as models to understand cell/tissue structure, cell signaling, in drug testing and may even replace animal models in few cases [7]. Using live cells as building blocks to make biological substitutes can be a more compatible solution than conventional transplants.

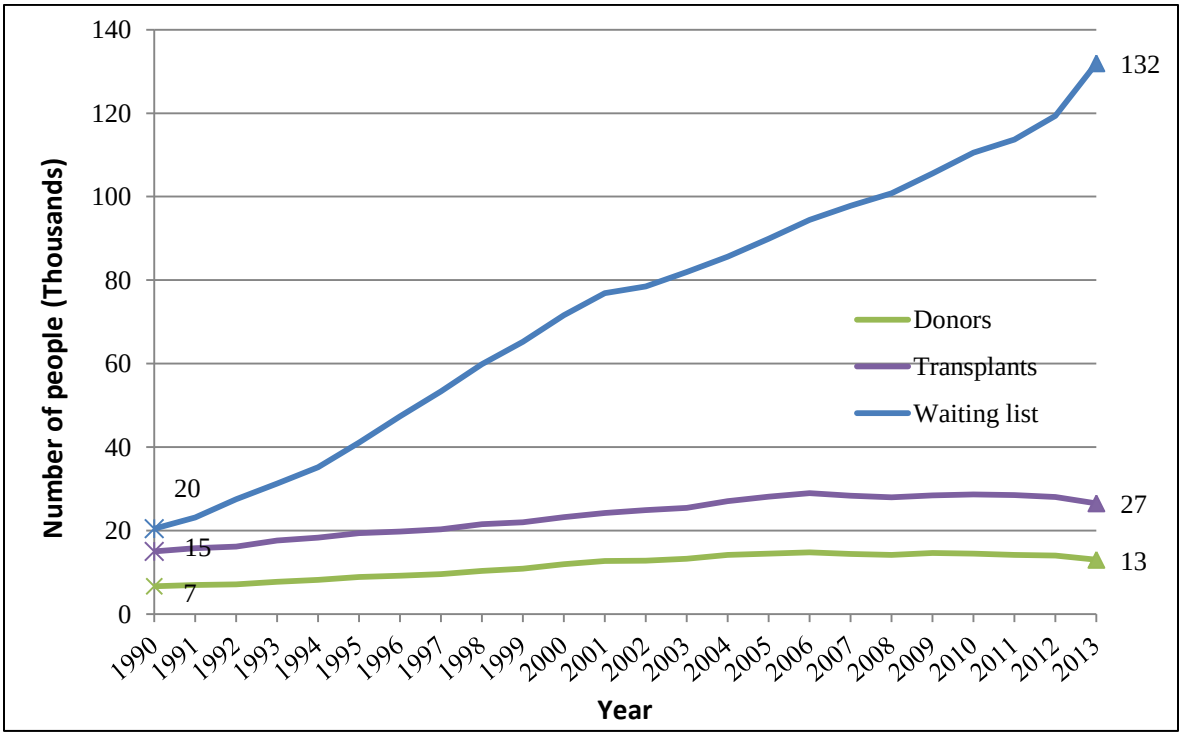

Figure 1 - 1 Number of donors , transplants and waiting list patients from 1990 to 2013 [4]

Table 1 - 1 Waiting list for organ transplants as of January 17, 2014 [4]

Organ	Waiting list
Kidney	106,330
Liver	16,366
Pancreas	1,182
Kidney / Pancreas	2,093
Heart	3,740
Lung	1,644
Heart / Lung	46
Intestine	253
All Organs	**131,654**

With advances in technology, two dimensional cell cultures are being translated into three dimensional (3D) configurations using TE constructs, culture media and bioreactors [8] [9]. 3D constructs better known as scaffolds offer a physiological context for the proliferating cells to organize into a regulated functional unit [10]. This scaffold based approach basically consists of two steps:

1) *in vitro* tissue formation using a porous biomaterial that promotes tissue formation in a controlled environment, and
2) *in vivo* tissue formation, where the laboratory grown tissue is implanted at the desired site and is expected to resume normal tissue regeneration and restore function.

Although TE offers promising solutions in creating biological substitutes, there are significant challenges that are to be addressed [11]. The scalability of this technology to physiologically relevant sizes which require better nutrient transfer mechanisms, higher control over starting materials (such as cell source, starting materials), transport and storage conditions are a few such challenges [12]. Overall, TE being a complex interdisciplinary

field, its success is dependent on better understanding and significant progress in all related areas of research.

1.2 Scaffolds in TE

A *scaffold* is defined as a support, delivery vehicle, or matrix for facilitating the migration, binding, or transport of cells or bioactive molecules used to replace, repair, or regenerate tissues (ASTM F2450-10) [13]. Scaffolds are designed to mimic the extracellular matrix (ECM) of the tissue being engineered [14]. They act as a temporary housing for culturing cells. They are designed to be biocompatible and promote cell proliferation while providing mechanical stability until tissue regeneration is complete.

Scaffold based TE can be thought of as implants or devices made of 'smart materials' i.e. live cells in a biodegradable housing. A flowchart with the various steps involved in autologous scaffold based TE is shown in Figure 1 - 2. The first step involves performing a biopsy to collect a sample of the native tissue from the donor [15]. Once the tissue sample is obtained, the desired cells are isolated from the ECM and expanded. When the desired cell count has been reached, the cells are harvested and seeded onto scaffolds. The cell proliferation within these scaffolds generates a functional implant for the patient.

Note that scaffolds can also be seeded with allogeneic (donor from same species), xenogeneic (donor from different species), or stem cells, depending upon the application [12]. This research focuses on the analysis of a 3D scaffold fabrication process since it has a significant impact on the subsequent step of cell seeding [8] which in turn plays a crucial role in tissue formation [9] [16].

Scaffolds require appropriate geometry, architecture and surface features to promote cell adhesion, signaling and migration [10]. This requirement can be cell or tissue specific as well. Cell culture experiments have demonstrated how 3D cell cultures bear closer resemblance to cellular morphology of native tissues when compared to 2D cultures [8].

Histological and scanning electron microscope (SEM) images of bone, liver and thymus cells (Figure 1 - 3) show a difference in cellular organization within 2D (B, E and H) and 3D matrices (C, F and I). It is observed that 3D cultures bear closer resembles to cells in the natural state (A, D and G). 2D substrates do not provide a unique ECM environment to cells causing them to adapt for survival. This in turn can alter cell metabolism and produce results that may not simulate actual tissue mechanism [8]. Hence, 3D cell cultures have gained importance over the past decade [17] and several techniques are being investigated to fabricate scaffolds with suitable physical and functional features.

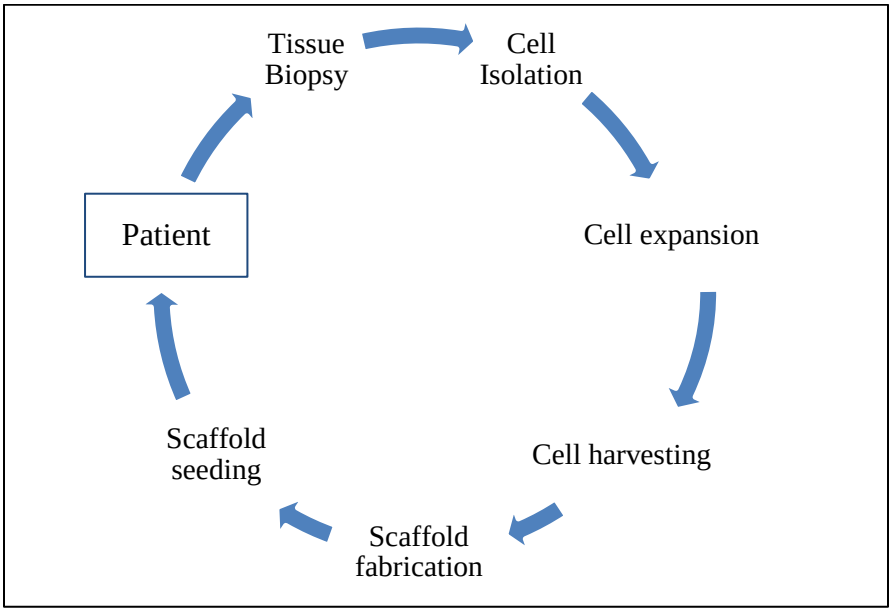

Figure 1 - 2 Flowchart of the steps involved in standard autologous scaffold based TE [11]

Porous scaffolds for TE can be fabricated with different types of biomaterials [18] (e.g.: poly(glycolic acid) (PGA), poly(l-lactic acid) (PLLA)) using various processes. These processes include conventional techniques [19] such as fiber bonding, solvent casting and particulate leaching, and electrospinning, or additive manufacturing (AM) processes [20]

such as stereolithography (SLA), selective laser sintering (SLS), fused deposition modeling (FDM), and 3D-Bioplotting. AM processes use data from a 3D computer model to fabricate structures in layers. Scaffolds made by these processes can be precisely controlled by the user to generate complex shapes as seen in Figure 1 - 4.

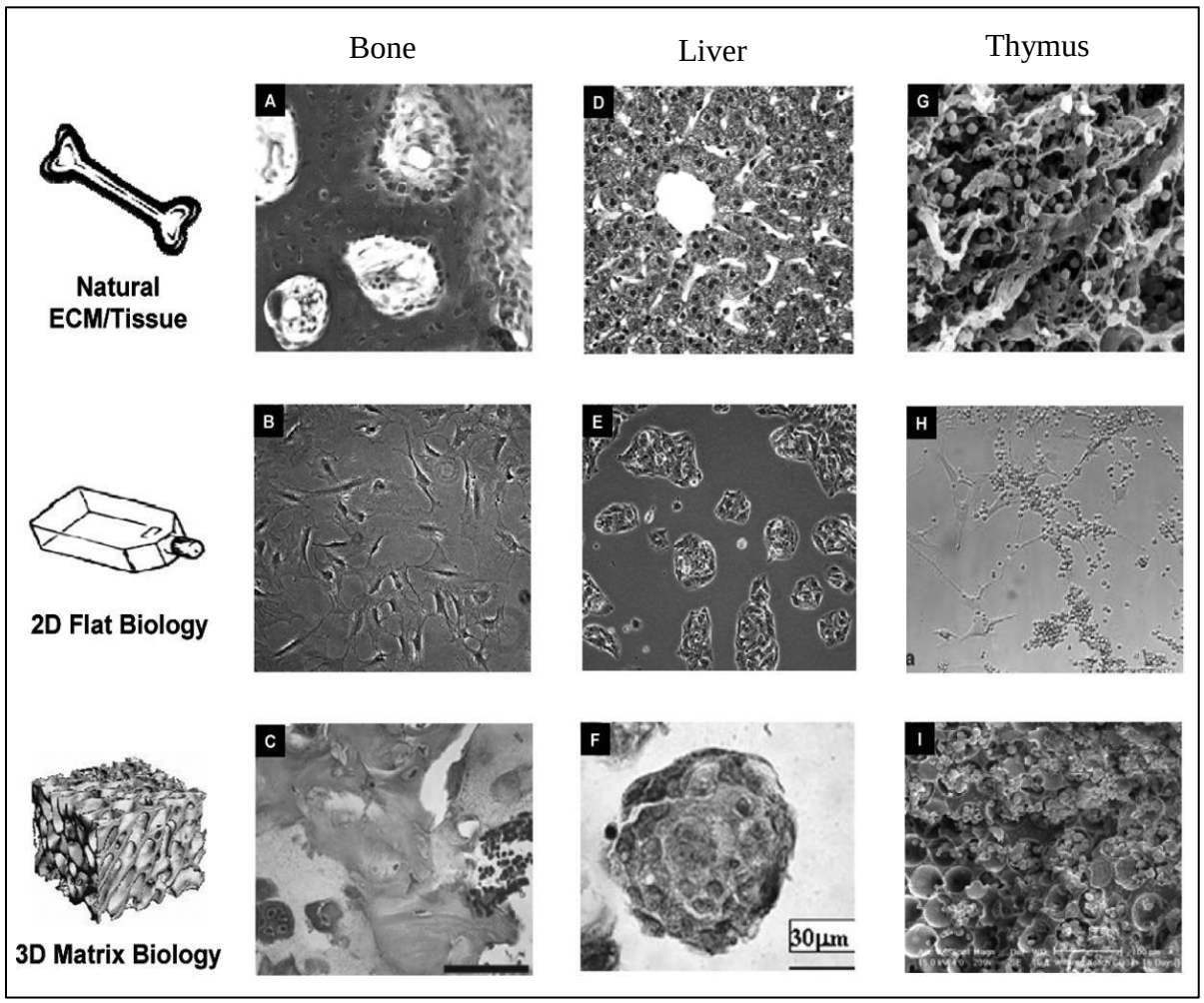

Figure 1 - 3 Comparison of cell morphology on 2D and 3D substrates to cells in the native tissue [8][21]; histological images of bone – (A) to (C), liver - (D) to (F) and thymus – (G) to (I) - SEM images

Although the AM processes generally offer greater control and flexibility compared to conventional methods by adopting a layered manufacturing approach, there are a few challenges. For example, their clinical applications can be limited due to high processing times, costs and equipment, also demanding focused collaborations between different disciplines [22]. These limitations can be overcome by focusing on the continuous improvement of these processes and developing models to optimize processing time and costs [22].

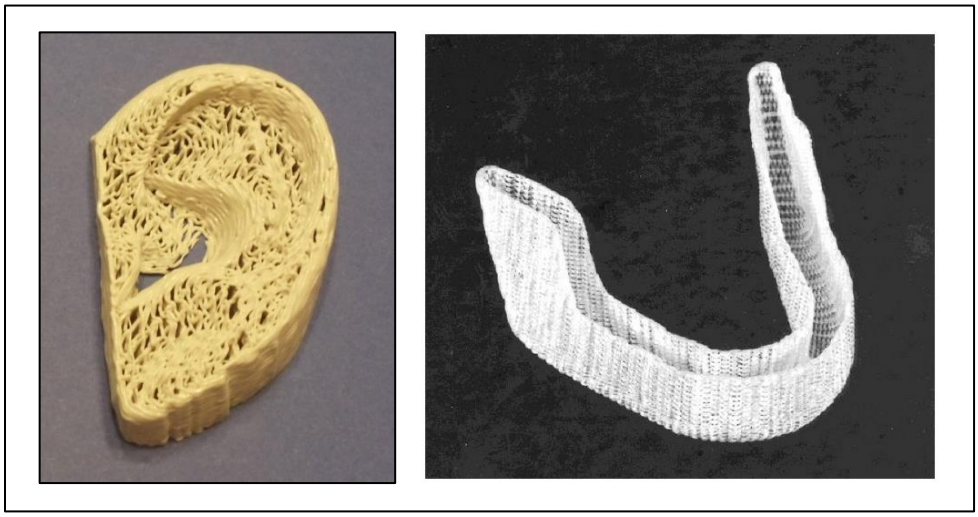

Figure 1 - 4 Example of 3D scaffolds used in TE; Left – Silicone ear; PLLA mesh used for regeneration of the jaw [23]

1.3 Motivation

Extrusion based AM processes have demonstrated the ability to fabricate scaffolds with fairly reproducible architectures [8]. Furthermore, some of these processes are capable of dispensing cell-based biomaterials. However, in order to scale up and translate such processes, a better understanding of the interactions between material properties and

processing parameters is required. Some of the important shortcomings of these processes include:

1) Sensitivity of process to the material viscosity at the nozzle tip [8]
2) Low mechanical strength of the fabricated structures [2] [9]
3) Calibration required for new material introduction [2] [9]

These inherent disadvantages limit the material selection and the mechanical strength of scaffolds fabricated using these processes is compromised. In addition, the time taken to develop a feasible range of processing parameters for newer biomaterial blends (e.g. Polycaprolactone (PCL) – Hydroxyapatite (HA) of varying proportions [24]) can be significantly high.

3D-Bioplotting is an extrusion based AM process that is compatible with the use of polymers, hydrogels and cell suspensions as raw materials. This technique involves the pneumatic extrusion of biomaterial melts in the form of strands through a nozzle. The strands are deposited onto a platform or into a plotting media to progressively build 3D structures in layers. This technique is advantageous as it allows plotting of a material within another material of comparable viscosity increasing the range of applicable materials [25].

The flow rate and flow behavior of the material are key parameters that influence the resulting scaffold architecture and mechanical characteristics in such extrusion based techniques [26]. Vozzi *et al.* [27] developed a model that could predict the strand size in a microsyringe deposition system, a technique similar to 3D-Bioplotting, to fabricate scaffolds. However, the application of this model is limited by the assumption that the dispensing material is a Newtonian fluid, where the fluid viscosity is independent of the shear rate. In reality, biomaterials and polymers exhibit non-Newtonian behavior which is more challenging to model. In these materials, the shear stress and shear strain do not vary linearly. Also, with the introduction of cell-hydrogel mixtures, temperature and pressure during the process can directly affect cell viability. Hence, there is a need for a model that can account

for the actual material flow behavior and processing parameters. With the use of polymer melts, it becomes critical to assess their rheological behavior since it plays a significant role on the resulting scaffold fabricated. A generic expression for polymer flow behavior is given by Equation 1- 1 [28].

$$\tau = \eta(T, \dot{\gamma}, P)\dot{\gamma} \qquad \text{Equation 1-1}$$

where,

τ is the shear stress induced in the polymer.

η (T, $\dot{\gamma}$,P) is the fluid viscosity at a temperature (T) with a deformation rate ($\dot{\gamma}$), pressure (P)

For any given polymer, the polymer viscosity is a function of temperature, pressure and deformation rate (Equation 1-1). A model that can account for the effect of all these parameters can be more accurate in characterizing the process. Such models are prerequisites to the fabrication of design-specific and consistent scaffolds. Due to the strong correlation between scaffold properties and biological functions, consistent scaffold production can directly impact the clinical success of scaffold based TE [16] [29]. This research aims to map the material-process-structure interactions during 3D-Bioplotting for one commonly used biopolymer. This can also be an essential step towards automating scaffold based TE. The research objectives and scope of the research is discussed in the subsequent section.

1.4 Research Objectives

This thesis aims to investigate the overall effect of processing parameters on scaffold characteristics during 3D-Bioplotting using an empirical approach. Additionally, data from rheological assessment of the polymer (conducted in parallel) is used to examine the effect of polymer viscosity during 3D-Bioplotting. This would minimize or eliminate the trial and error approach of identifying a feasible set of process parameters for a given material. The broader goal is to develop an approach that can be applicable to a wider range of biomaterials.

This thesis focuses on establishing critical relationships between polymer viscosity, processing parameters (nozzle diameter, extrusion temperature, extrusion pressure, dispensing speed) and resultant characteristics of the fabricated scaffolds (geometry and strength). The list of the process parameters and scaffold characteristics that have been used in this study is summarized in Table 1 - 2. PCL is the primary biomaterial under consideration used to fabricate scaffolds on a 3D-Bioplotter™ system from Envisiontec. In order to meet the broader objective, the specific aims defined for this research are listed below:

Table 1 - 2 List of parameters used in this study

3D-Bioplotting process parameters	Scaffold characteristics
Extrusion temperature	Strand width
Nozzle diameter	Strand separation distance
Dispensing speed	Porosity
Extrusion pressure	Swell ratio
Material Viscosity	Compression strength

Aim 1: To determine the feasible range of processing parameters for 3D-Bioplotting of PCL

- Determine feasible levels of extrusion temperature, extrusion pressure and dispensing speed for a given nozzle diameter to extrude continuous strands of PCL.

Aim 2: To investigate the effect of 3D-Bioplotting process parameters on the resultant scaffold characteristics

- Determine the effects of feasible processing parameters (from Aim 1) on resultant scaffold characteristics (geometry and compression strength) using a DOE.

Aim 3: To establish a relationship between the rheological properties of PCL and the extrusion temperature

- Determine the rheological characteristics and sensitivity of PCL by at different shear rates over time
- Determine the apparent viscosity of PCL during 3D-Bioplotting
- Compare the viscosity of different molecular weights of PCL. Table 1 - 3 shows the different molecular weights of PCL used in these studies.

Table 1 - 3 PCL blends used in this experiment

Name	Polymer form	Brand	Molecular Weight (kDa)
PCL 767	Pellets	Tone Polymers	43 – 50
PCL 15	Flakes	Sigma-Aldrich	15

1.5 Thesis Outline

Chapter 2 reviews some of the relevant literature on scaffold design and fabrication processes with an emphasis on extrusion based techniques. Chapter 3 describes the experimental setup, procedure and results obtained from the scaffold fabrication experiments. Chapter 4 presents the materials, experimental approach and results obtained in the rheological characterization of PCL. The thesis concludes in Chapter 5 with a summary and directions for future research.

1.6 Chapter Summary

TE is an emerging field combining principles of engineering and life sciences which aims to revolutionize treatment of various diseases and disorders by creating biological substitutes. One of the approaches in this discipline is the use of 3D matrices or scaffolds for creating these substitutes. These scaffolds are porous and biodegradable acting as temporary housing for cells which eventually proliferate to form organized tissue systems. 3D scaffold

requirements are stringent and specific. The fabrication of these scaffolds is critical to the clinical success of this approach. The main motivation behind this research is to minimize the time taken for scaffold fabrication for an AM technique, namely, 3D-Bioplotting. This thesis aims to characterize this process for PCL by investigating the effect of PCL viscosity and 3D-Bioplotting process parameters on the resulting scaffold characteristics.

CHAPTER 2: LITERATURE REVIEW

In this chapter, selected literature pertaining to TE scaffold design and fabrication processes is presented. Extrusion-based AM fabrication processes and the importance of material rheology in such processes are reviewed in greater detail due to their relevance to this thesis.

2.1 Functional Requirements of TE Scaffolds

Most cells in human tissues reside in a fibrous, interconnected network of functional proteins and polysaccharides, such as collagen and elastin and glycosaminoglycans (GAGs) referred to as the ECM (Figure 2 - 1) [10].

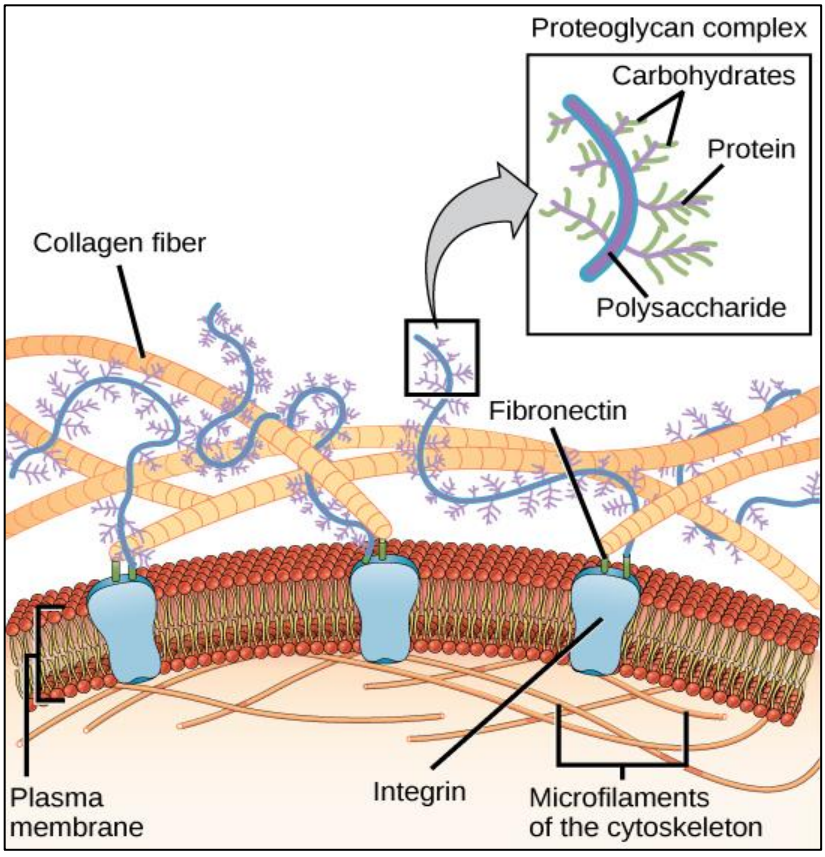

Figure 2 - 1 Schematic diagram of the ECM [30]

The macromolecules that constitute the ECM are secreted, oriented and modified by the cellular components of tissues. These in turn, exert control over many cellular processes (e.g., growth and wound healing) [31]. The ECM provides structural support and the physical environment for cells to reside in. The ECM also imparts mechanical properties (e.g., rigidity, elasticity), provides bioactive cues for regulating cell activities, acts as a reservoir of growth factors and provides dynamic degradable environment to allow tissue healing and remodeling [14].

The fundamental role of TE scaffolds is to simulate and mimic the ECM of cells temporarily, promoting tissue regeneration. This can be extremely challenging since the interaction between cells and the ECM is a dynamic process and is continually changing [8]. For instance, cartilage is a tissue largely composed of collagen as the ECM, and the amount of collagen produced is of the order of 100 µm per day. Since cartilage is a load bearing tissue, the ECM is modified and remodeled in response to mechanical deformations. So, the ECM has both a structural and an informational component, and it is important to consider both of these in scaffold based TE [2].

2.2 Scaffold Materials

The scaffold material plays a critical role in tissue regeneration since it in direct contact with the cells while acting as a substrate. Material selection for TE scaffolds is based on a few important criteria, such as [32] [33]:

1. Biocompatibility – the scaffold material must not elicit a foreign-body reaction or inflammation when used *in vivo* [34]. Collagen is an example of a naturally derived, highly biocompatible material [8].

2. Biodegradability – the macromolecular degradation of the materials *in vivo* should leave no traces behind and should not exhibit cytotoxicity. This degradation rate should be controlled and in sync with the tissue regeneration rate (explained further in Section 2.3).

The average degradation rate for few commonly used scaffold materials is shown in Table 2 - 1 [35] [19].

3. Mechanical properties – the bulk material properties should match that of the tissue being engineered. This has been explained in greater detail in section 2.1.2.

4. Processibility – the selected material should be capable of being fabricated into desired structures using a suitable fabrication technique and retaining the above mentioned criteria post processing [36]. The different scaffold fabrication techniques employed are discussed in Section 2.5.

Table 2 - 1 Degradation rates of different biopolymers for a given scaffold geometry; (note: this is also dependent on molecular weight, local environment pH value and source) [35] **[19]**

Material	Degradation rate (months)
Hydroxyapatite (HA)	5 - 60
Polyglycolic acid (PGA)	12 - 48
PCL	24 – 36
Poly(D, L-lactic acid)	12 – 48
Collagen	2 – 24

2.2.1 Scaffold material classification

Four types of biomaterials have been experimentally and/or clinically studied as scaffold materials for TE applications [32] :

1) synthetic organic materials (e.g. Aliphatic polyesters)
2) synthetic inorganic materials (e.g. HA)
3) organic materials of natural origin (e.g. collagen)
4) inorganic material of natural origin (e.g. coralline HA)

Naturally derived materials such as collagen, fibrin, GAGs, chitosan, alginates, and starch, can be directly extracted from plants, animals, or human tissues and do not invoke a foreign body response when introduced *in vivo* [1,7]. These natural polymers have been used in conjunction with synthetic polymers such as PLLA, PGA and PCL to impart superior mechanical properties and also improve cell interactions [33]. Collagen with electrospun nanofibers have been used as scaffolds for bone and cartilage [33]. Collagen-GAG scaffolds that have been used clinically for skin regeneration and have shown potential in engineering different systems with the use of mesenchymal stem cells (MSCs) [37].

Bioceramics which encompass HA, bioglass, tri-calcium phosphate (TCP) closely mimic bone tissues and have therefore been used widely in bone TE. These materials provide an osteoconductive environment where bone ECM proteins are absorbed, resulting in osteoblasts adhering and proliferating [24]. Ceramics have mostly been used in conjunction with polymers as composite scaffolds to compensate for their brittle properties.

Polymers are generally chosen over other materials because of their ease of processing and tailorable properties [18]. They also give predictable results compared to naturally derived materials [10]. Different materials that are applicable as scaffold materials as summarized in Table 2 - 2.

Table 2 - 2 List of scaffold materials [10]

Material		Examples	Advantages
Polymers	Natural	collagen, fibrin, chitosan, alginates	good biocompatibility and low toxicity, properties easily tailored Ease of processing
	Synthetic	PLA, PGA and PCL	
Ceramics		Hydroxyapatite (HA), Tri-calcium phosphate (TCP)	Naturally occurring bone mineral Easily absorbed by the body

PCL, used in this research, is a biopolymer that is being extensively investigated as a biomaterial and shows an increasing trend in TE applications (Figure 2 - 2) [38]. PCL is known to possess stable rheological properties, low glass-transition temperature and high decomposition temperature [8] and can be processed using a multitude of techniques. PCL scaffolds have been employed in research efforts to engineer bone, cartilage, skin and cardiovascular systems [38]. There are a number of drug-delivery devices fabricated with PCL that have FDA approval which makes this a favorable polymer for commercialization and clinical translation [38][39]. Another advantage of PCL is that it can be easily combined into blends with other materials and manipulated to fabricate scaffolds of desired specifications [33].

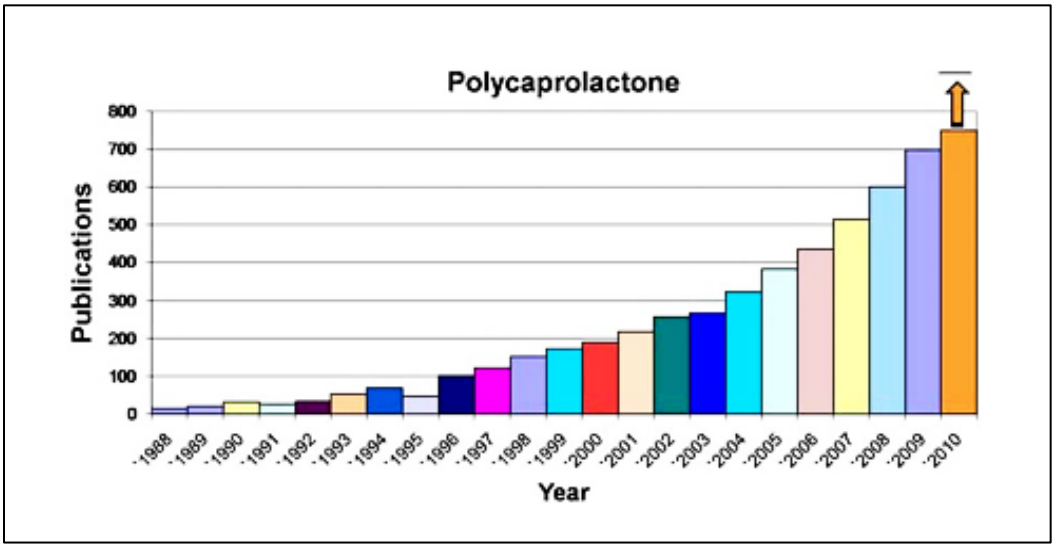

Figure 2 - 2 Publications using PCL in the field of biomaterials and TE from 1988 to 2010 [38]

2.3 Scaffold Architecture

Scaffold architecture is critical to cell proliferation since mass transport mechanism in TE scaffolds is primarily through diffusion [40]. Nutrient supply to cells *in vivo* is through

capillaries, which are usually situated within 100 μm from any given cell [16]. Static cell cultures in 3D scaffolds for TE have shown tissue formation only 100 to 200μm into the peripheral regions of the scaffolds due to diffusion limitations [40]. The diffusion of nutrients and waste in and out of cells is mainly influenced by scaffold architecture (pore size and porosity), material degradation characteristics and surface topography, which is covered in this section.

2.3.1 Pore size and porosity

The size of pores in 3D scaffolds is one of the main parameters which affect subsequent cell seeding, in-growth of tissue as well as cell attachment. Cellular responses of angiogenesis, inflammation, foreign body capsule formation and tissue infiltration, *in vivo*, have been shown to be dependent on average pore size and pore size distribution [41][42]. Cell dimensions and interactions have to be taken into account while designing scaffolds since different cell types have different pore size requirements (Table 2 - 3) [18][43].

Table 2 - 3 Pore size requirements of different cell types [10], [17], [19], [31]

Cell type		Pore size
Bone	Minimum size based on cell dimension	>100 um
	To promote new bone formation	>300um
Fibroblast and endothelial cells		50 to 90 um
Hepatocytes		20 um
Vascular smooth muscle cells		63 – 150 um
Keratinocytes & Skin cells		20 - 125 um

In addition to the average pore size, scaffolds can be characterized and evaluated by the overall porosity. Scaffold porosity is the space available for cells to migrate and for

vascularization of the tissue [10]. The mass transport of oxygen and nutrients within a scaffold depends on the total porosity and pore interconnectivity Micro-porosity is important for capillary ingrowth and interactions between cells and the ECM, while macro-porosity is vital for nutrient supply and waste removal from cellular metabolism [10]. Scaffolds should ideally be designed to have a high porosity, high surface area to volume ratio and an inter-connected geometry for any given shape [16].

Several techniques are available to determine scaffold porosity (often expressed as a percentage). Porosity characterization by measuring scaffold density is widely found in literature and is represented by Equation 2 -1 (ASTM F2450-10) [13]. It is an estimate of pore volume within a scaffold using the scaffold dry weight.

$$V_P = V_T - (m_s/\rho) \qquad \text{Equation 2- 1}$$

where, V_P is volume of pores, V_T is total scaffold volume, m_s is the mass of the scaffold (measured using a weighing scale) and ρ is the density of the scaffold material.

V_T is calculated using the scaffold dimensions and material density for a non-porous solid scaffold. Scaffold pore volume V_P is then calculated using Equation 2-1.

Porosity is expressed as a percentage using Equation 2- 2 represented as follows [20]:

$$\text{Porosity} = (V_P/ V_T)*100 \qquad \text{Equation 2- 2}$$

Equations 2-1 and 2-2 are applicable to random geometries. Landers et al [44] developed a theoretical approach in calculating the porosity for regular structures built using AM processes. This is applicable to structures that have alternate layers arranged orthogonally (Equation 2- 3).

$$Total\ Porosity\ (\%) = 1 - \left(\frac{\pi {d_1}^2}{4 d_2 d_3}\right) * 100 \qquad \text{Equation 2 - 3}$$

where, d_1 is filament diameter, d_2 is repeat length and d_3 is layer thickness (Figure 2 - 3).

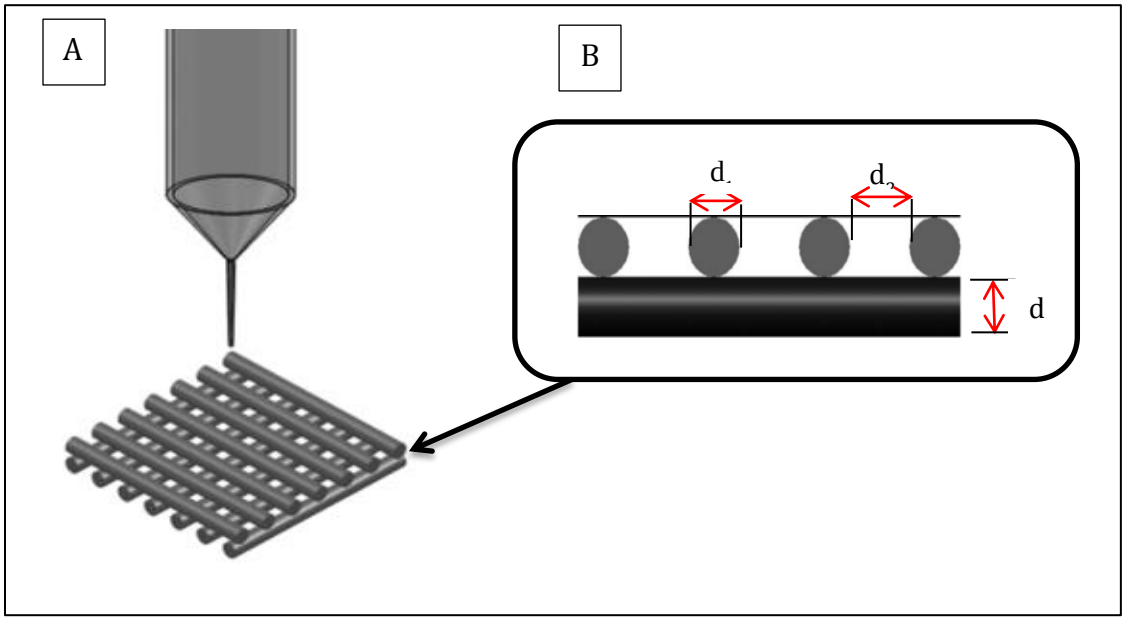

Figure 2 - 3 Porosity calculation for structures with orthogonally arranged layers (A) 0°_90° laydown patter (B) dimensions used for porosity calculations [45]

It is also important to consider the increase in pore size when the material degrades *in vivo* as it results in changes in pore structure and interconnectivity with time [19]. Scaffold design should account for this rate of degradation which is described in the following subsection.

2.3.2 Rate of degradation

Scaffolds should be fabricated with biocompatible materials that do not exhibit any cytotoxic behavior and/or elicit an immunological response from the host system [35]. The rate of resorption or degradation of these scaffolds should be designed such that the strength of the scaffold is retained until the tissue has recovered and/or remodeled to take over their role [8].

Two broad strategies have been outlined for material selection based on degradation rate [34]. In the first strategy, the scaffold is retained until the engineered transplant is completely ready to perform its structural role. In this approach, the implant possesses comparable mechanical properties to the host tissues and is commonly used in bone regeneration. The

second approach consists of retaining the scaffold material properties only during the *in vitro* phase. A premature tissue with sufficient strength is then implanted into the host. This strategy is illustrated in Figure 2 - 4 with respect to a heart valve transplant [34]**.**

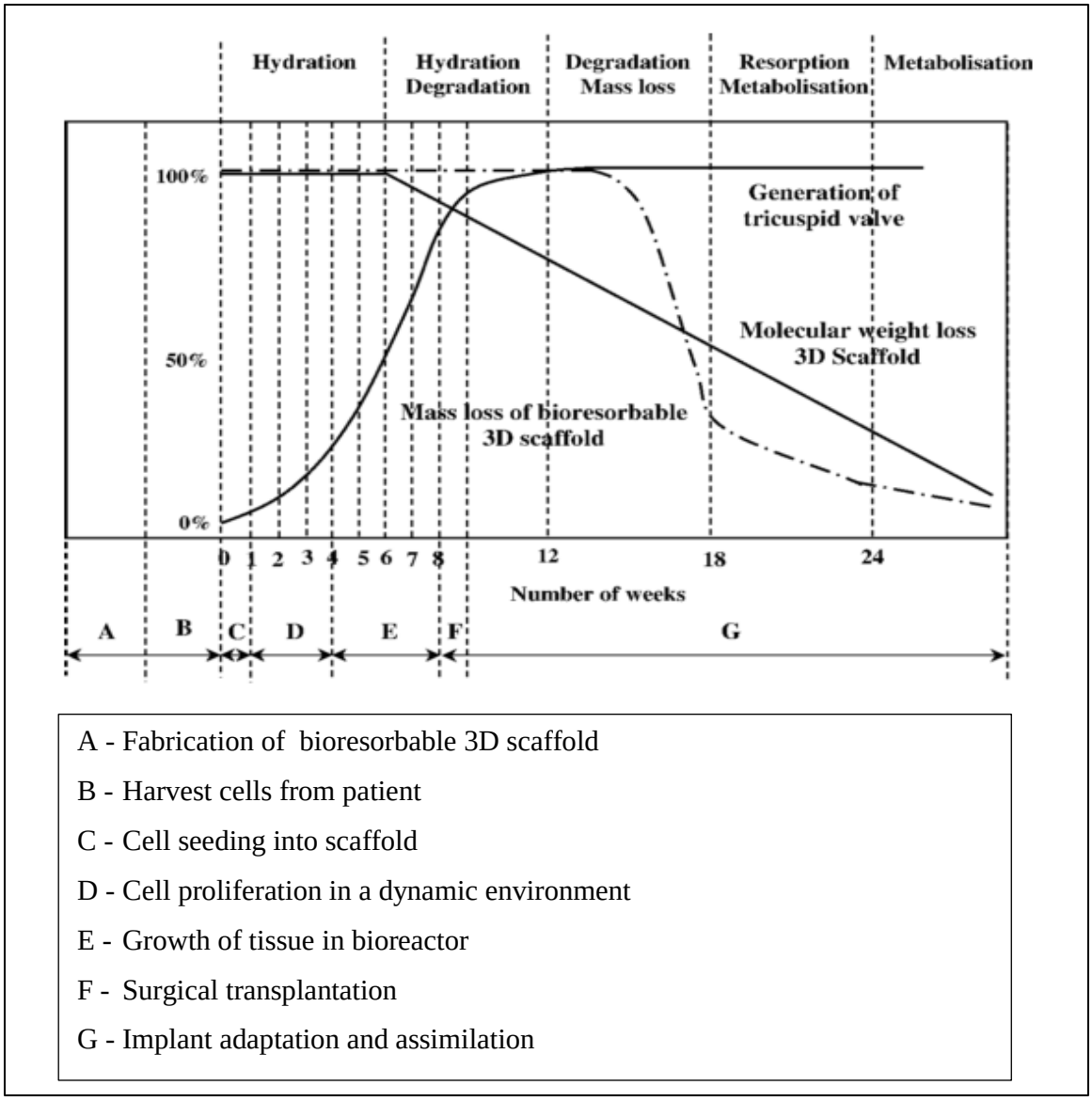

Figure 2 - 4 Graphical illustration of polymer selection strategy using degradation rate of a 3D scaffold over time for engineering a heart valve [34]

The graph shows the complex interactions between the mass loss of the 3D scaffold with respect to the time taken for tissue regeneration and remodelling. In addition to this, the actual geometery of the scaffold, the processing technique and material used influence the degradation rate.

2.3.3 Surface topography

Regulation of cellular activities is done through mechanical signaling via the ECM, which include physical cues such as changes in surface topography [46]. Cell adhesion and interactions are affected when such signaling is simulated in scaffold cell cultures as well [47]. Kiang *et al.* [16] demonstrated that smooth muscle cells respond to changes in surface roughness. In general, surface roughness increases cell adhesion, migration and ECM production [16]. Surfaces with nodes, pores and patterns have been shown to exhibit pronounced cellular activities, morphological changes and have been associated with the

production of regulatory factors [16]. Yin *et al.* [48] cultured cardiac cells on grooves 50 mm deep and 120 mm wide to investigate the topography-driven changes in cardiac electro-mechanics. Their results demonstrated that the microstructure had a direct influence on cardiac function [48]. There are extensive studies being conducted in mechano-signaling responses in cell cultures [16], which play an important role in scaffold design. The material and fabrication technique selected dictates the surface topographical features as well. Scaffold fabrication techniques are discussed in detail in section 2.5.

2.4 Mechanical Properties

The mechanical properties of TE scaffolds should be tailored to resemble the native or host tissue. Most natural tissue systems possess anisotropic and non-linear material properties which poses a challenging problem to replicate using artificial scaffolds [9]. Various research efforts have been channeled into determining mechanical properties of different organ/tissue systems [49]. Table 2 - 4 shows examples of different tissues and some of their mechanical properties [2].

Scaffolds should have sufficient mechanical strength to resist deformation against pulsatile pressures and *in vivo* stresses in a physiological environment, while maintaining their shape to promote cellular ingrowth [17]. Scaffolds used in bone regeneration, require the ability to bear loads and retain mechanical stability till the bone tissue is restored [50]. Whereas, scaffolds for vascular regeneration need to withstand cyclic strain over extended periods of time [17]. The mechanical properties of scaffolds are determined by the inherent bulk properties of the constituent material and are also influenced by the scaffold geometry. For instance, crystalline polymers show increased tensile strength and porous geometry affects the load bearing capacity of scaffolds [18] [40] .

Table 2 - 4 Mechanical properties of different tissues [2]

Material	Elastic Modulus (MPa)	Yield Stress (MPa)	Strain (%)
Collagen Fibers	500	50	10
Elastin	100	300	300
Cartilage	10	20	70 - 200
Skin	35	15	100
Muscle Fascia	350	15	270
Tendon	700	60	10

The selection of the scaffold material should be based on the mechanical properties of the tissue being engineered, i.e. the inherent material property should closely match that of the native/host tissue. The mechanical properties of the host tissue can vary with age and gender as well [51]. One example of this is the difference observed with respect to bone density of different individuals (Figure 2 - 5) [51]. The scaffold mass and architecture, which in turn affect the degradation rate of the scaffold, also need to be tailored to retain mechanical strength till the tissue is repaired or remodeled. The basic overall requirements for a TE scaffold with respect to material and physiological aspects are summarized in Figure 2 - 6.

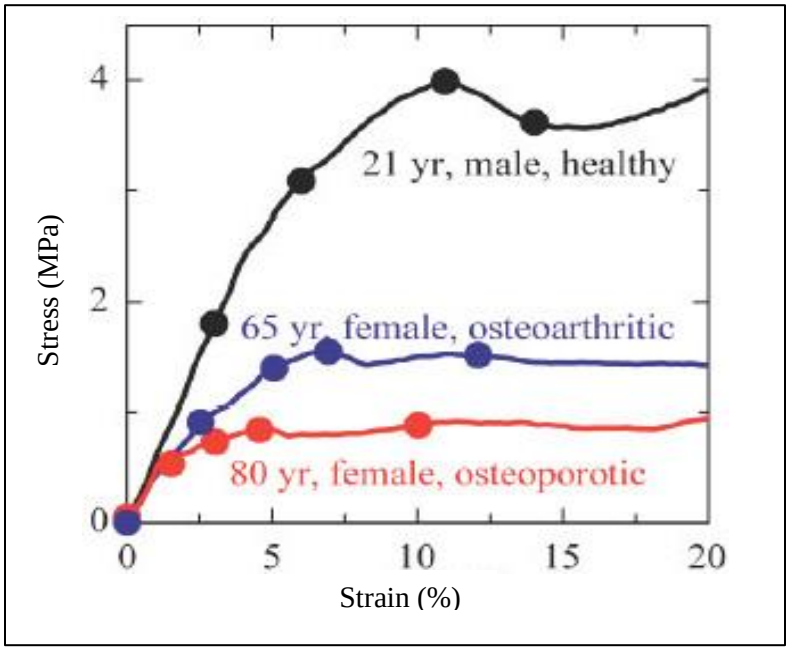

Figure 2 - 5 Variation in bone strength between gender, age and physical fitness levels [51]

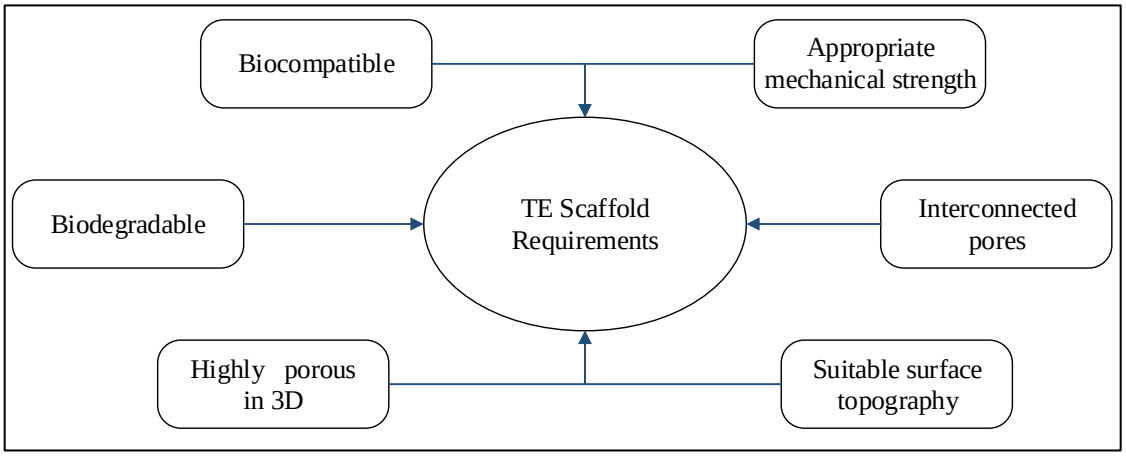

Figure 2 - 6 Basic requirements of a TE scaffold [22]

2.5 Scaffold Fabrication Techniques

The biomaterial and the fabrication technique chosen to build TE scaffolds are key parameters in controlling their performance [25][52]. To cater to the broad spectrum of design requirements which have been discussed in the previous sections, an ideal scaffold fabrication technique should provide the user with a high degree of control capable of producing tissue-specific scaffolds and maximize effectiveness of tissue regeneration.

The fabrication of scaffolds can be broadly classified into non-deterministic or stochastic techniques and AM processes. This classification is based on the degree of a control offered by the process in generating a porous structure. Some of techniques that fall under these categories are discussed in the subsequent subsections.

2.5.1 Nondeterministic Techniques:

Non-deterministic or stochastic techniques include methods such as solvent casting and particulate leaching, freeze dying, phase separation and electrospinning [19]. These techniques produce scaffolds with pore size, volume and distribution that are random or stochastic in nature [52]. In general, these techniques use a heterogeneous mixture which consists of a porogen that is removed using chemical or thermal processing, leaving behind a porous structure.

1) Solvent casting and particulate leaching

Solvent casting and particulate leaching is one of the oldest techniques used to generate porous structures [10]. It uses a solvent to cast a polymer into a desired shape with embedded water soluble particles. The particle dimensions are chosen based on the porosity requirement of the scaffold. These particles are eventually removed using a solvent leaving a porous polymer cast (Figure 2 - 7). Commonly used porogen agents are sodium chloride, ammonium bicarbonate and varying particle sizes of glucose. The application of this technique is mostly in scaffolds for engineering soft tissues [53].

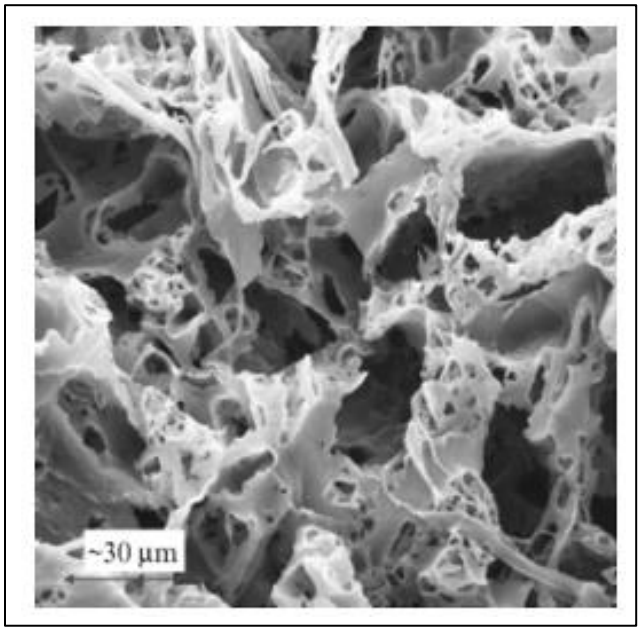

Figure 2 - 7 Scaffold fabricated by solvent casting and particulate leaching [54]

2) Electrospinning

Electrospinning (Figure 2 - 8) employs the principle of electrostatic repulsion to eject a polymer stream to produce continuous fibers. This stream is directed towards a grounded target where fibers with diameters ranging from 3nm to 5µm are generated [36]. This method has been used to make scaffolds for guided regeneration of smooth muscle cells [16]. Figure 2 - 8 shows electrospun PLLA scaffolds seeded with chondrocytes.

3) Freeze drying

Freeze drying is another technique which uses a solvent-polymer mixture to produce porous structures [8]. The solvent, usually water, sublimes under specific conditions of temperature and pressure leaving behind a porous spongy structure. This produces scaffolds with porosities up to 90% and pore diameters in the range of 15 µm - 35 µm [1] [13]. These scaffolds usually possess a closed pore morphology and have been used in dermal regeneration in the form of a porous sheet [12].

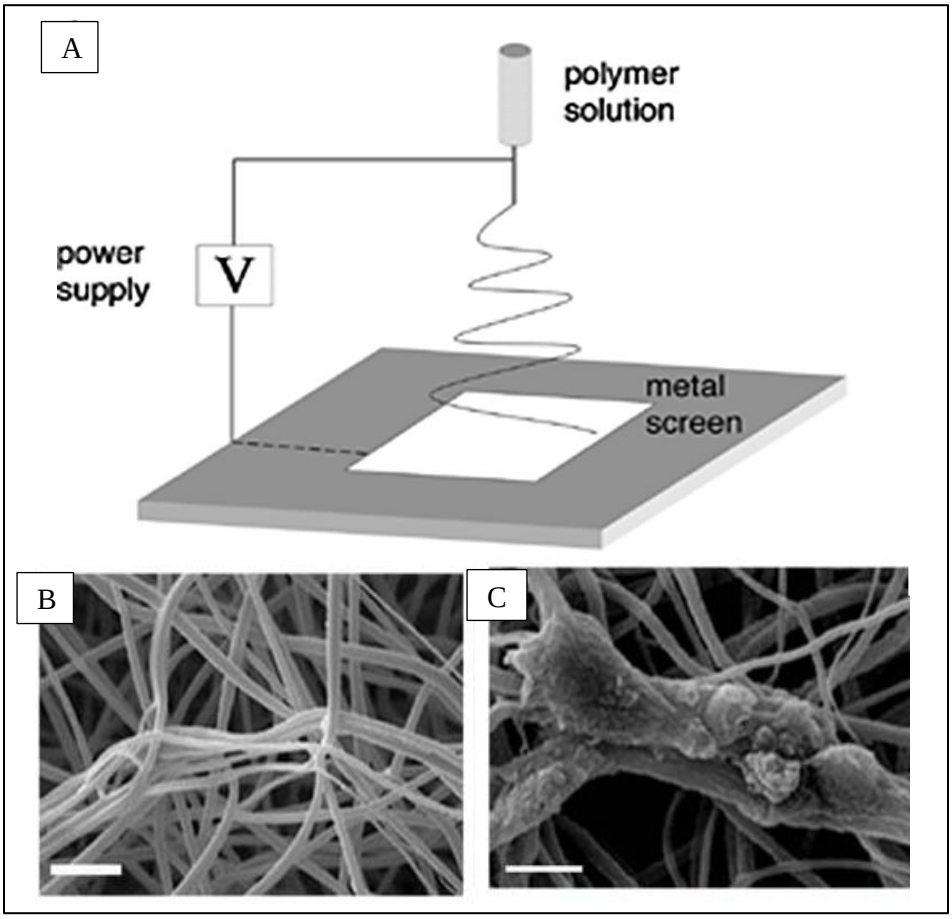

Figure 2 - 8 (A) Graphical illustration of electrospinning [55]**; (B) and (C) SEM images of electrospun PLLA scaffolds seeded with chondrocytes (R)** [55]

Some of the other non-deterministic techniques include fiber bonding, membrane lamination, melt molding and phase separation. Table 2 - 5 provides a summary of the some specifications and characteristics of conventional fabrication techniques discussed above.

Control over scaffold architecture using these conventional techniques is process dependent rather than design dependent [25]. These processes are also limited by their inability to control the internal geometry of the scaffolds. AM processes (described in the next section) aims to overcome these limitations by adopting a layered manufacturing approach.

Table 2 - 5 Summary of conventional techniques for scaffold fabrication [19] [1] [13] [36] [53]

Process	Specifications	Strength & Weakness
Solvent casting and particulate leaching	93% porosity [19] 500 µm pore sizes	*Advantages:* • Independent control of porosity by controlling porogen size • Highly porous scaffolds produced *Disadvantages:* • Limited to thin films and membranes - upto 3mm thick [52]. • Solvent residue may be harmful • Shape dependent on mold design
Electrospinning	3 nm to 5 µm fiber diameters [36]	*Advantages:* • Inexpensive and simple setup • Can produce highly porous scaffolds and generate micro and nano fibers. *Disadvantages:* • Limited mechanical properties • Limited range of materials that can be processed
Freeze drying	90% porosity pore diameters 15 to 35 µm [53]	*Advantages:* • Independent control of porosity by controlling porogen size • Highly porous scaffolds produced *Disadvantages:* • Solvent residue may be harmful • Unpredictable pore size and distribution

2.5.2 Additive manufacturing processes

AM also known as Solid Freeform Fabrication (SFF) include a set of processes that build 3D scaffolds by assembling two dimensional objects in layers. These processes offer higher control over the fabrication process of scaffolds with a predictable structure. Complex shapes which cannot be generated using conventional methods can be constructed using AM processes since the input is in the form of a 3D computer aided drawing (CAD) [56]. Different AM processes are being employed by researchers to fabricate scaffolds for cell culture experiments [20].

Recent advances in AM have enabled the inclusion of live cells as a scaffold material in the form of cell-hydrogel mixtures (Figure 2 - 9) [57]. This recently developed AM technique has also been shown to possess the ability to build hybrid scaffolds with multiple cell populations [58]. Fabrication of hybrid structures would be a significant breakthrough in organ regeneration since most organs are composed of more than one cell type [59]. The promising results of these techniques for TE scaffold fabrication have made them a research focus over the past decade.

AM processes stand out distinctly in comparison with traditional nondeterministic methods. Some of the main characteristics of these processes with respect to TE scaffold fabrication are highlighted below [22] [56] [60] [25]:

1) Machine-controlled layered manufacturing ensures that material deposition is precise and repeatable.
2) Customized patient-specific implants and complex architectures can be fabricated since AM processes use CAD models to generate the overall shape, as opposed to using molds. This also enables control over the internal geometry of the fabricated structure.
3) Increased pore interconnectivity in the porous scaffolds allows cells to migrate and nutrients to diffuse into the scaffold, resulting in improved cell seeding and proliferation.
4) It can be adapted to include hydrogels, living cells and growth factors as a part of the fabrication process to manufacture hybrid scaffolds.

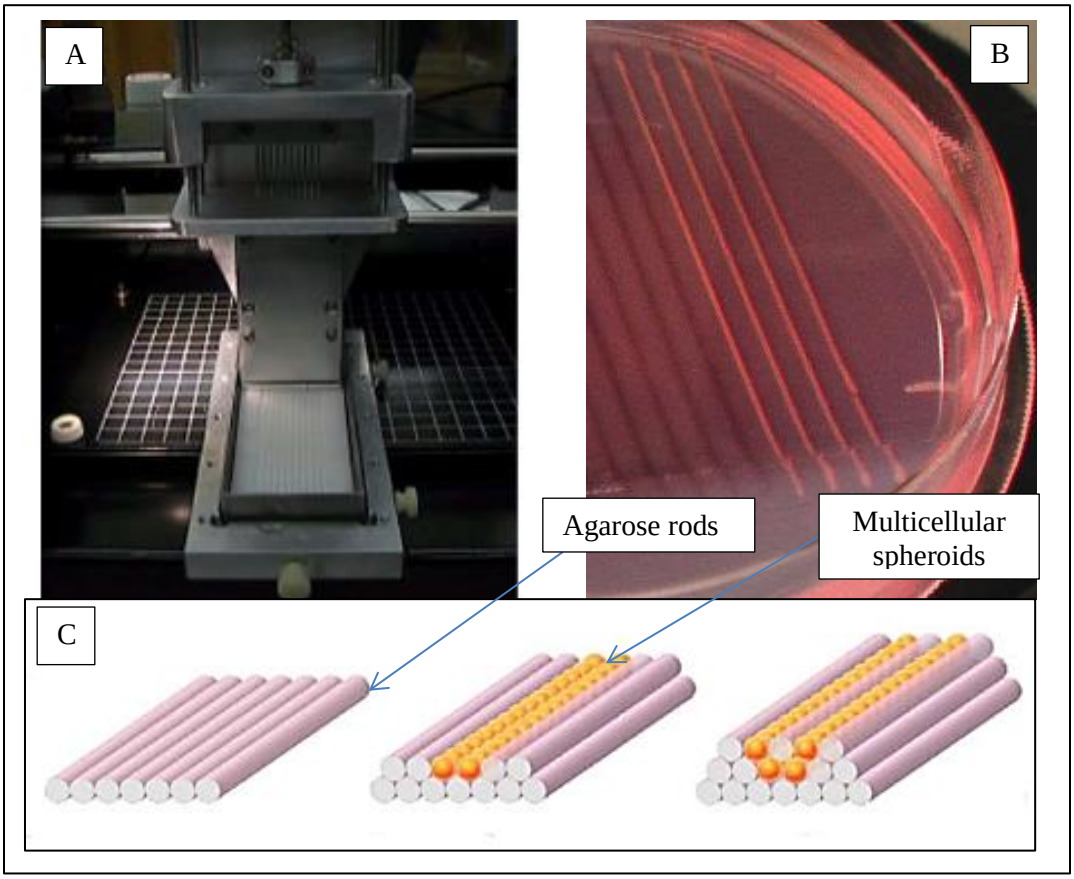

Figure 2 - 9 The concept of printing cells; (A) Bioprinter designed to extrude multicellular spheroids (human skin fibroblasts) (B) Non-adhesive agarose mold for deposition (bioink) (C) Illustration of deposition pattern of agarose mold and multicellular spheroids [57] [61]

Some of the AM processes used to fabricate TE scaffolds are reviewed in this section with a brief description of the process along with a few examples from literature.

1) Stereolithography (SLA)

SLA uses selective polymerization of photosensitive materials to fabricate a desired part [62]. An ultraviolet (UV) laser beam is used to trace the path of the object (CAD model) over a molten photosensitive material to cure the polymer layer by layer in the desired shape. The model is then cured in a UV oven and usually followed by a finishing process [25]. SLA can build complex geometries with a pore size starting with 250µm [60]. It has been used to

fabricate heart valves that could be used without suturing [63]. It has also been used to build HA prototypes for bone tissue scaffolds (Figure 2 - 10). SLA is limited by the range of materials that can be used and also due to the number steps involved before a finished product is obtained [20].

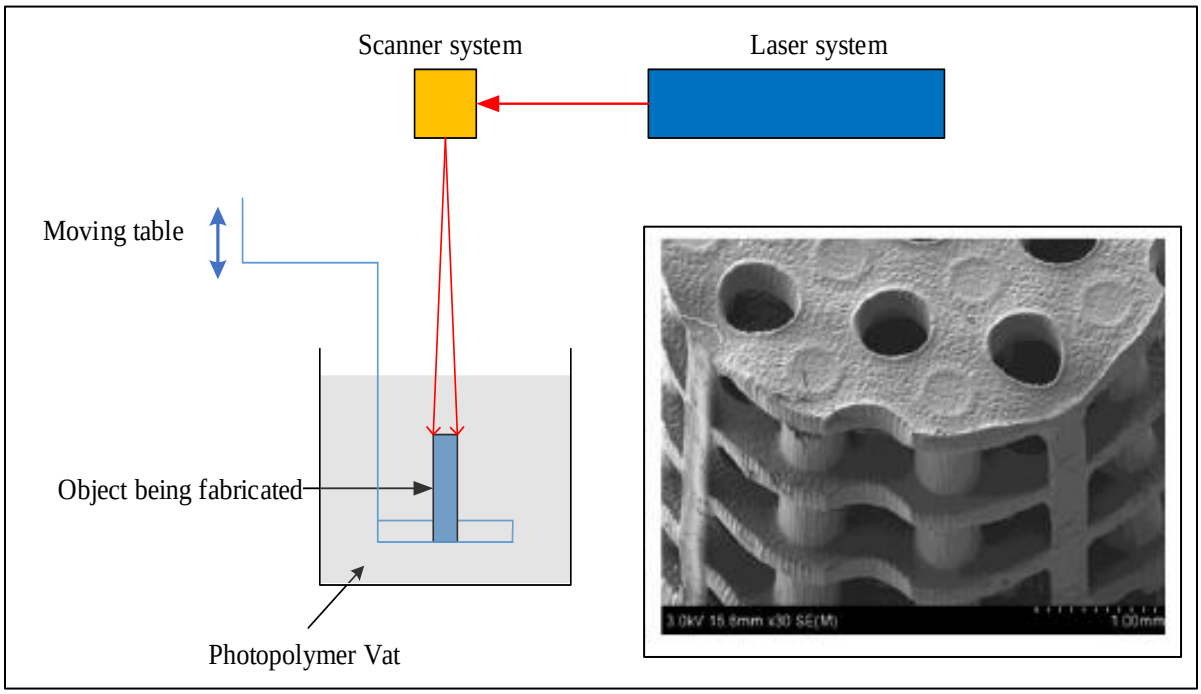

Figure 2 - 10 Pictorial illustration of SLA [62]; INSET: Scaffold fabricated using SLA for a critical sized bone defect using poly(propylene fumarate)/diethyl fumarate [64] [65]

2) Selective Laser Sintering (SLS)

SLS (Figure 2 - 11**)** uses a laser beam to sinter powdered raw material to build 3D models in layers using their CAD equivalent [62] . The laser beam locally melts the powdered raw material and is replaced by a roller after every layer. SLS has been employed to manufacture ceramic bone implants [66] and clinical implants using Ultra High Molecular Weight Polyethylene (UHMWPE) [67].

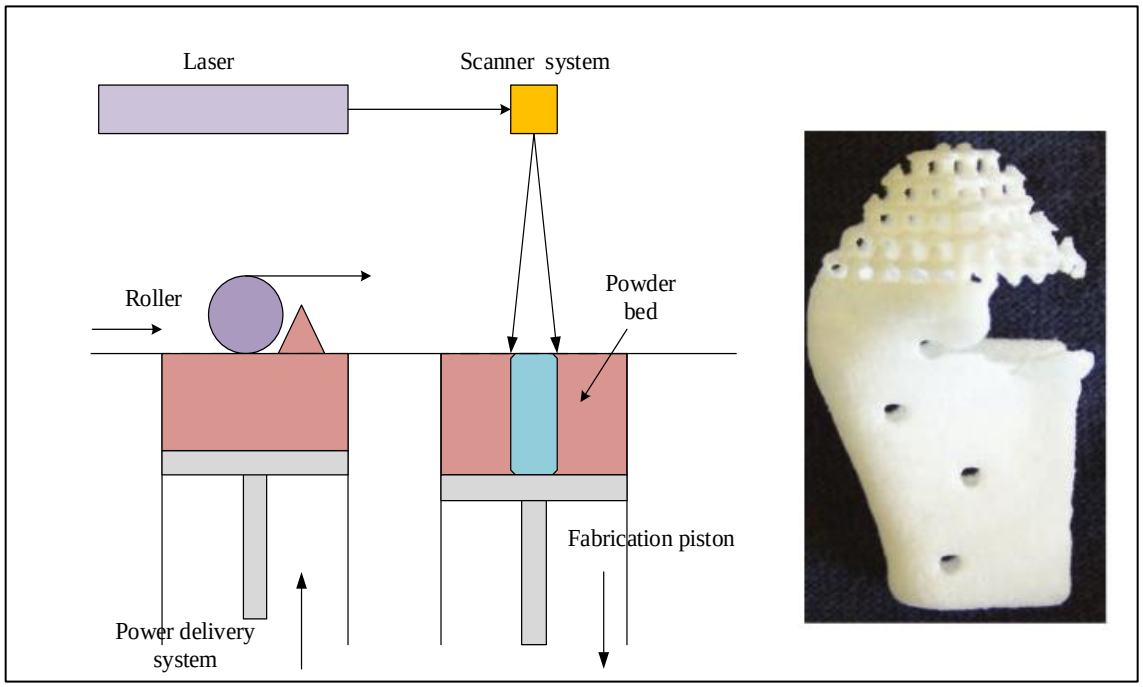

Figure 2 - 11 Illustration of SLS; INSET: a mandibular condyle PCL scaffold fabricated using SLS [62]

3) Extrusion based AM processes

Extrusion based AM processes involve the melt extrusion of a chosen material through a nozzle in a layered fashion, guided by the computer model. Each layer of the 3D model consists of multiple parallel strands of the material deposited in a desired pattern. This section describes extrusion based techniques in detail as it is pertinent to this research. In general, extrusion based techniques can fall into one of the following three systems [68]:

1) Conventional Roller feed system or Fused deposition modeling (FDM)
2) Compressed air extrusion system (e.g. 3D-Bioplotting)
3) Screw-extrusion system

FDM based system (Figure 2 - 12) uses a heated, computer-controlled nozzle to extrude raw material which is in the form of filaments. The material is deposited as semi-molten strands onto a movable platform (in the z-axis) [18]. Chim *et al.* [69] fabricated PCL and PCL-HA

scaffolds using FDM to fabricate porous implants for bone TE. Scaffold fabricated using FDM have shown controlled pore sizes, porosity and total pore interconnectivity [18].

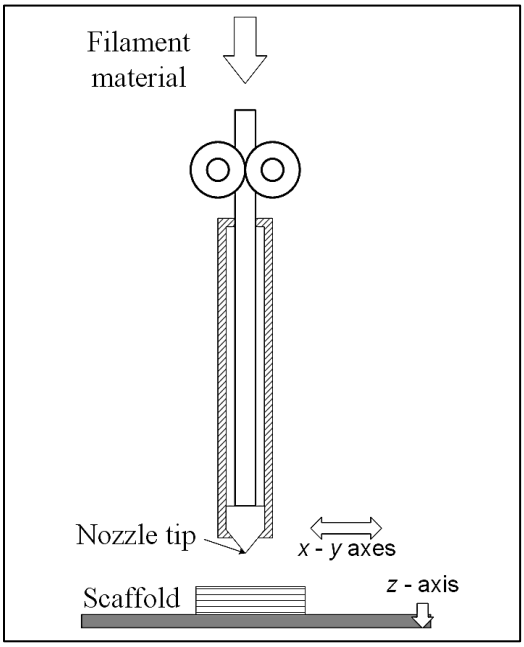

Figure 2 - 12 Process setup for Fused Deposition Modeling (FDM) [70]

Compressed air extrusion system such as 3D-Bioplotting (Figure 2 - 13) is used to print a range of materials using the principle of melt extrusion. This technique uses pneumatic pressure to extrude the molten material onto a platform through a nozzle of a desired diameter [71]. 3D-Bioplotting is also capable of handling support structures and printing into a plotting media of comparable viscosity. This technique supports the use of polymer, hydrogels and cell suspensions as raw materials [72].

Screw-extrusion based system (Figure 2 - 14) consists of a robotic arm which controls the movement of a barrel. The barrel is integrated with a heater that melts the material in it which is extruded using a screw-feed to generate pressure [68]. Precision extrusion deposition (PED) and BioExtruder are examples of this type of systems [73] [70].

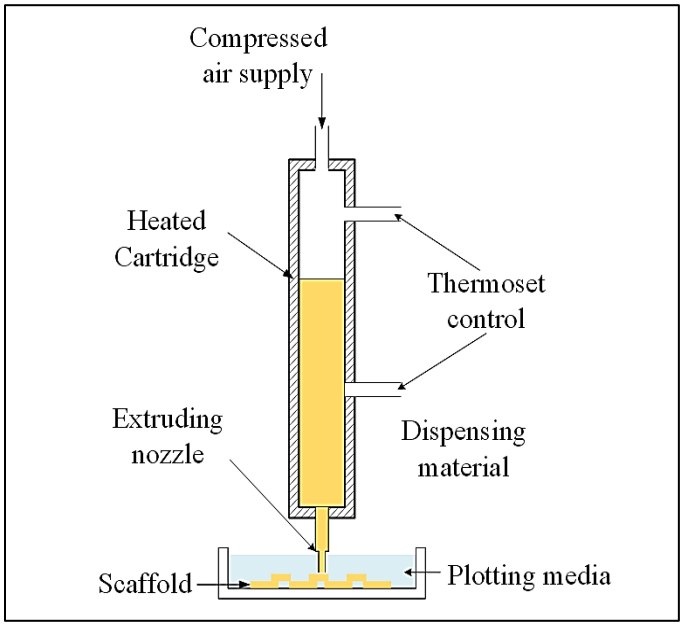

Figure 2 - 13 3D-Bioplotting setup [71]

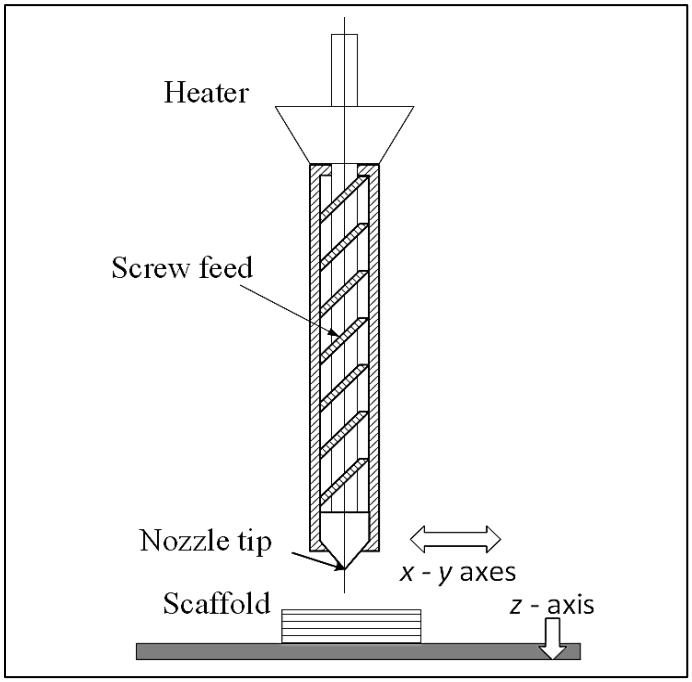

Figure 2 - 14 Screw-extrusion deposition system

These systems are considered tedious to be maintained because without proper cleaning of the rotational screw there can be contamination of the extruding material. The advantage is the thorough mixing of the polymer with no trapped air bubbles [74]. Table 2 - 6 presents a summary of different AM processes discussed in this section along with their advantages, disadvantages and different areas of application.

Table 2 - 6 Summary of AM processes [20] [25]

AM process	Resolution (µm)	Strength	Weakness	Application
SLA	366	Control over external and internal morphology	Multiple steps involved	Heart valve reconstruction, bone TE, Orthopaedics
		Easy to remove support materials	Limited by photo-polymerizable and biodegradable materials	
		Easy to achieve small features		
SLS	500	No support structure needed	Materials must be in powder form	Mandibular condyle, bone TE
		Enhanced range of materials	High temperature	
		Higher strength of parts	Trapped materials hard to remove	
FDM	250	Good Mechanical strength	High temperature	Bone TE, craniofacial , auricular cartilage, spinal reconstruction
		Versatile lay-down patterns	Need filament type material	
3D-Bioplotting	250	Enhanced range of materials	Low mechanical strength, slow processing	Bone & cartilage engineering, dental
		Can incorporate biomolecules	Calibration needed for new material	

2.5.3 Process characterization studies of extrusion based AM processes

A review of recent literature shows that FDM and 3D-Bioplotting are commonly used extrusion based AM techniques [22]. Research efforts related to process characterization and modeling of extrusion based AM techniques is presented in this section. Mechanical properties, porosity achieved and surface roughness are some of the parameters that have been studied for different types of extrusion based processes [75] [76] [77] [68] [78].

Mechanical properties of scaffolds fabricated using these processes have been given a considerable amount of attention. Lee et al [75] printed scaffolds on a 3D-Bioplotter™ using PCL and measured compressive modulus and cellular response. They demonstrated that 3D printed scaffolds are 20 to 50 times stronger compared to a salt leached scaffold (Figure 2 - 15). They attempted to enhance the elastic modulus and yield strength of the PCL strand by using an oscillating nozzle system. Their results indicate that the elastic modulus of the strand increased with the oscillating amplitude, but the oscillating frequency of the nozzle was found to have no significant effect on the elastic modulus of the PCL strand.

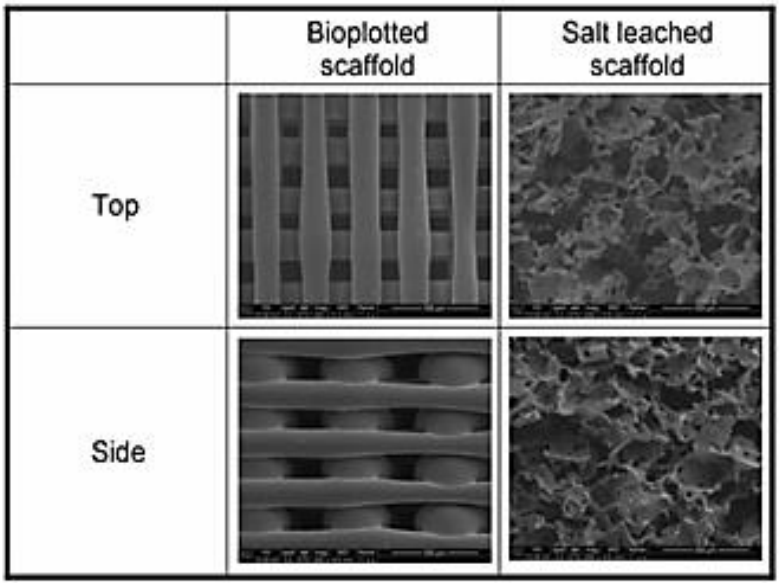

Figure 2 - 15 SEM images comparing a salt leached scaffold with a 3D printed scaffold [**75]**

Sood *et al.* [76] also studied the mechanical properties of structures fabricated using FDM. They considered layer thickness, orientation, raster angle, raster width and raster gap to parametrically model tensile, flexural and impact strength using response surface methodology. *Layer thickness* is defined as the height of the layer deposited by the nozzle; *orientation* is the angle between successive layers deposited in the XY plane; *raster angle* is the direction of deposition; *raster width* being the strand thickness and *raster gap* is the distance between successive parallel strands (shown in Figure 2 - 16). The results show a significant interaction between parameters showing that FDM is a complex process to model with respect to strength.

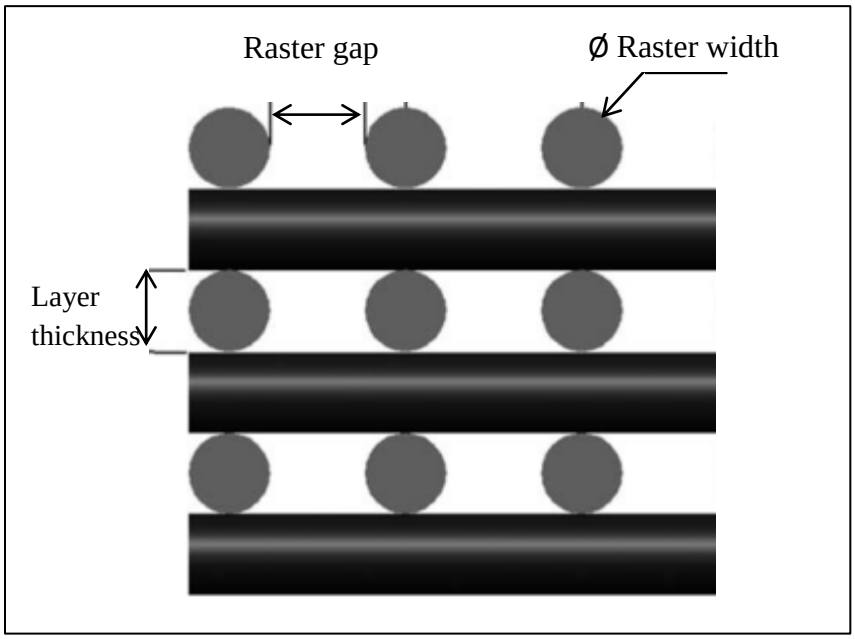

Figure 2 - 16 Cross section of a 3D printed structure with 0_90 orientation [70]

Scaffold porosity was studied in scaffolds with a honeycomb inner structure pattern and porosity ranging from 48 - 77% fabricated using FDM [77]. The compressive stiffness of these scaffolds ranged from 4MPa to 77MPa showing a direct correlation between porosity and mechanical properties under compression. Ang and Leong [79] also used a DOE

approach to determine significant parameters affecting the porosity and mechanical properties of scaffolds printed using FDM. They found that air gap and raster width greatly influenced the scaffold properties. They observed that the relationship between mechanical properties and porosity was logarithmic.

Hutmacher and Schantz [80] used FDM to print PCL scaffolds (Figure 2 - 17) with a porosity of 61± 1% and tested biocompatibility with fibroblasts and osteoblasts. The mechanical testing of these scaffolds showed a compressive stiffness of 41.9±3.5 MPa and yield strength of 3.1±0.1 MPa. They found that this process was highly reproducible and that cells were able to proliferate, showing the correlation between porosity and cell seeding as well. Gibson *et al.* [68] fabricated PLLA-TCP scaffolds with 80% porosity for bone TE intended for medium load bearing application using a screw extrusion based system. The mechanical testing under compression showed a maximum stress of 3.06 MPa. Their results also showed increased osteopontin synthesis in the 3D composite scaffolds compared to the 2-D tissue culture polystyrene.

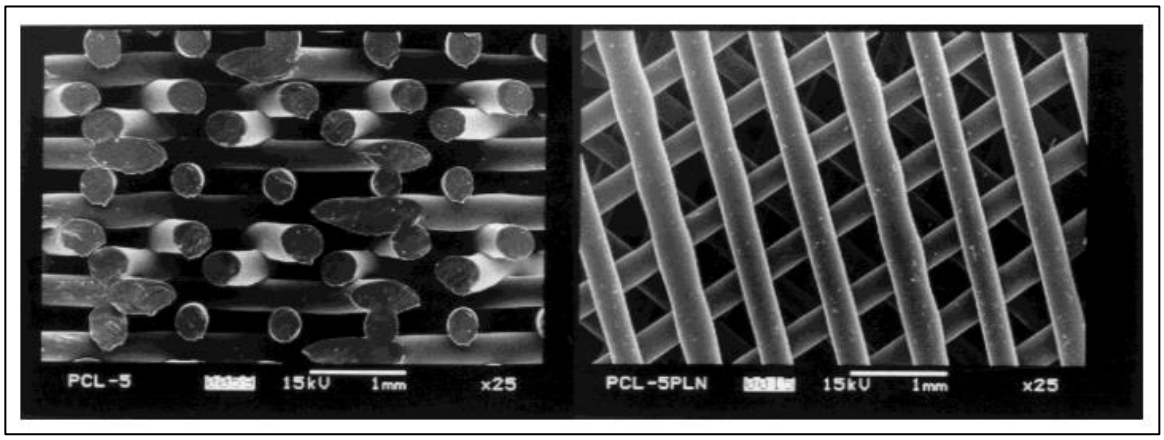

Figure 2 - 17 Side view (L) and top view (R) of PCL scaffolds fabricated using FDM [80] [81]

Anitha et al [78] studied the surface roughness of scaffolds fabricated using FDM. The effect of process variables on the surface roughness of scaffolds was investigated using a statistical

design of experiments. They found that the layer thickness greatly affects the surface roughness employing a statistical DOE approach.

Federovich *et al.* used 3D Bioplotting to print bone grafts with two different cell populations in hydrogel suspensions. They demonstrated that cells survive the process and are viable to differentiate post extrusion [58]. In another study, MSCs and endothelial cells were used to print bone grafts and promote vascularization in them. They also tested these grafts *in vivo* by implanting them in mice which resulted in the formation of bone tissue [59]. A summary of significant findings is included in Table 2 - 7.

Table 2 - 7 Summary of process characterization studies in extrusion based AM

Process	Significant finding	Reference
3D-Bioplotting	Scaffolds fabricated by 3D-Bioplotting are 20 to 50 times stronger compared to a salt leached scaffold	[75]
	Using an oscillating nozzle increased elastic modulus of the extruded strands with increasing amplitude; the oscillating frequency of the nozzle was found to have no significant effect on the elastic modulus	[75]
FDM	Scaffold layer thickness, orientation, raster angle, raster width and raster gap was used to parametrically model tensile, flexural and impact strength showing significant interaction and high complexity as a process with respect to strength.	[76]
	Scaffolds with porosity ranging from 48 - 77% exhibited a compressive stiffness ranging from 4MPa to 77MPa showing a direct correlation between porosity and mechanical properties.	[77]
	Air gap and raster width greatly influence the scaffold properties.	[79]
	Mechanical properties and porosity show a logarithmic relation	[79]
	Layer thickness greatly affects the surface roughness	[78]
	PLLA-TCP scaffolds with 80% porosity for bone TE showed a maximum stress of 3.06 MPa. 3D composite scaffolds showed increased osteopontin synthesis compared to the 2-D culture.	[68]

A review of the literature revealed a gap in studies with respect to process characterization using a 3D-Bioplotter™, which this thesis aims to cover. The rheological properties of the material along with the process parameters influences the scaffold output in extrusion based processes which are reviewed in the following section.

2.5.4 Rheology in extrusion

In all extrusion based processes, material rheology has been found to be critical in defining the characteristics of the scaffold generated [28]. The main drawback of these processes is their high sensitivity to the material viscosity at the nozzle tip [74]. Since these techniques have been shown to produce reliable and repeatable results with good cell attachment [74], establishing a rheological profile of the material melt used can be an essential step to modeling the process. This can be challenging with the use of most polymers and hydrogels as they are non-Newtonian fluids [26]. Hence research efforts which include rheological characterization of materials for extrusion based processes are a focus in this section. The relationship between processing parameters and material viscosity during extrusion based scaffold fabrication has been studied and reported by various researchers [5] [26] [82].

Liang et al [28] proposed a modified viscosity model during extrusion by studying melt viscosity in steady shear flow for four polymers. They verified the consistency of their model with static measurements made using a capillary Rheometer. The empirical relationship derived in this paper for the melt shear viscosity uses a referent shear rate which is the smallest shear rate affecting apparent viscosity.

Jiang et al [82] used a mini-deposition system to fabricate PCL and PCL/HA scaffolds with a porosity of 54.6%. They characterized the scaffolds based on flow behavior, mechanical properties and wettability. An investigation of the flow properties of the polymer melts showed that the viscosity of the polymer increased with the inclusion of HA (Figure 2 - 18). They also found that the compressive modulus increased from 26.5 MPa to 49.8 MPa and the water uptake ratio increased from 8 to 39% with the inclusion of HA.

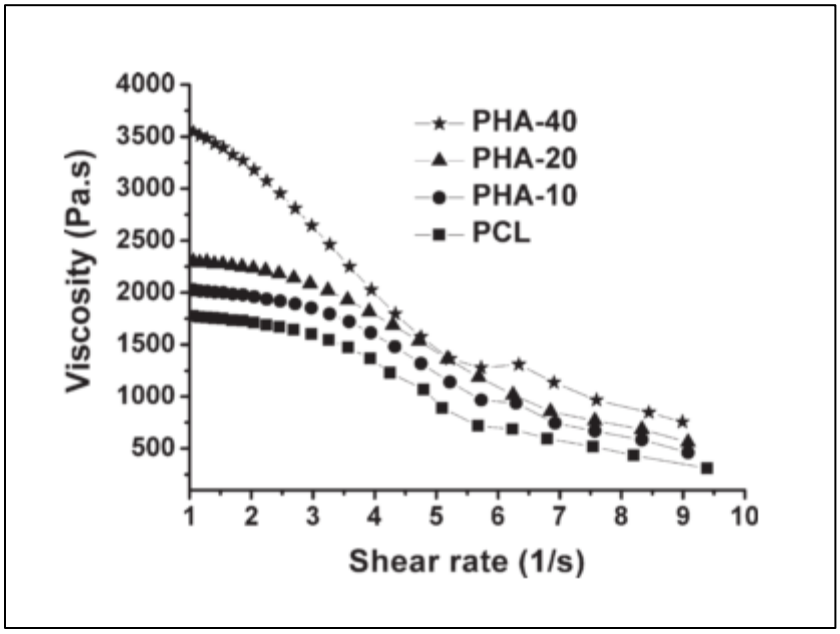

Figure 2 - 18 Viscosity versus shear rate for PCL and PCL/HA blends with varying proportions of HA (10%, 20% and 40%) at 120°C which exhibits shear-thinning [82]

Extrusion based processes have also been studied using mathematical and simulation models [26] [83]. Ke and Chen [26] studied the influence of fluid flow behavior on scaffold porosity in fluid dispensing RP techniques through a simulation model. Some of the important findings from this paper are highlighted as follows:

1) Higher driving pressures, low viscosity materials and a wider nozzle radius result in lower porosity for a given feed rate.
2) The flow rate and porosity do not vary linearly with driving pressure and nozzle radius and is primarily dependent on the surface tension of the biomaterial used.
3) There is a critical value of flow index (*K*) beyond which there is a reduced effect of the material viscosity on the process.

Ramnath et al [83] studied the effect of rheological properties of PCL during FDM using Finite Element Analysis (FEA). They modeled the melt flow behavior of a polymer along with a velocity profile using the power law for Non-Newtonian fluid. Their analysis

demonstrated that the melt flow behavior is affected by the nozzle diameter, nozzle angle and pressure gradient. The velocity profiles showed smooth flow along the melt channel (Figure 2 - 19). They developed a graphical user interface to determine melt flow behavior of other biomaterials. The results from the rheological analysis (using Equation 2- 4) indicated that PCL exhibits shear thinning or pseudo-plastic behavior with a power law index of 0.42.

$$\eta = K\dot{\gamma}^{n-1} \qquad \text{Equation 2- 4}$$

where,

K = consistency index

n = power law index.

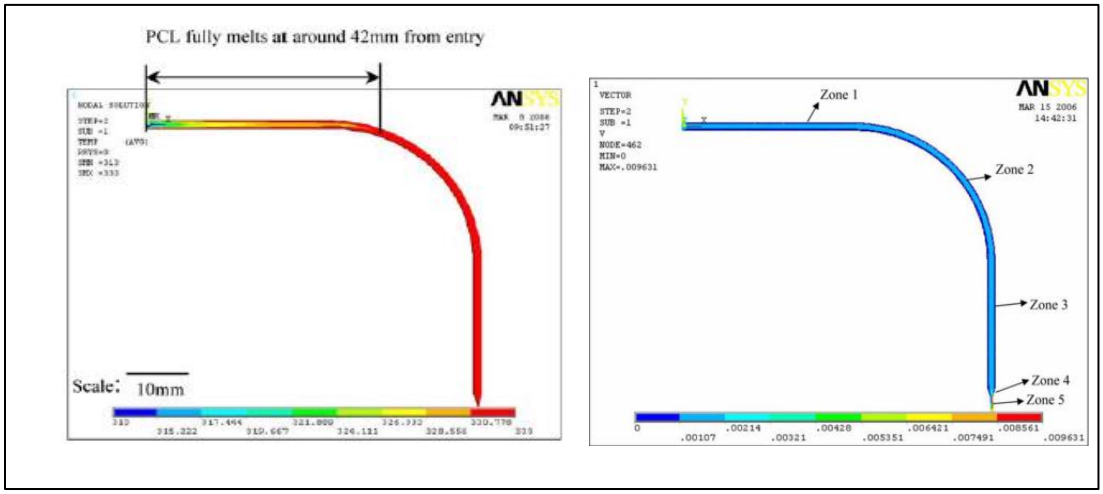

Figure 2 - 19 Temperature distribution plot (L) and velocity profile(R) for PCL obtained by finite element analysis during FDM [83]

Rheological properties of polymers have also been independently investigated to assess their processability. Ramkumar and Bhattacharya [84] characterized thermal and rheological properties of biodegradable aliphatic polyesters – PLA, PCL and polyhydroxybutyrate-co-hydromerate (PHBV) as most processing techniques employ these materials in a molten

state. PCL is shown to exhibit shear thinning and shows reduced toughness at lower viscosities. Their analysis also showed that the molecular weight of PCL greatly affected its viscosity.

2.6 Chapter Summary

This chapter includes a description of the basic design requirements of TE scaffolds, which are essentially porous, biodegradable matrices of mechanical strength comparable to the host or native tissue. Scaffold architecture influences the subsequent step of cell seeding and cell proliferation within a scaffold. The material and the fabrication technique used also determine the clinical success of scaffolds. Different scaffold materials (polymers, ceramics or composites) can be selected based on the scaffold requirements. These requirements are diverse and vary with cell/tissue being engineered, age and gender of the host. Scaffold fabrication techniques mainly fall into two categories – non-deterministic and AM processes based on the degree of control they offer on scaffold fabrication. Non-deterministic techniques produce scaffolds with a random pore distribution and do not offer control over internal geometry. AM techniques use CAD models to build 3D scaffolds in layers, offering control over the pore distribution as well as the inner structure of the scaffolds. These techniques include SLA, SLS and extrusion based techniques like FDM and 3D-Bioplotting. Extrusion based techniques have been found to be sensitive to material viscosity at the nozzle tip. A review of literature of these techniques indicates their potential application to the field of TE. This review also reveals a gap in literature with respect to process characterization using 3D-Bioplotting which this thesis aims to fill.

CHAPTER 3: SCAFFOLD FABRICATION

This chapter discusses the evaluation of the process of scaffold fabrication on a 3D-Bioplotter™. The material used and experimental approach employed in this study is described in Section 3.2 and 3.3 respectively. The detailed results and their inferences are presented in Section 3.4.

3.1 Introduction

This chapter addresses specific aims 1 and 2 defined in Section 1.4 of Chapter 1. The first objective is addressed by means of screening experiments designed to determine a feasible range of processing parameters on a 3D-Bioplotter™ for PCL of two different MWs. The second set of experiments, corresponding to specific aim 2, is designed to further investigate scaffold fabrication using one of the MWs of PCL. This consists of a DOE to examine the effect of 3D-Bioplotting process parameters on scaffold geometry and strength.

3.2 Materials

PCL with two different molecular weights (MW) were used in this study: 43 - 50kDa (Tone Polymers, Union Carbide [85]) and 15kDa (Sigma - Aldrich, [86]). The properties of these two types of PCL as specified by the manufacturers are summarized in Table 3 - 1.

Table 3 - 1 Properties of PCL

Name	PCL 767	PCL 15
Supplier	Union Carbide	Sigma - Aldrich
Molecular weight	43 to 50 kDa	15 kDa
Melting point	60°C	55°C
Density	1.145 g/cc	1.145 g/cc
Physical form	Pellets (Ø 3mm)	Flakes

A feasible range of process parameters was determined for both types of PCL. Scaffold fabrication and characterization studies were then performed using PCL 767 since it has been more widely used in literature.

3.3 Experimental methodology

3.3.1 3D-Bioplotting

A 3D-Bioplotter™ (Envisiontec, Germany) (Figure 3 - 1) was used to fabricate the PCL scaffolds in this study. This technique involves the pneumatic extrusion of molten material to form 3D structures [87]. The final structure is fabricated by deposition of molten strands in a layered fashion. An STL file serves as an input to generate the outer form of these structures. The inner structure can be defined by the user. The working mechanism of the 3D-Bioplotter™ and its process parameters are discussed below.

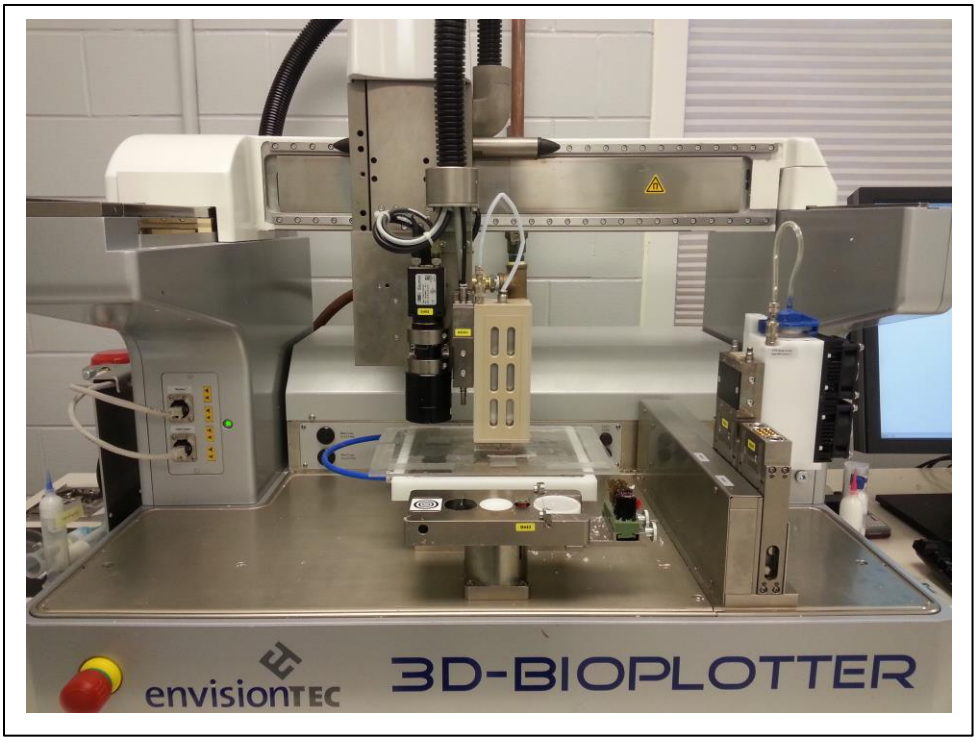

Figure 3 - 1 3D-Bioplotter™ from Envisontec [87]

The 3D-Bioplotter™ consists of two dispensing head frames - low and high temperature (integrated with thermal controls), each of which houses a cartridge. The material in this cartridge is extruded using compressed air. The tool path is generated by the machine by using coordinates imported directly from the STL file. This study uses the high temperature dispensing head with a glass plate fixed on the platform as a base.

The high temperature head includes a 10 mL stainless steel cartridge (Figure 3 - 2) which is filled with the chosen material (PCL) and fitted with a luer-lock nozzle (Figure 3 - 2). The nozzle diameter is selected based on the material flow properties. The whole cartridge mount is then placed in the dispensing head before an operation is run. The primary processing parameters for a certain nozzle diameter are – extrusion temperature, extrusion pressure and dispensing speed (or feed rate). All these parameters are set by the user.

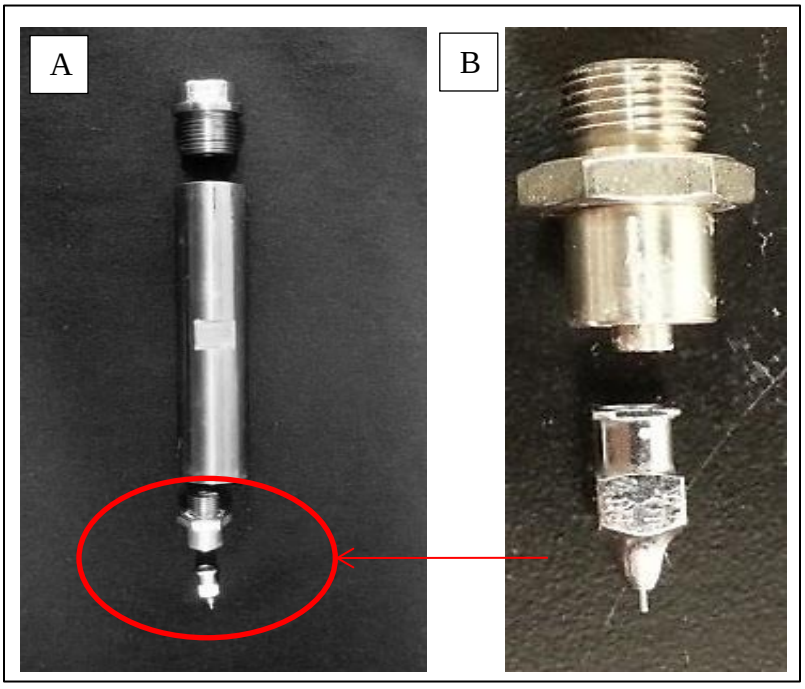

Figure 3 - 2 Stainless steel high temperature cartridge with the nozzle attachment used in this experiment

The extrusion temperature is the temperature of the cartridge in the dispensing head. The pressure required to extrude the material through the nozzle is referred to as the extrusion pressure. The dispensing speed is the movement of the high temperature head (or dispensing head) in the working (X-Y) plane. The extrusion pressure and dispensing speed can be controlled dynamically during the operation of the machine. The internal diameter of the nozzle is referred to as the nozzle diameter. The procedure for fabricating scaffolds on a 3D-Bioplotter™ (Figure 3 - 3) is briefly summarized in the following three steps:

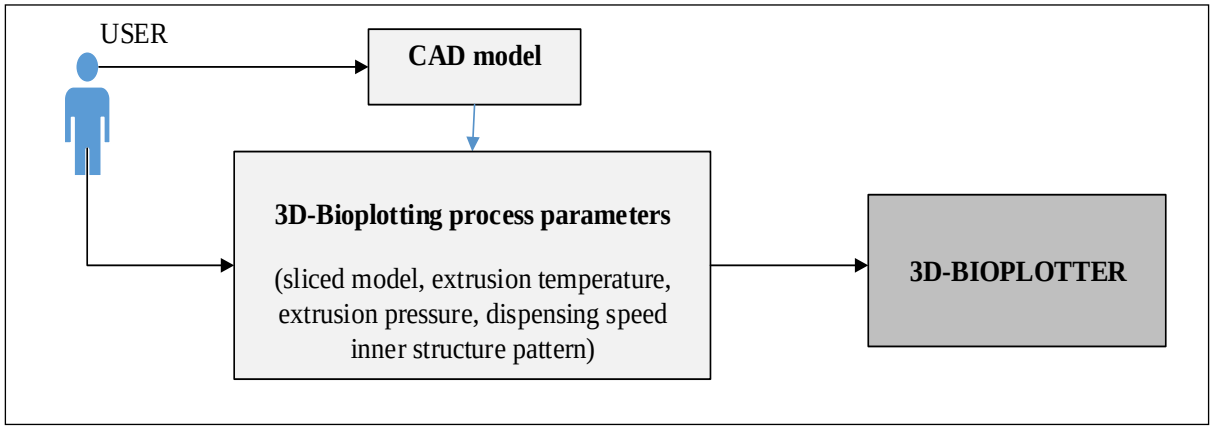

Figure 3 - 3 Steps for fabricating structures using a 3D-Bioplotter™

1. **Sliced model generation:** An STL file of a 3D model generated using *SolidWorks* is divided into layers by importing it into *3D-Bioplotter* slicing software (Figure 3 - 4). The height of the model is divided into a multiple layers upwards. The layer height selected for the sliced model is 80% of the nozzle diameter [87].

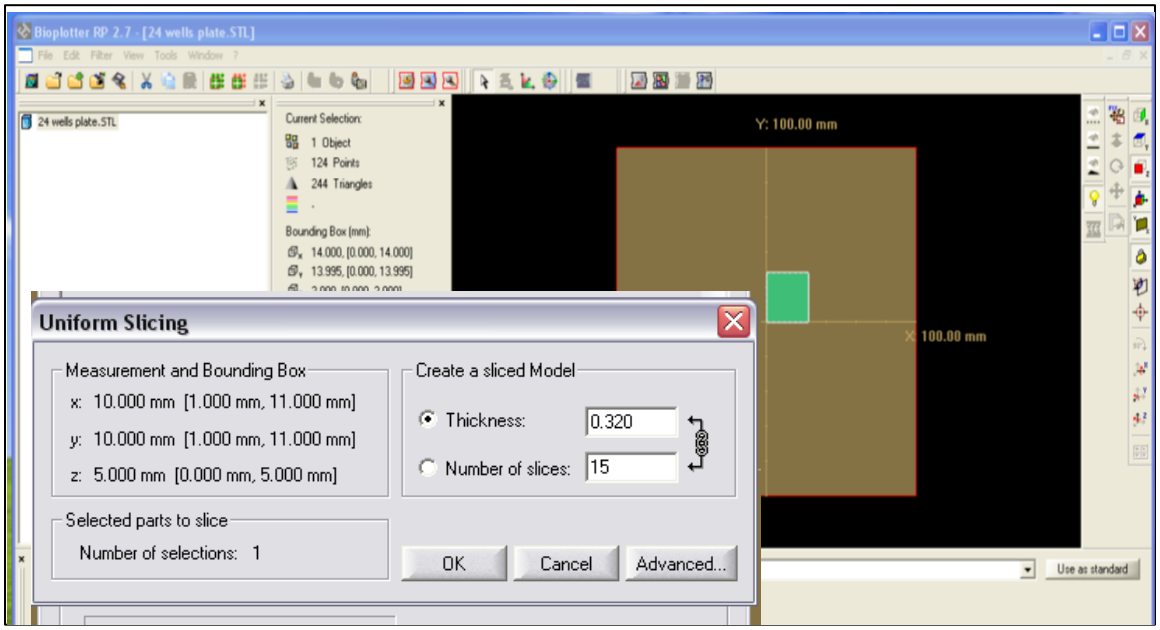

Figure 3 - 4 Snapshot of the software that slices the model into desired layer height

2. **Material specific parameter selection:** The sliced model is imported in '*VisualMachines'* software and are built according to specific processing parameters entered in the '*MaterialEditor'* tab (Figure 3 - 5). These parameters can be saved as default values for a given material.

3. **Inner structure pattern:** The angular orientation of every second layer of a model being built can be specified. The strands in a particular layer are always deposited parallel to each other. This is referred to as the inner structure pattern which is defined by the user (*Inner Structure Pattern Editor).* The following values need to be specified by the user to define this pattern:

   (i) Distance between strands: The distance between adjacent strands in the XY plane in a single layer

   (ii) Angle: The orientation of adjacent layers with respect to the X-plane (1° to 179.9°).

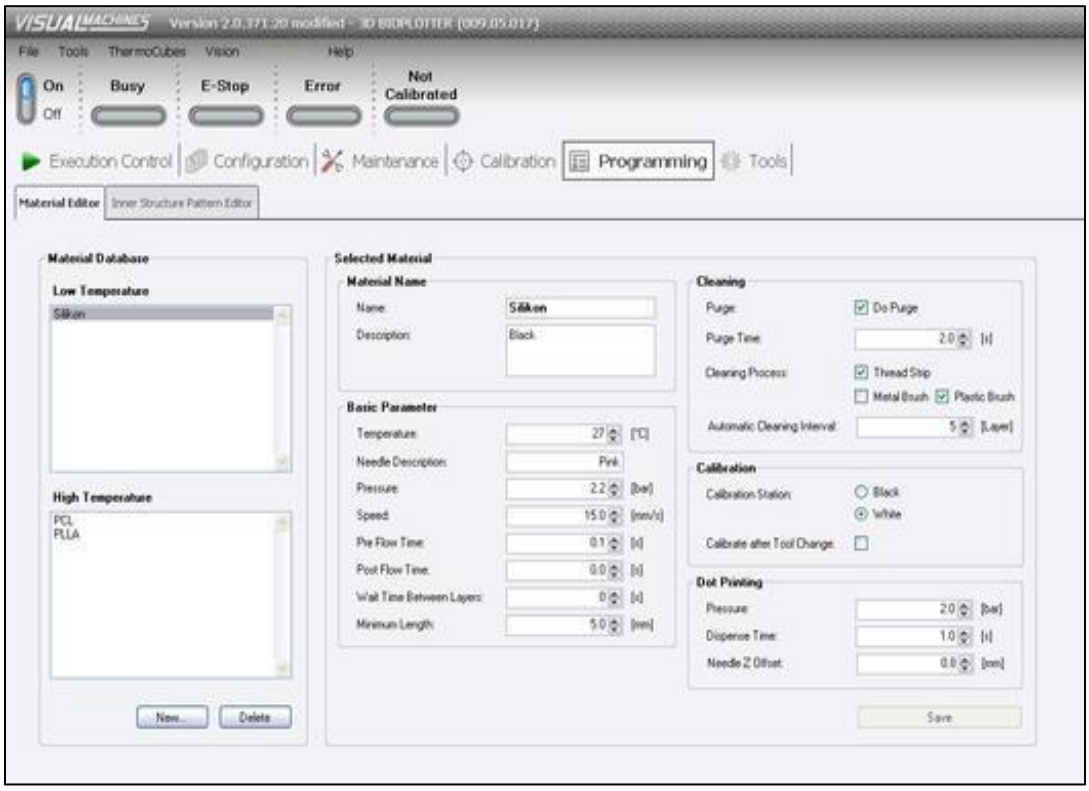

Figure 3 - 5 *MaterialEditor* in the *VisualMachines* software

3.3.2 Parameter Screening and selection

A set of screening experiments were carried out to determine a feasible range of process parameters for 3D-Bioplotting using PCL 767. The factors that influence the process of 3D-Bioplotting were analyzed using a fishbone diagram (Figure 3 - 6).

An initial extrusion temperature of 70°C was selected since extrusion temperatures are required to be higher than the material melting point [74] and PCL has a melting point of 60°C [80]. This was incremented in steps of 10, up to 100°C. The upper temperature limit was restricted to 100°C to avoid thermal degradation of the PCL. Extrusion of PCL was tested for nozzle diameters 0.2 mm, 0.3 mm and 0.4 mm.

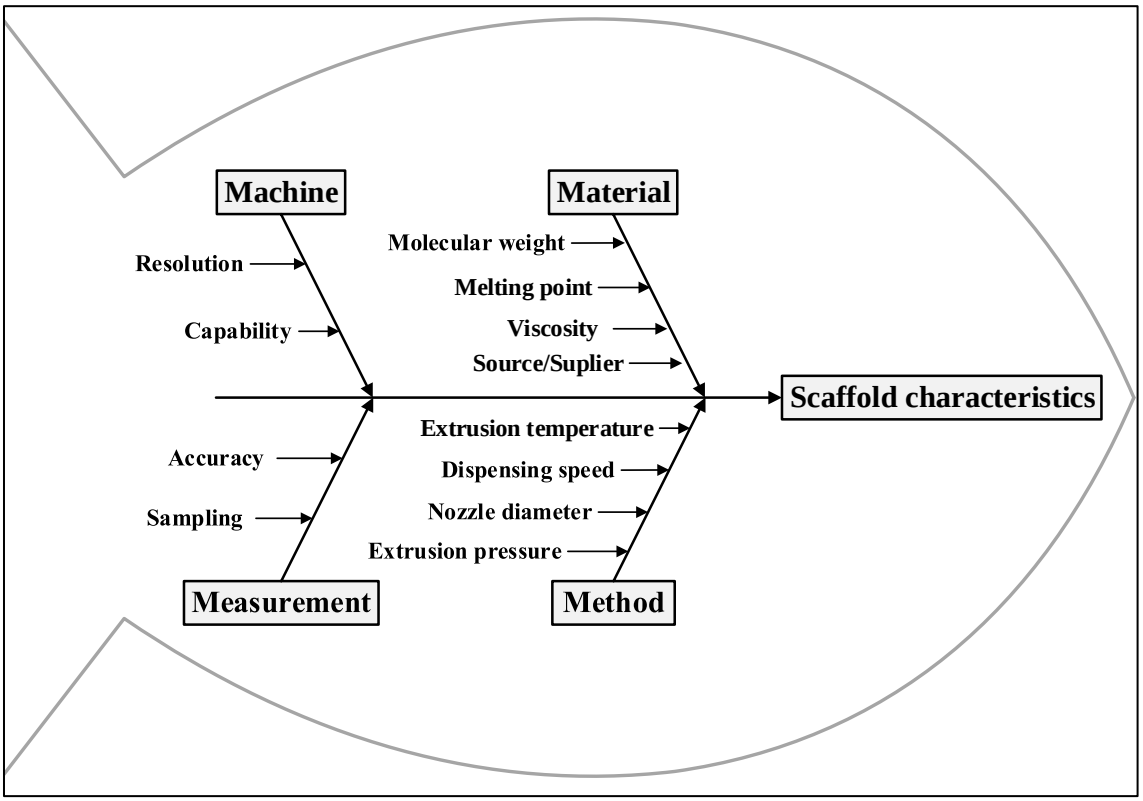

Figure 3 - 6 Fishbone diagram of the factors affecting scaffold characteristics

For each extrusion temperature - nozzle diameter combination, the extrusion pressure and dispensing speed were determined using the dynamic control setting. The different levels of each parameter tested in this study are summarized in Table 3 - 2.

Table 3 - 2 Parameter screening levels to determine feasible 3D-Bioplotting parameters for PCL

Parameter	Levels
Extrusion temperature (C)	70, 80, 90, 100
Nozzle diameter (mm)	0.2, 0.3, 0.4
Pressure range (bar)	5 to 3.5 (steps of 0.1)
Dispensing speed (mm/s)	1 to 1.5 (steps of 0.1)

The effect of extrusion temperature and nozzle diameter on scaffold fabrication was further investigated in this thesis. A working extrusion pressure and dispensing speed was determined at each temperature – nozzle diameter combination. These two values were then kept constant in the process characterization study explained in the next section.

3.3.3 Scaffold design and fabrication

PCL 767 was used to fabricate scaffolds on the 3D-Bioplotter™ using the feasible range of parameters determined previously. These scaffolds were designed to fit a 24-well culture plate. The total height was limited to 2 mm. This is the recommended height in cell culture experiments to ensure diffusion of nutrients [88]. The model was drafted using the modelling software *SolidWorks*® and then sliced using the layer creation software. The sliced model and design specifications are summarized in Table 3 - 3.

Table 3 - 3 Design specifications of the porous scaffolds

Scaffold property		Specification
Scaffold diameter (mm)		14
Scaffold height (mm)		2
Orientation (degrees)		0°_90°
Distance between strands (mm)	0.3mm nozzle	1
	0.4mm nozzle	1.75
Number of layers	0.3mm nozzle	7
	0.4mm nozzle	5
Wait time between layers (s)		3

The high temperature cartridge was filled with 4 g of PCL pellets and allowed to stand in the dispensing head for 30 minutes at each temperature level before the fabrication process was run. The wait time between layers is a pause between layers to allow solidification of the

polymer melt before the next layer is printed. Scaffold strand width, strand separation distance and compression strength were measured in this study. Scaffold porosity and swell ratio which are functions of scaffold strand width was also calculated. The measurement of these scaffold features are described in the next section.

3.3.4 Scaffold Metrology:

The scaffolds fabricated in this study were measured using a KH-7700 HIROX digital microscope with 70x magnification [89].

1) Strand width and strand separation

The measurements were made from the topmost layer of each scaffold (Figure 3 - 7).

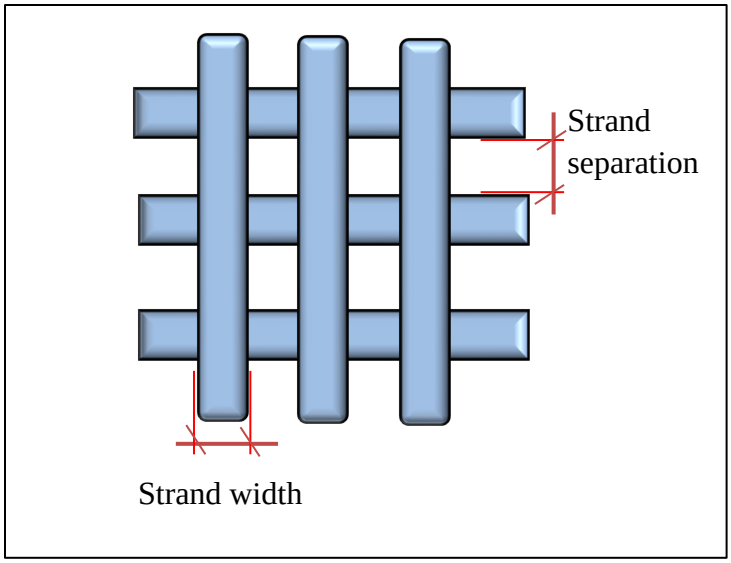

Figure 3 - 7 Scaffold measurements made using digital microscopy

2) Scaffold porosity:

The porosity of the scaffolds was calculated using two methods listed below:

a) Relative density method: (Equation 3 – 1 and Equation 3 – 2)

$$V_P = V_T - (m_s/\rho) \quad \text{Equation 3- 1}$$

$$Porosity = (V_P/ V_T)*100 \quad \text{Equation 3- 2}$$

where,

V_P = volume of pores

V_T = total scaffold volume

m_s = the mass of the scaffold (measured using a weighing scale)

ρ = is the density of the PCL (ρ = 1.145).

V_T is calculated using the scaffold dimensions and material density for a non-porous solid scaffold. Scaffold pore volume V_P is then calculated using Equation 3 – 1 and expressed as a percent using Equation 3 - 2.

b) Using scaffold metrology: which consists of the following steps:

- Calculate rectangular area (A_1) of strand width (*SW*) per layer (Equation 3 – 3). The total chord length (*length*) was calculated according to the scaffold design dimensions.

$$A_1 = SW * length \quad \text{Equation 3 - 3}$$

- Calculate volume occupied by the strands per layer by multiplying area with layer height.

$$V_1 = A_1 * Layer\ height \quad \text{Equation 3 – 5}$$

- Use these values to determine porosity which is a ratio of volume of empty space to total solid volume.

$$Porosity = (1 - V_1)/V_T * 100 \quad \text{Equation 3 - 6}$$

3) Swell ratio:

The swell ratio (Equation 3 – 6) is the ratio of the measured strand width to the ideal strand width (i.e. nozzle diameter) of the scaffold. This was estimated for the strand width measured at each experimental level.

$$Swell\ ratio = \frac{d_1}{d_2} \qquad \text{Equation 3 – 6}$$

where,

d_1 = measured strand width (mm)

d_2 = nozzle diameter (mm)

3.3.5 Statistical analysis

A statistical DOE was formulated using feasible levels of extrusion temperature and nozzle diameter. The DOE consisted of an (*m* x *n)* factorial design with *m* levels of extrusion temperature and *n* levels of nozzle diameter. The values of *m* and *n* were determined in the screening experiments. The response measured was the scaffold strand width. The effect of extrusion temperature and nozzle diameter on scaffold strand width was compared using ANOVA models. The computations and analysis were performed using statistical software JMP Pro (SAS, Cary, NC). An alpha level (α) of 0.05 was used for all statistical tests. The strand width and strand separation distance was measured for each scaffold by dividing it into four quadrants or zones (Figure 3 - 8).

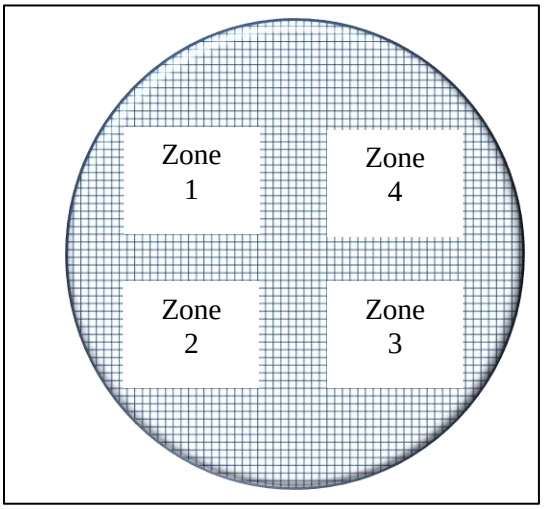

Figure 3 - 8 Strand width and strand separation distance measured in each zone of the scaffold

Three measurements of strand width and strand separation were sampled from each zone at random. The mean strand width and strand separation distances were calculated from the twelve measurements made across the scaffold. The strand width data was also fit to a least square regression model against extrusion temperature to develop a predictive model.

3.3.6 Compression Testing:

The scaffolds were tested in compression on an ATS 1605C universal tester (Figure 3 - 9). The specimens were compressed between steel plates at the rate of 0.002 mm/sec starting at zero load. Each sample was loaded till 50% deformation. The peak load at this point has been reported in the results. Five samples from each level were tested in compression. The compression modulus is the slope of the linear portion of the stress-strain curve obtained during compression.

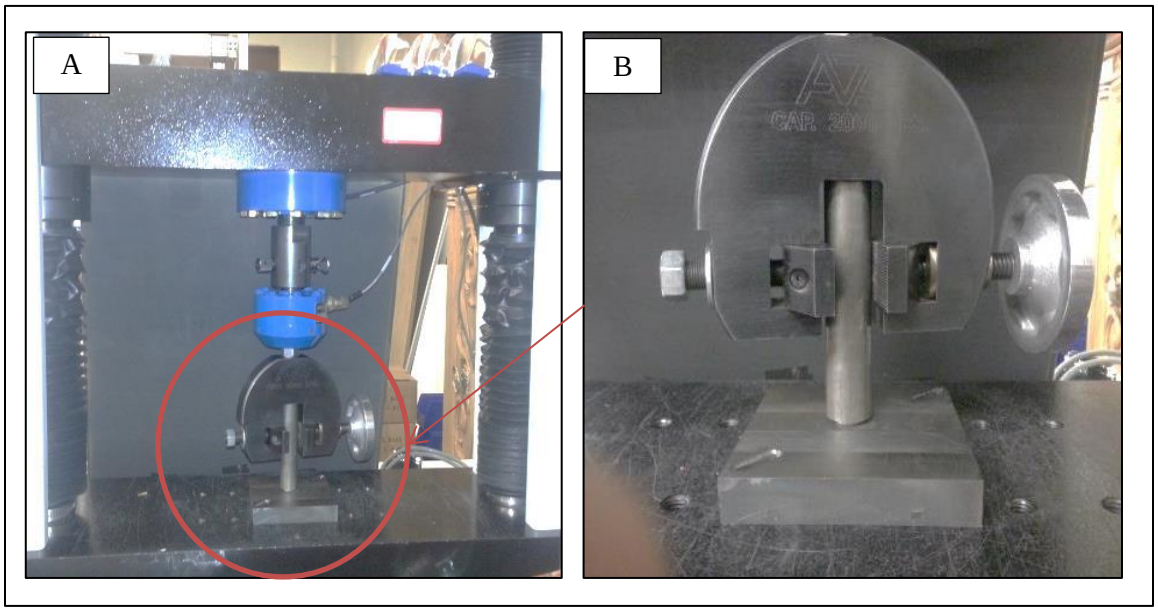

Figure 3 - 9 (A) Compression testing setup on the ATS 1605C; (B) closer view of the parallel plates setup

3.4 Results and Discussion

3.4.1 Parameter screening and selection

The results obtained are summarized below (Figure 3 - 10):

- Extrusion of PCL 767 strands using a nozzle diameter of 0.2 mm was infeasible for extrusion temperatures between 70°C to 100°C.
- PCL strands extruded at 70°C for nozzle diameters 0.3 mm and 0.4 mm were discontinuous and non-homogenous.
- Extrusion temperatures of 80°C, 90°C and 100°C for nozzle diameters 0.3 mm and 0.4 mm were found to be feasible, resulting in homogenous continuous strands.
- A minimum extrusion pressure of 3.5 bar with a maximum dispensing speed of 1.2 mm/s was found to be feasible for temperatures 80°C, 90°C and 100°C for PCL 767.
- PCL 15 could be extruded between 70°C to 100°C using a nozzle diameter of 0.2 mm, 0.3 mm and 0.4 mm with a pressure of 2.2 bar and a higher dispensing speed of 2 mm/ s.

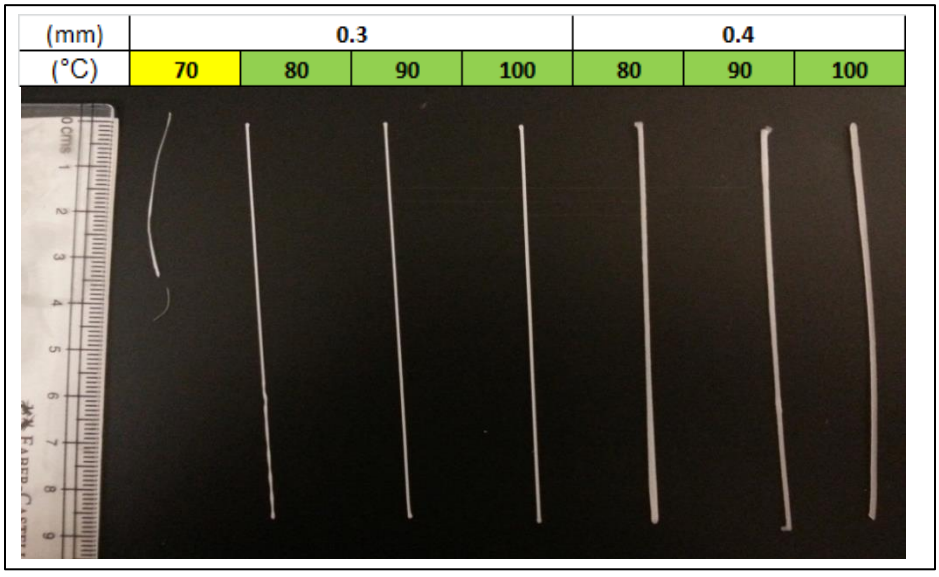

Figure 3 - 10 Continuous strands generated using the different extrusion temperature – nozzle diameter combinations for PCL 767

Table 3 - 4 presents a summary of the above mentioned results for all extrusion temperature-nozzle diameter combinations. Since PCL with a molecular weight of 43 – 50 kDa has been more widely used in literature, the feasible parameters determined for PCL 767 were further investigated (Table 3 - 5).

Table 3 - 4 Parameter screening and selection for 3D-Bioplotting with PCL

Extrusion temperature (°C)	PCL 767			PCL 15		
	Nozzle diameter (mm)			Nozzle diameter (mm)		
	0.2	0.3	0.4	0.2	0.3	0.4
70						
80						
90						
100						

→ Extrusion not possible

→ Extrusion possible; inconsistent strands

→ Feasible

Table 3 - 5 Feasible Bioplotting parameters for PCL 767

Input Parameters	PCL 767	PCL 15
Extrusion Temperature(°C) (*m*)	80, 90, 100	70, 80, 90, 100
Nozzle diameter (mm) (*n*)	0.3 , 0.4	0.2, 0.3, 0.4
Extrusion pressure (bar)	3.5	2.2
Feed (mm/s)	1.2	2

3.4.2 Scaffold fabrication using PCL 767

A sample of a single scaffold fabricated using every combination of extrusion temperature and nozzle diameter at constant dispensing speed and pressure is shown in Figure 3 - 11. The total time taken to fabricate a single scaffold including the wait time between layers was 17 minutes. The time taken to completely utilize a full cartridge containing 4 g of PCL was approximately 5 hours. Scaffolds fabricated using the 0.4 mm nozzle at an extrusion temperature of 100°C was excluded from this study. This was because the strand width of the scaffolds fabricated at this level exceeded 1.75 mm which was the selected distance between strands (Section 3.3.3). The strands merged together to form a non-porous structure (Figure 3 - 11). The total number of samples fabricated at each level (Table 3 - 6) served as replicates for each experimental level.

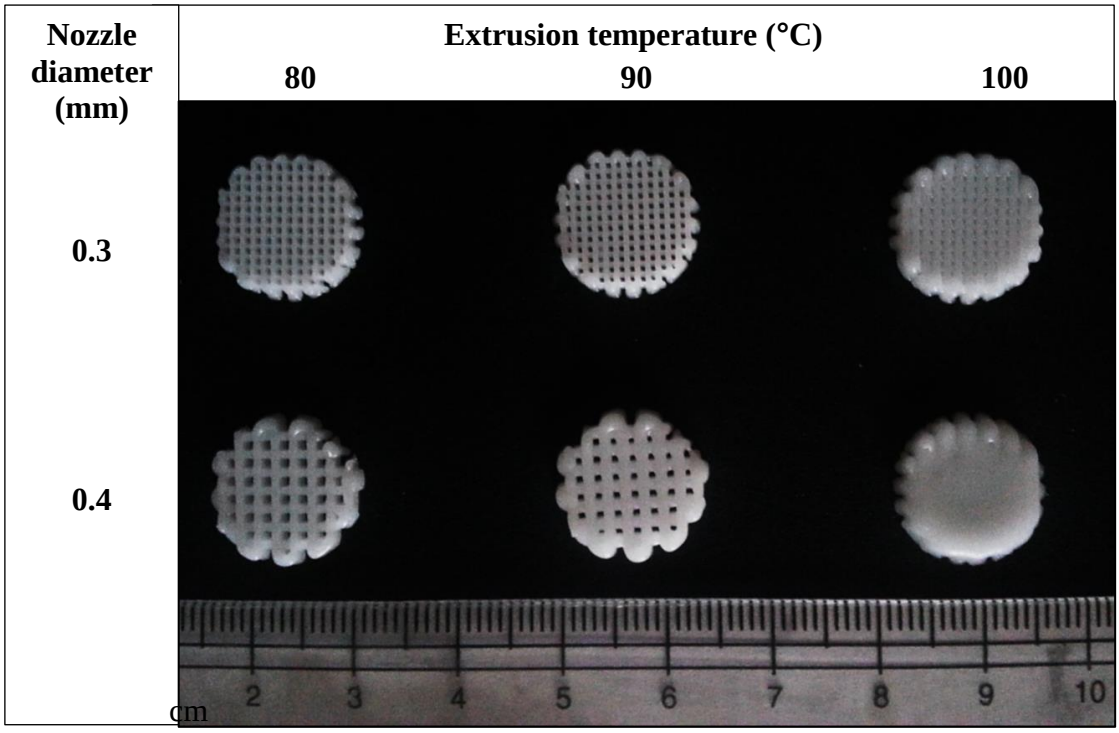

Figure 3 - 11 PCL scaffolds fabricated at different extrusion temperature – nozzle diameter combinations (one sample)

Table 3 - 6 Number of samples (replicates) fabricated at each experimental level

Nozzle diameter (mm)	Extrusion temperature (°C)	Number of scaffolds
0.3	80	20
	90	19
	100	13
0.4	80	12
	90	12

3.4.3 Scaffold metrology

Scaffolds fabricated for this study were measured using digital microscopy as detailed in Section 3.3.5 (Figure 3 - 12).

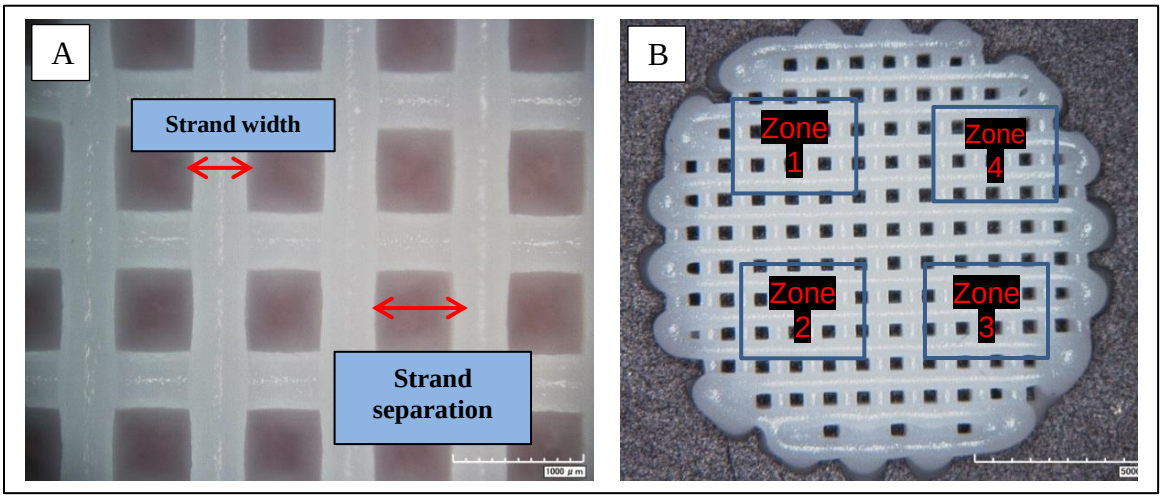

Figure 3 - 12 Scaffold metrology - Strand width and strand separation distance (A) measured in each zone (B)

Figure 3 - 13 shows a sample of microscopic images with a 70X magnification of scaffolds taken across the three extrusion temperatures for scaffolds fabricated using a nozzle diameter

of 0.3 mm. The twelve measurements made on each scaffolds were averaged and used in further analysis.

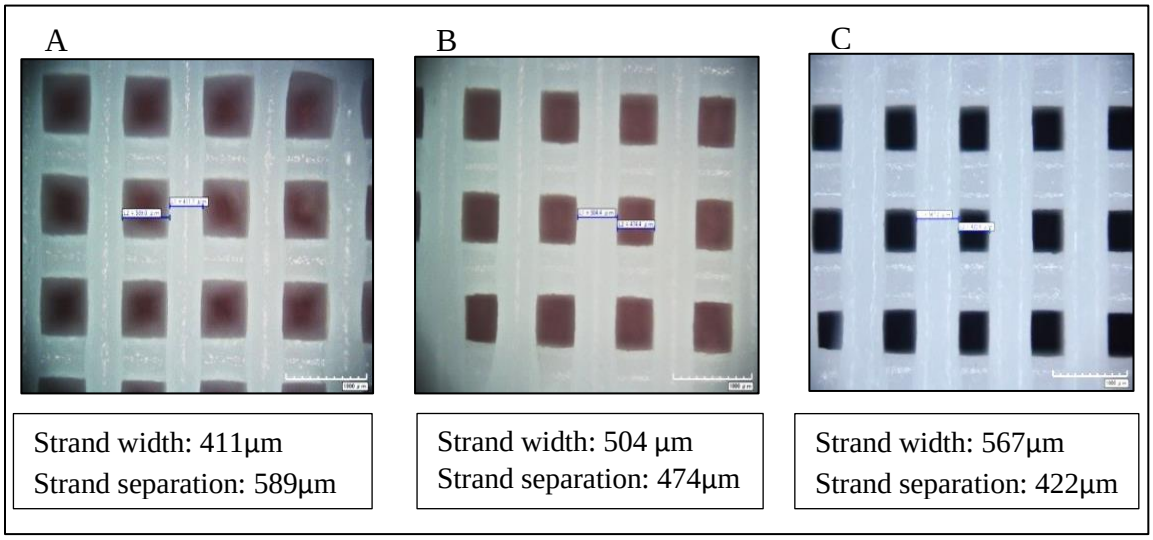

Figure 3 - 13 Microscope images – 70X Magnification; PCL 43-50kDa Nozzle ID 0.3mm; (A) to (C): Extrusion temperatures 80°C, 90°C, 100°C respectively; measurements made on these images are displayed below the image

3.4.4 Statistical analysis

1) Scaffold strand width (PCL 767)

A scatter plot (Figure 3 - 14) of the mean strand width against extrusion temperature using nozzle diameters of 0.3 mm and 0.4 mm for PCL 767 shows an increasing trend. The following analyses were performed with the data set:

- One way ANOVA to measure the effect of extrusion temperature on strand width for each nozzle diameter – 0.3 mm and 0.4 mm.
- Full factor ANOVA to measure the effect of extrusion temperatures – 80°C and 90°C and nozzle diameters – 0.3 mm and 0.4 mm and their interaction on the strand width.
- Regression model of scaffold strand width against extrusion temperature

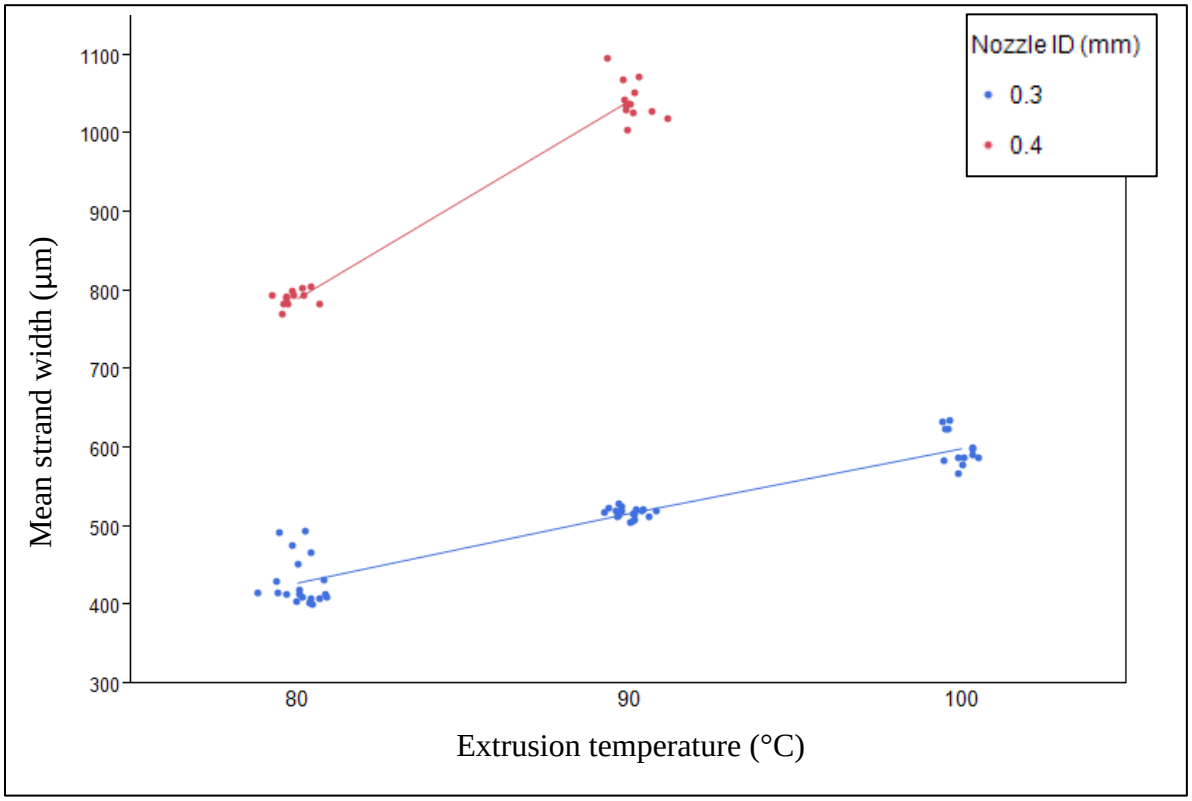

Figure 3 - 14 Scatter plot of mean strand width against extrusion temperature for nozzle diameters 0.3mm and 0.4mm showing an increasing trend

- Effect of extrusion temperature on scaffold strand width for each nozzle diameter

The strand width data was modeled using a one-way ANOVA model represented by Equation 3 – 3. The statistical design parameters are represented in Table 3 - 7. The response variable Y_{ij} (strand width) is represented as follows:

$$Y_{ij} = \mu + a_i + \varepsilon_{ij} \qquad \text{Equation 3 - 3}$$

i = 1, 2, 3 (0.3 mm nozzle)

i = 1, 2 (0.4 mm nozzle)

$$\varepsilon_{ij} \sim iid\ N(0, \sigma^2)$$

where,

μ = overall (grand) mean

α = main effect of extrusion temperature

Table 3 - 7 One-factor statistical design parameters

Factor	Level	Variable
Extrusion temperature (°C)	80	α_1
	90	α_2
	100	α_3

The *p*-value of the one-way ANOVA tests the null hypothesis that the mean strand width at different levels of extrusion temperatures is equal. The null hypothesis is represented by:

H_0: $\mu_{80} = \mu_{90} = \mu_{100}$

where,

μ_{80} = Mean strand width at extrusion temperature of 80°C

μ_{90} = Mean strand width at extrusion temperature of 90°C

μ_{100} = Mean strand width at extrusion temperature of 100°C (omitted for 0.4mm nozzle)

ANOVA results indicate that extrusion temperature has statistically significant ($p < 0.0001$) effect on the mean strand widths of PCL scaffolds fabricated using a nozzle diameter of 0.3 mm (Table 3 - 8) and 0.4 mm (Table 3 - 9). These results were further examined by computing the mean and standard deviations (SD) of scaffold strand width with a 95% confidence interval (Table 3 - 10).

Table 3 - 8 ANOVA results for strand width data using a nozzle diameter of 0.3 mm

Source	DF	Sum of squares	Mean square	*F*-ratio	*p*-value
Extrusion temperature (°C)	2	235232.18	117616	244.02	<.0001*
Error	49	23617.07	482		
Total	51	258849.24			

Table 3 - 9 ANOVA results for strand width data using a nozzle diameter of 0.4 mm

Source	DF	Sum of squares	Mean square	*F*-ratio	*p*-value
Extrusion temperature (°C)	1	379835.80	379836	991.2785	<.0001*
Error	22	8429.91	383		
Total	23	388265.71			

The effect of different levels of extrusion temperature on scaffold strand width was compared using a Tukey's HSD test. This test indicated that the strand width is significantly differs between different extrusion temperatures for a nozzle diameter of 0.3 mm (Table 3 - 11) and 0.4 mm (Table 3 - 12). Experiment levels that are significantly different are represented by different letters. Figure 3 - 15 shows that the mean strand width at each extrusion temperature for different nozzle diameters.

Table 3 - 10 Mean and SD of strand width with a 95% CI for all experiment levels

Nozzle diameter (mm)	Level (°C)	Sample size	Mean (µm)	SD (µm)	Lower 95% (µm)	Upper 95% (µm)
0.3	80	20	428.81	30.04	414.76	442.88
	90	19	517.17	6.05	514.26	520.09
	100	13	599.62	21.99	586.33	612.92
0.4	80	12	790.76	9.91	784.50	797.10
	90	12	1042.37	25.84	1025.9	1058.8

Table 3 - 11 Tukey HSD output for strand width data; nozzle diameter: 0.3 mm

Level (°C)	Grouping			Mean strand width (µm)
100	A			599.62
90		B		517.17
80			C	428.81

Table 3 - 12 Tukey HSD output for strand width data; nozzle diameter: 0.4 mm

Level (°C)	Grouping		Mean strand width (µm)
90	A		1042.37
80		B	790.76

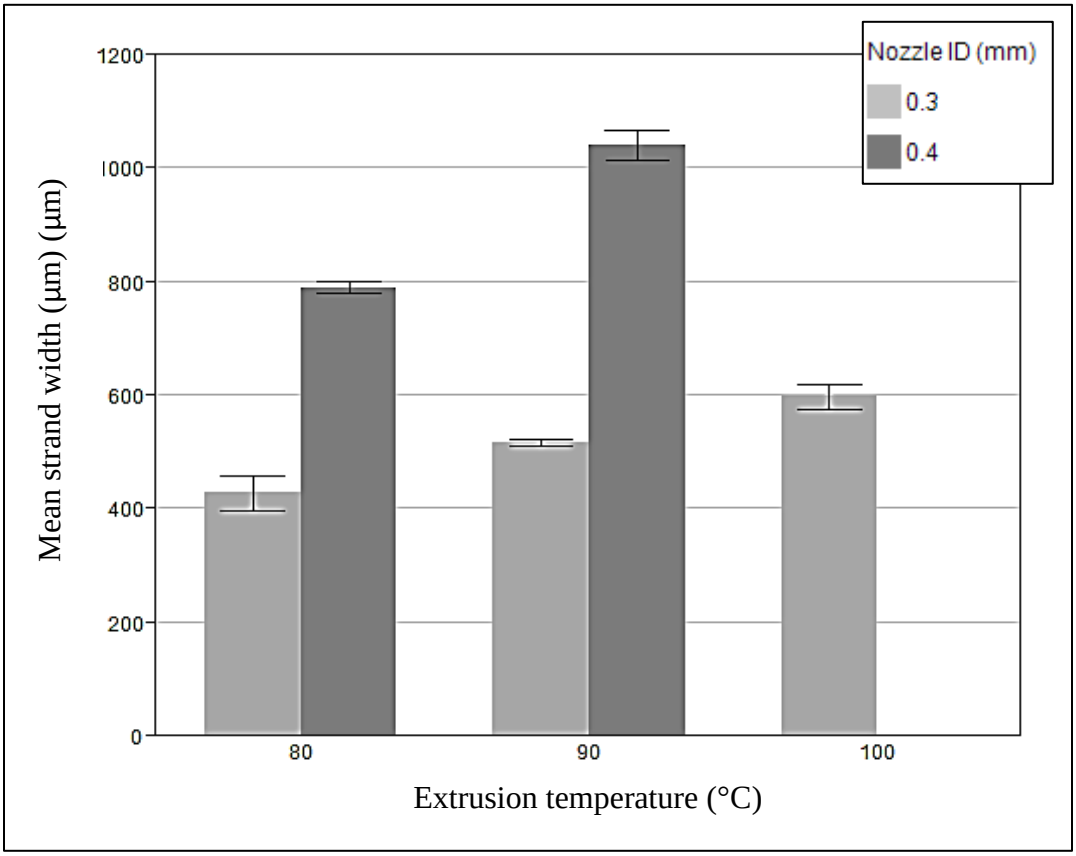

Figure 3 - 15 Bar graph of mean strand width at the three extrusion temperatures using a nozzle diameter of 0.3 mm and 0.4 mm; error bar showing one standard deviation

This set of experiments shows that an extrusion temperature of 90°C and a nozzle diameter of 0.3 mm generate PCL scaffolds with the least variance in strand width (Figure 3 - 34). For

an extrusion temperature of 90°C, scaffolds fabricated using a nozzle diameter of 0.3 mm was found to have a lower SD in strand width (6.05 µm) when compared to those fabricated with a nozzle diameter of 0.4 mm (25.84 µm). This indicates the possibility of a combined effect of extrusion temperature and nozzle diameter on the scaffold strand width.

- Full factor ANOVA

The effect of extrusion temperatures – 80°C and 90°C and nozzle diameters – 0.3 mm and 0.4 mm and the effect of an interaction between the two factors on scaffold strand width were studied using a full factor ANOVA. The model of this equation can be represented by Equation 3 – 2.

$$Y_{ijk} = \mu + \beta_1 x_1 + \beta_2 x_2 + \beta_3 x_1 x_2 + \varepsilon_i \qquad \text{Equation 3 - 2}$$

$$i = 1 \text{ to } n \text{ (sample size)}$$

$$\varepsilon_i \sim iid\ N(0, \sigma^2)$$

where,

μ = overall (grand) mean or intercept

β_1 = effect of extrusion temperature on strand width

β_2 = effect of nozzle diameter on strand width

β_3 = interaction term for effect of extrusion temperature and nozzle diameter on strand width

x_1= indicator variable for extrusion temperature = $\begin{cases} 1 \text{ if extrusion temperature} = 90°C \\ 0 \text{ otherwise } (80°C) \end{cases}$

x_2= indicator variable for nozzle diameter = $\begin{cases} 1 \text{ if nozzle diameter} = 0.4 \text{ mm} \\ 0 \text{ otherwise } (80°C) \end{cases}$

This test assumes that the strand width of the scaffolds printed with different temperatures and nozzle diameters are independent of the chosen spacing between the strands since the chosen spacing was higher for the 0.4mm nozzle. The ANOVA output along with the effects test for the parameters is shown in Table 3 - 13 and Table 3 - 14. The model shows that the effect of the interaction between extrusion temperature and nozzle diameter is statistically

significant (*p*-value < 0.0001). The plot (Figure 3 - 16) shows non-parallel lines which visually indicate an interaction. This implies that the effect of extrusion temperature on scaffold strand width is dependent on nozzle diameter and vice-versa.

Table 3 - 13 Full factor ANOVA output

Source	DF	Sum of squares	Mean square	*F*-ratio	*p*-value
Extrusion temperature (°C)	3	3394076.5	1131359	2543.8	<.0001*
Error	59	26239.4	445		
Total	62	3420315.9			

Table 3 - 14 Effects test

Source	DF	Sum of squares	*F*-ratio	*p*-value
Extrusion temperature (°C)	1	76071.29	171.0486	<.0001*
Nozzle diameter (mm)	1	982542.47	2209.276	<.0001*
Extrusion temperature (°C) * Nozzle diameter (mm)	1	98960.27	222.5151	<.0001*

In the presence of a significant interaction between the experimental factors, the main effects cannot be interpreted directly; hence we examine the simple effects. In this case, the interaction can be classified as a simple interaction since the effect of the individual factors on scaffold strand width is predictable. An analysis of the simple effects of nozzle diameter and extrusion temperature reveals a *p*-value of < 0.0001. This indicates that for a given level of nozzle diameter, extrusion temperature has a significant effect on the strand width and vice-versa.

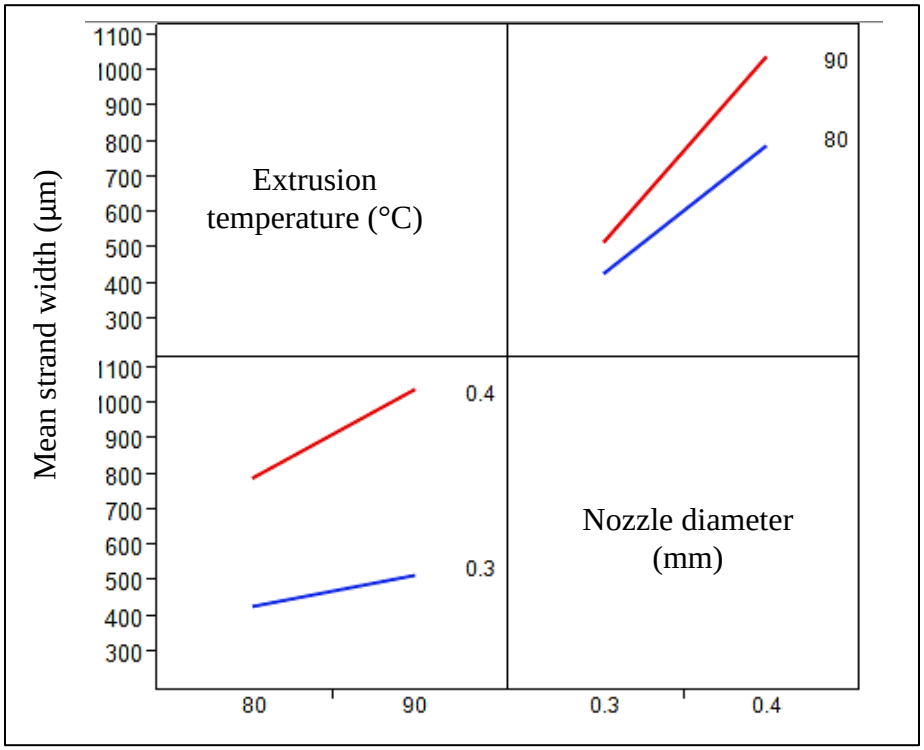

Figure 3 - 16 Interaction plots for mean strand width against nozzle diameter and temperature

- Regression model of strand width against extrusion temperature

In order to develop a predictive model for the strand width obtained, the data was fit to a least square regression. Two regression models were obtained by modeling the strand width data against extrusion temperature which are described as follows. In both cases, the standard assumptions of simple linear regression were verified.

1) Regression model for a nozzle diameter of 0.3 mm

The strand width data for scaffolds fabricated using a nozzle diameter of 0.3 mm was fit to a simple linear regression using extrusion temperature as the dependent variable. The prediction expression for strand width (y) is represented by Equation 3 – 3.

$$(y) = \beta_0 + \beta_1 * Extrusion\ temperature + \varepsilon_i \qquad \text{Equation 3 – 3}$$

where,

β_0 = intercept

β_1 = slope of the regression line

ε_i = error term

Table 3 - 15 Parameter estimates for regression of strand width against extrusion temperature (Nozzle diameter = 0.3 mm)

Term	Estimate	Std. error	*t*-ratio	*p*-value
Intercept (β_0)	-255.4451	34.2377	-7.46	<.0001*
Temperature (°C) (β_1)	8.5642	0.3846	22.26	<.0001*

Here the intercept is negative (= -255.445) which is equal to the strand width at zero extrusion temperature. This value loses its meaning in this context. The slope of the line (β_1) represents the increase in strand width per degree increase in extrusion temperature. This model is valid under the constant extrusion pressure and dispensing speed used in these experiments. The summary of fit (Table 3 - 16) and the regression plot (Figure 3 – 17) indicate that this model accounts for the variation in the data set since the *R-square* value is close to 1.

Table 3 - 16 Summary of fit for regression plot

Parameter	Value
R^2	0.9083
Adjusted R^2	0.9065
Root Mean Square Error	21.7809

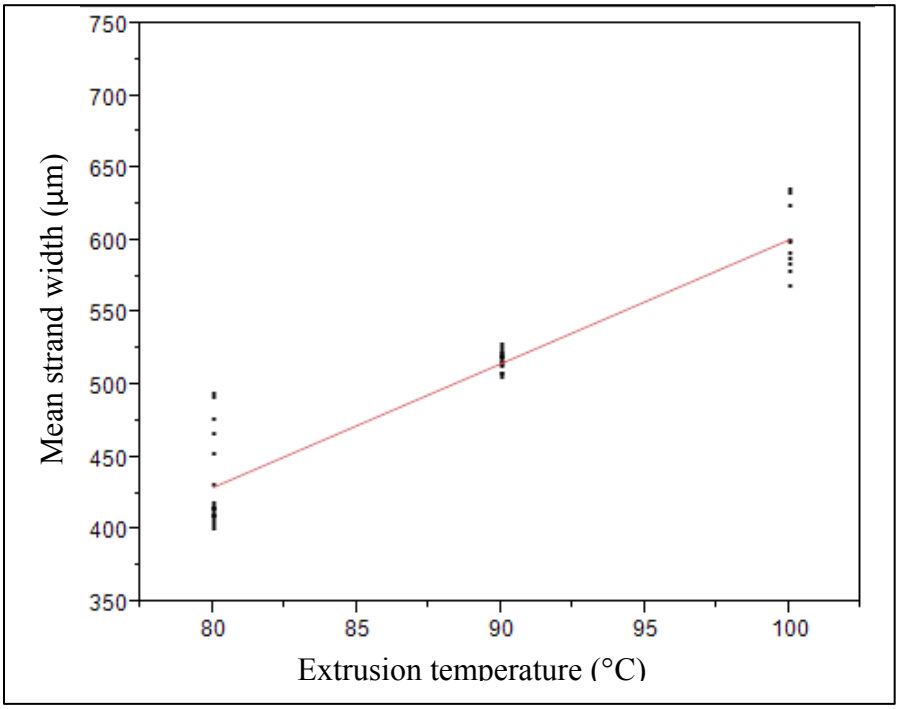

Figure 3 - 17 Regression plot for strand width against extrusion temperature for a nozzle dia 0.3 mm

The final regression expression for strand width against extrusion temperature at a constant extrusion pressure and dispensing speed can be represented by Equation 3 – 4.

$$(y) = -255.445 + 8.5642 \ * Extrusion\ temperature + \varepsilon_i \qquad \text{Equation 3 – 4}$$

2) Regression model of strand width against extrusion temperature and nozzle diameter

The strand width data of scaffolds fabricated using two levels of extrusion temperature and two levels of nozzle diameter was modeled using least square regression (Equation 3 – 4). The regression plot and the summary of fit for this model are represented in Figure 3 -18 and Table 3 – 17 respectively.

$$(y) = \beta_0 + \beta_1 x_1 + \beta_2 x_2 + \beta_3 (x_1 - 84.9206) x_2 + \varepsilon_i \qquad \text{Equation 3 – 5}$$

where,

β_0= intercept

β_1= parameter associated with extrusion temperature

x_1= extrusion temperature (C) ($80 \leq x_1 \leq 100$)

β_2 = parameter associated with nozzle diameter

x_2 = nozzle diameter = $\begin{cases} 1 \text{ if nozzle diameter} = 0.4 \text{ mm} \\ 0 \text{ otherwise } (= 0.3 \text{ mm}) \end{cases}$

This equation treats extrusion temperature as a continuous variable and nozzle diameter as a discrete variable. The parameter estimates (Table 3 - 17) obtained shows a significant interaction term between these two factors.

Table 3 - 17 Parameter estimates for the linear regression model for scaffold strand width

Term	Estimate	Std. Error	t Ratio	*p*-value
Intercept (β_0)	-278.0562	57.4389	-4.84	<.0001
Temperature (°C) (β_1)	8.8359	0.6756	13.08	<.0001
Nozzle diameter (mm)[0.4-0.3] (β_2)	442.2753	5.4717	80.83	<.0001
(Temperature (°C)-84.9206)* Nozzle diameter (mm)[0.4-0.3] (β_3)	16.3248	1.0944	14.92	<.0001

The summary of fit (Table 3 - 18) for the regression plot (Figure 3 - 18) gives a high value for R^2 indicating that this model is a good fit for the data set.

Table 3 - 18 Summary of fit for regression plot shown in Figure 3 - 18

Parameter	Value
R^2	0.9923
Adjusted R^2	0.9919
Root Mean Square Error	21.78091

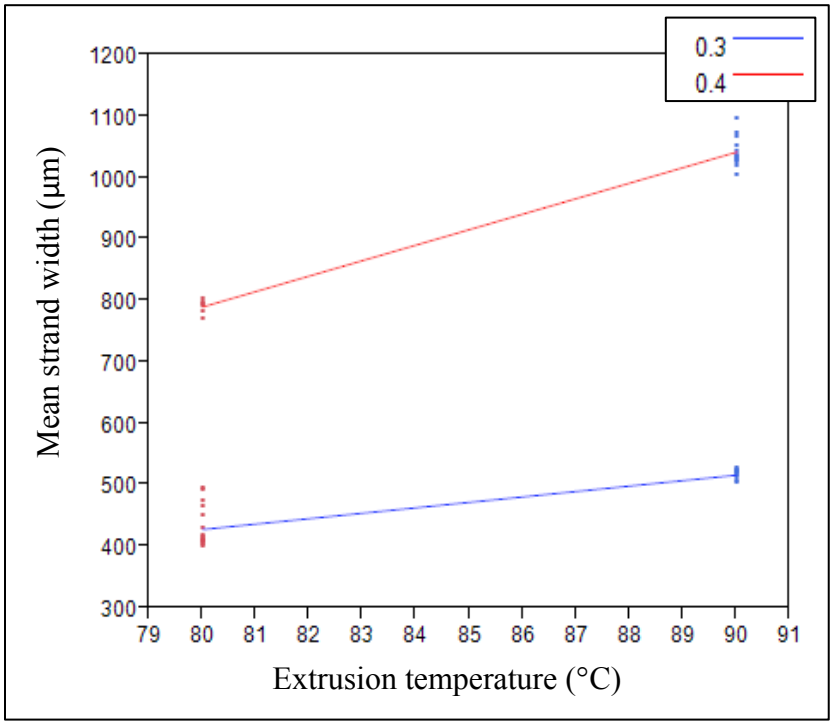

Figure 3 - 18 Regression plot for strand width against extrusion temperature for scaffolds fabricated using nozzle diameters – 0.3 mm and 0.4 mm

The best fitting line for the model for strand width predicts a positive relationship between strand width and extrusion temperature for a given nozzle diameter. The prediction expression for the strand width based on the estimates obtained can be represented by Equation 3 – 6.

$$(y) = \mu + 8.8359x_1 + 442.2753x_2 + 16.3248(x_1 - 84.9206)x_2 + \varepsilon_i \qquad \text{Equation 3 - 6}$$

3) Scaffold porosity

A scatterplot of the porosity (Figure 3 - 19) calculated using both methods show a similar trend of decreasing porosity with increase in extrusion temperature. It can be seen that an

increase in strand width would cause a decrease in porosity for given scaffold geometry, nozzle diameter at a constant extrusion pressure and dispensing speed. Strand width analysis showed significant differences for different extrusion temperatures and nozzle diameters and the interaction of these two factors (p-value < 0.0001). This can be extended to scaffold porosity as well since they are directly related. This was further examined by tabulating the mean and SD with a 95% CI for both methods (Table 3 - 19 and Table 3 - 20). Overall, the porosity of the scaffolds shows a decreasing trend with increasing an extrusion temperature.

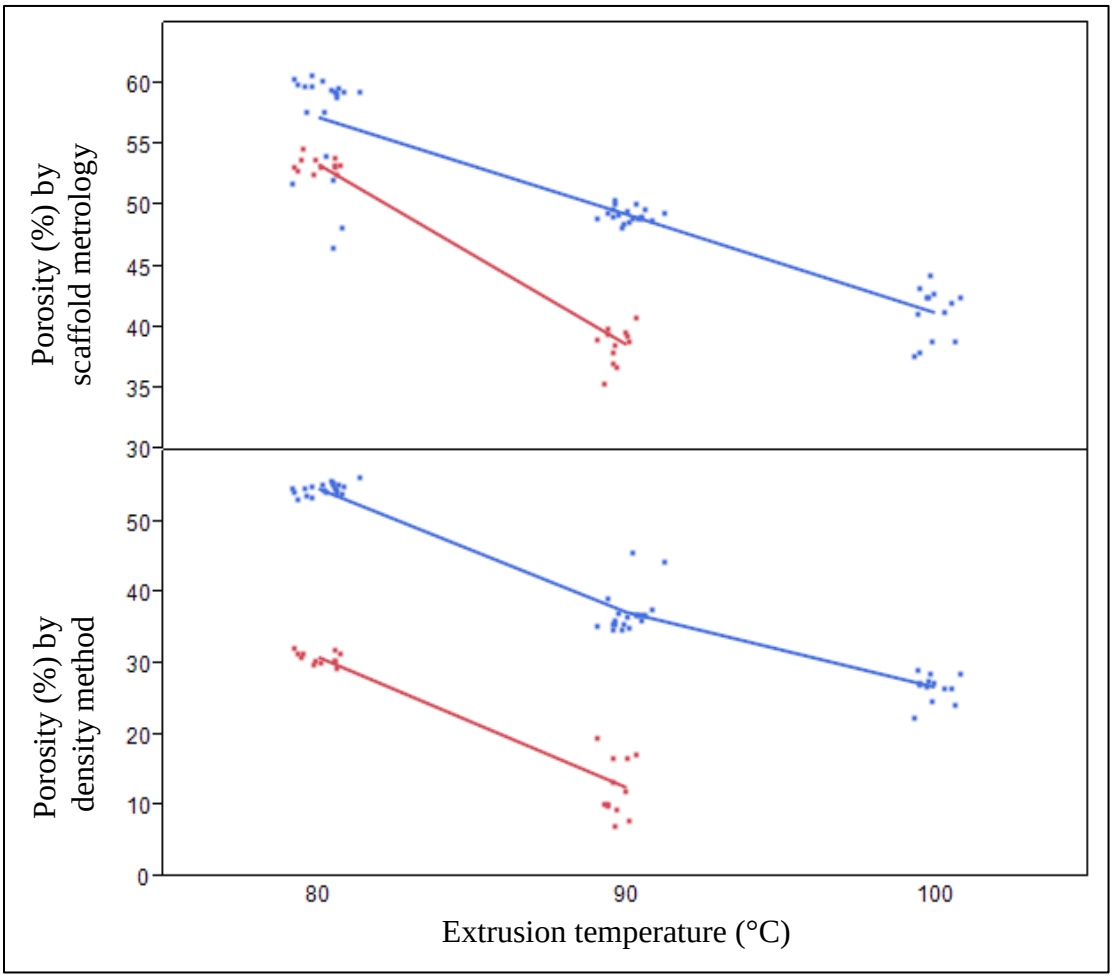

Figure 3 - 19 Scatterplot of scaffold porosity against extrusion temperature for nozzle diameters 0.3 mm and 0.4 mm

Table 3 - 19 Mean and SD of scaffold porosity (%) using relative densities

Nozzle diameter (mm)	Level (°C)	Sample size	Mean (%)	SD (%)	Lower 95% CI	Upper 95% CI
0.3	80	20	54.7	0.78	54.37	55.11
	90	19	37.3	2.96	35.88	38.74
	100	13	26.7	1.90	25.61	27.92
0.4	80	12	30.9	0.86	30.44	31.54
	90	12	12.6	4.06	10.04	15.28

Table 3 - 20 Mean and SD of scaffold porosity (%) using scaffold metrology data

Nozzle diameter (mm)	Level (°C)	Sample size	Mean (%)	SD (%)	Lower 95% CI	Upper 95% CI
0.3	80	20	57.2	4.25	55.30	59.29
	90	19	49.3	0.59	49.03	49.60
	100	13	41.2	2.15	39.94	42.54
0.4	80	12	53.4	0.58	53.05	53.80
	90	12	38.6	1.52	37.64	39.57

The mean porosities obtained for both methods are summarized in Table 3 - 21 and in bar graph (Figure 3 - 20). The porosity values for the two nozzle diameters cannot be compared since the strand separation distances chosen in the scaffold design were different. However, there was a difference observed in the porosity results obtained using the two methods.

Table 3 - 21 Comparison of mean scaffold porosity calculated using both methods

Nozzle diameter (mm)	Level (°C)	Sample size	Relative density		Scaffold metrology	
			Mean porosity (%)	SD (%)	Mean porosity (%)	SD (%)
0.3	80	20	54.7	0.78	57.2	4.25
	90	19	37.3	2.96	49.3	0.59
	100	13	26.7	1.90	41.2	2.15
0.4	80	12	30.9	0.86	53.4	0.58
	90	12	12.6	4.06	38.6	1.52

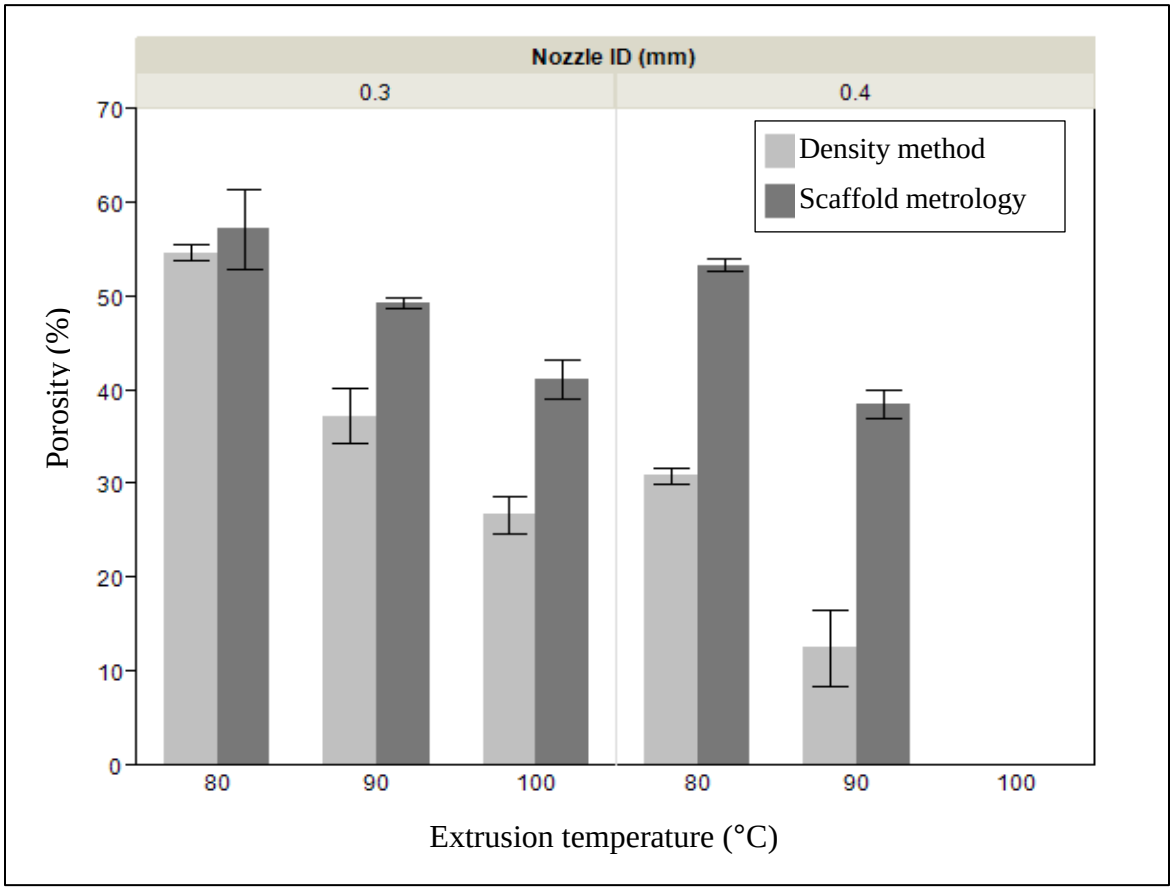

Figure 3 - 20 Bar graph comparing the two methods used to measure porosity of scaffolds; error bar displaying one standard deviation

4) Swell Ratio

The distribution of the swell ratio calculated for the PCL scaffolds is seen in Figure 3 - 22. The trend in this data was further examined by tabulating the mean and SD (Table 3 - 22).

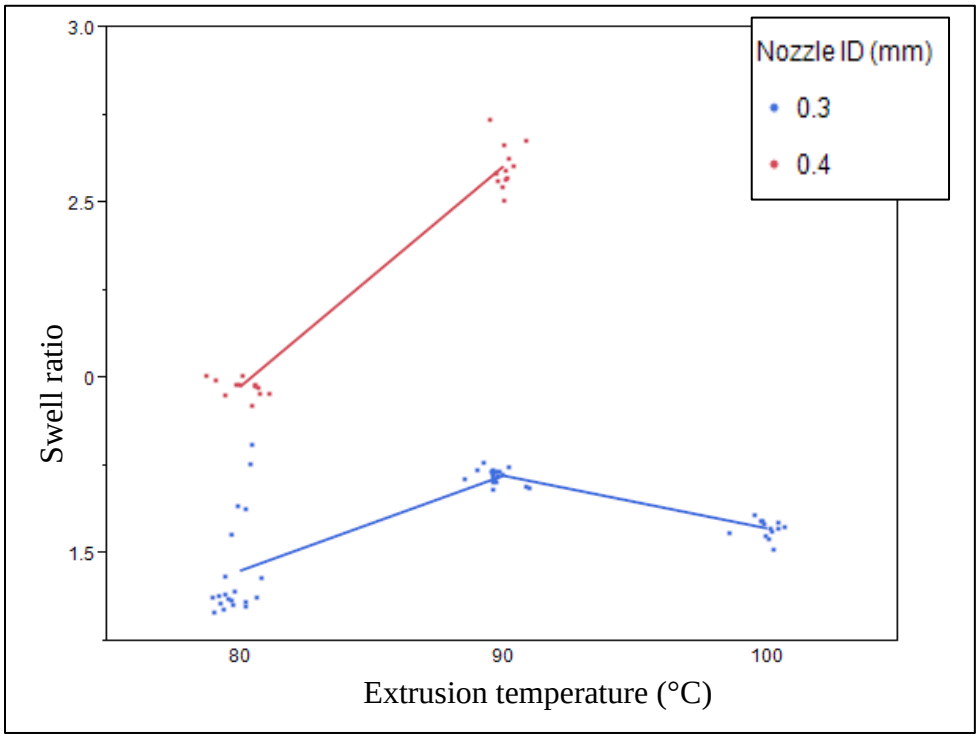

Figure 3 - 21 Scatter plot of swell ratio against extrusion temperature for scaffolds fabricated using nozzle diameters – 0.3 mm and 0.4 mm

The results show that the swell ratio differs significantly for different extrusion temperatures and for both nozzle diameters (p <.0.0001). This is consistent with previous results which show significant differences in scaffold strand width. Additionally, the swell ratio of scaffolds fabricated at 90°C was observed to be the highest (= 2.6) while using a nozzle diameter of 0.3 mm. This behavior in polymers is attributed to the viscoelastic nature of the materials, where the material tends to regain its original state after deformation causing swell

of the extrudate. The overall values obtained for mean swell ratio with one standard deviation are represented graphically in Figure 3 - 22.

Table 3 - 22 Mean and SD of swell ratio with a 95% CI

Nozzle diameter (mm)	Level (°C)	Sample size	Mean	SD	Lower 95% CI	Upper 95% CI
0.3	80	20	1.45	0.14	1.38	1.52
	90	19	1.72	0.02	1.71	1.73
	100	13	1.57	0.02	1.55	1.58
0.4	80	12	1.97	0.02	1.96	1.99
	90	12	2.60	0.06	2.56	2.64

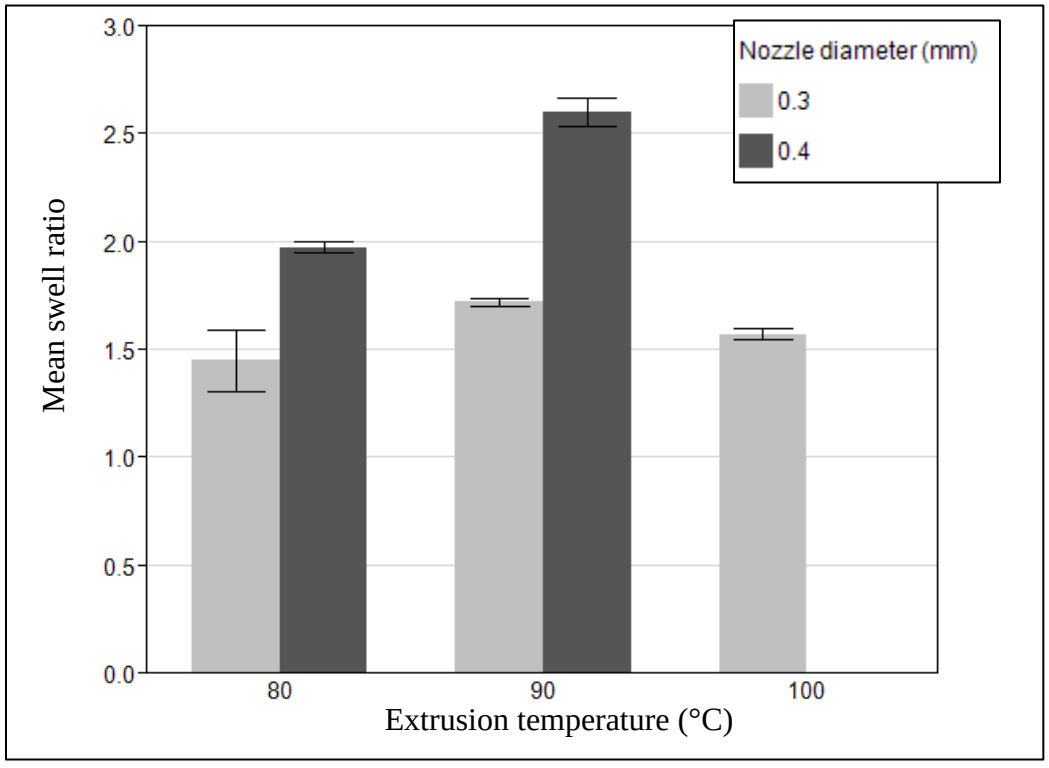

Figure 3 - 22 Distribution of strand swell ratio; error bar showing one standard deviation

3.4.5 Compression testing results

The compression test results conducted on five randomly drawn samples from each temperature and nozzle diameter combination are presented in this section. The load - displacement graphs for scaffolds fabricated at 80°C, 90°C, 100°C using a nozzle diameter of 0.3 mm (Figure 3 - 23,Figure 3 - 24,Figure 3 - 25) and at 80°C and 90°C using a nozzle diameter of 0.4 mm (Figure 3 - 29 and Figure 3 - 30) were generated. Similarly, stress - strain graphs for scaffolds fabricated using a nozzle diameter of 0.3 mm (Figure 3 - 26, Figure 3 - 27, Figure 3 - 28) and 0.4 mm nozzle (Figure 3 - 31and Figure 3 - 32) were also generated. The peak load and compression modulus was calculated from these plots and averaged over the five samples (Table 3 - 23).

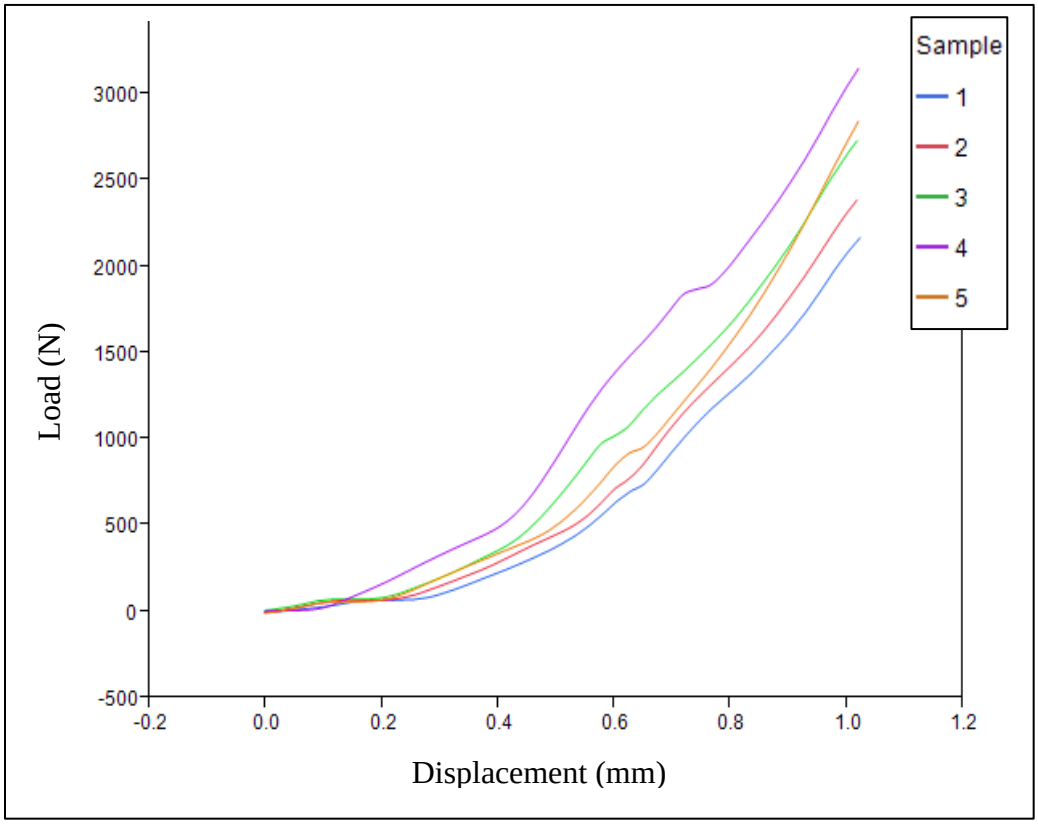

Figure 3 - 23 Load - displacement graph for scaffolds printed at 80°C with 0.3mm nozzle

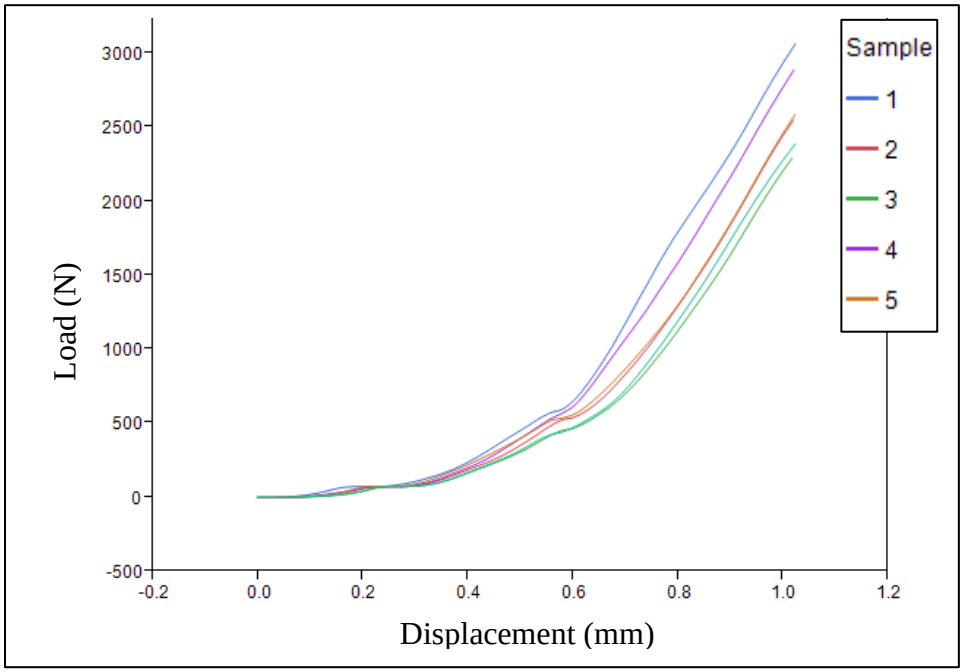

Figure 3 - 24 Load - displacement graph for scaffolds printed at 90°C with 0.3 mm nozzle

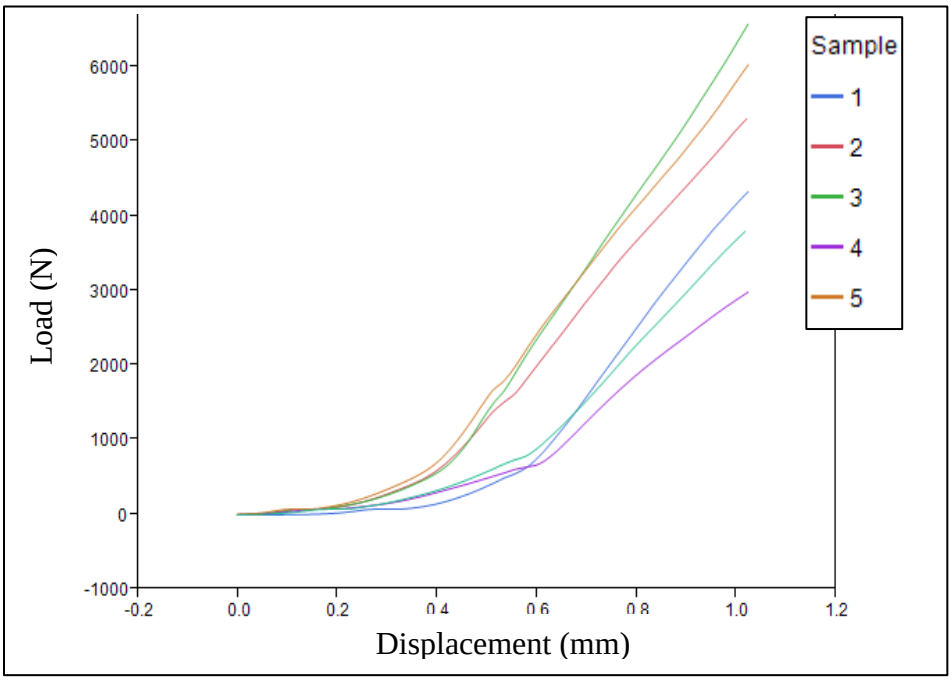

Figure 3 - 25 Load - displacement graph for scaffolds printed at 100°C with 0.4mm nozzle

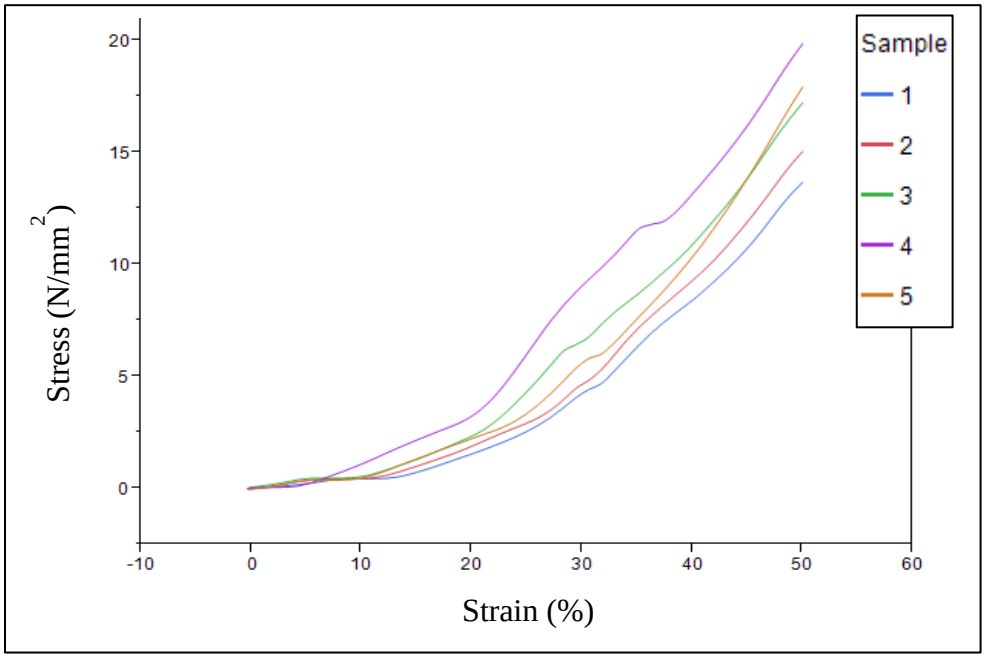

Figure 3 - 26 Stress - strain curve for scaffolds printed at 80°C with 0.3mm nozzle

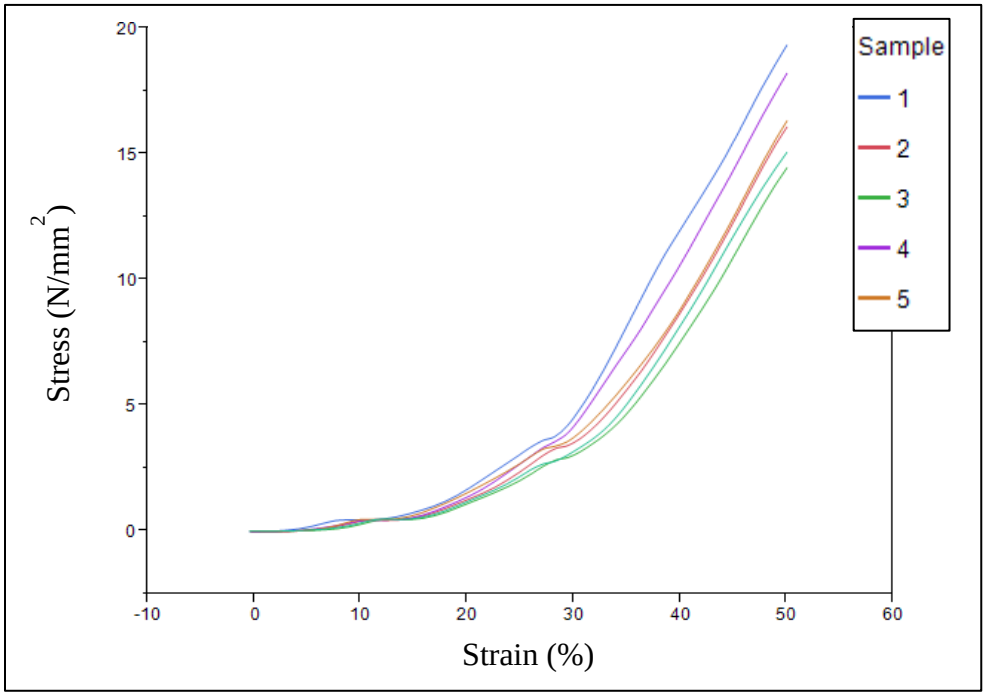

Figure 3 - 27 Stress - strain curve for scaffolds printed at 90°C with 0.3mm nozzle

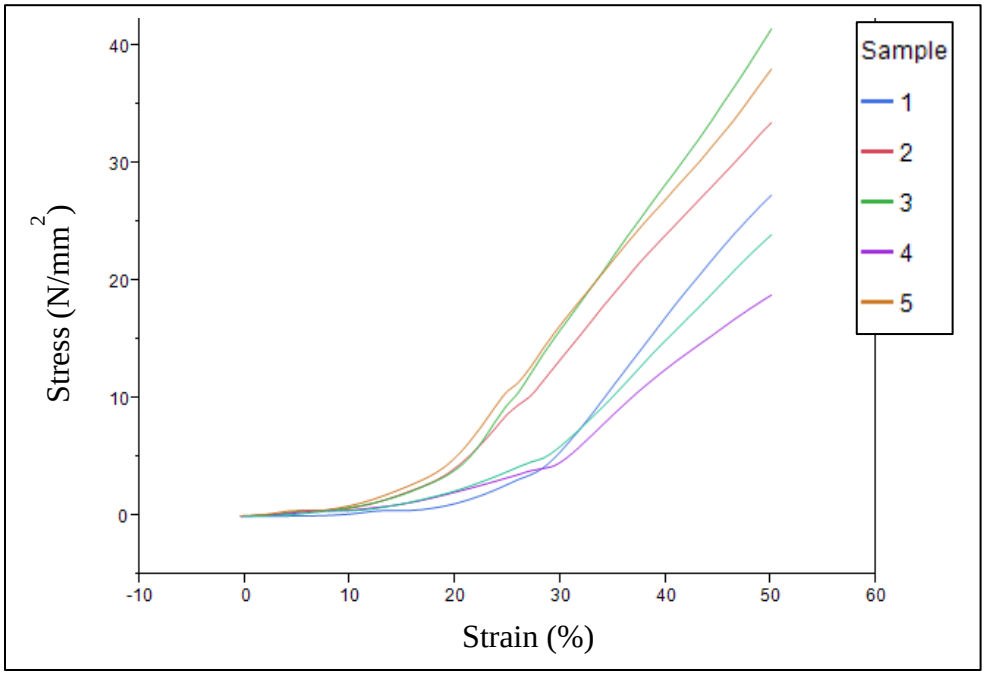

Figure 3 - 28 Stress - strain curve for scaffolds printed at 100°C with 0.3mm nozzle

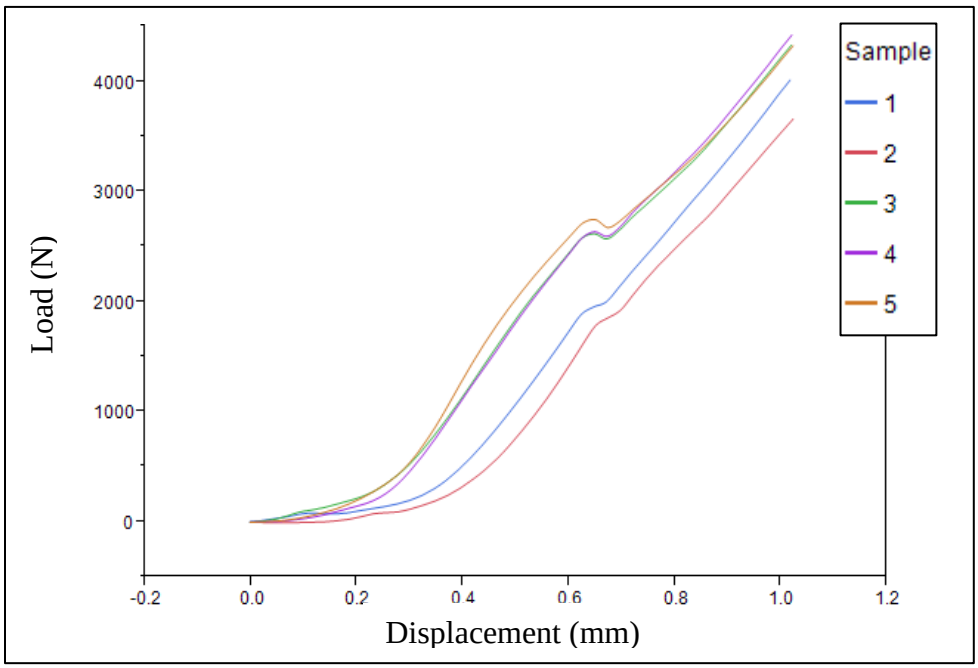

Figure 3 - 29 Load - displacement graph for scaffolds printed at 80°C with 0.4mm nozzle

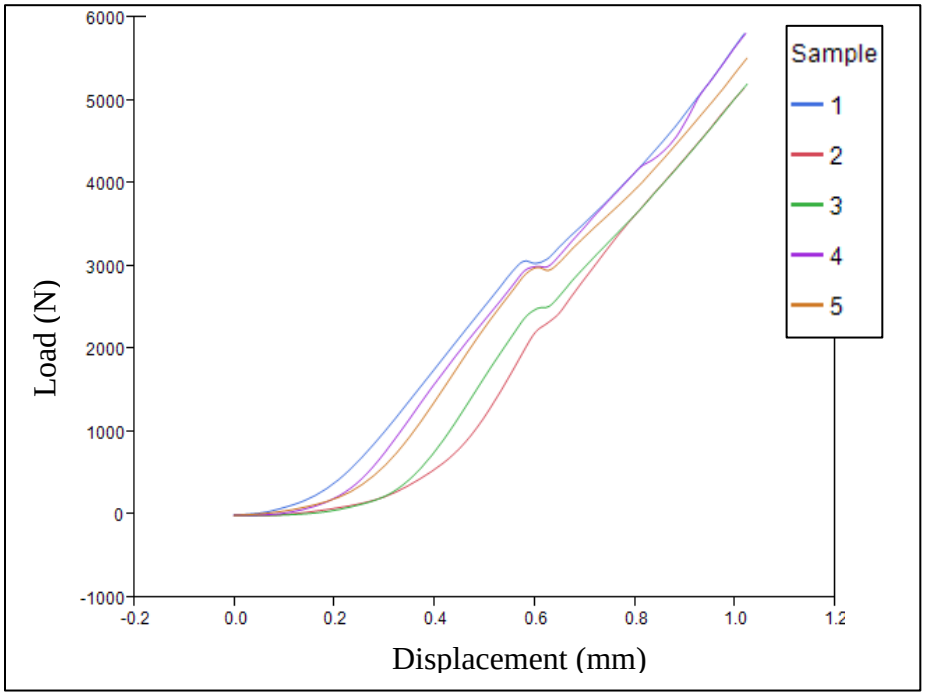

Figure 3 - 30 Load - displacement graph for scaffolds printed at 90°C with 0.4mm nozzle

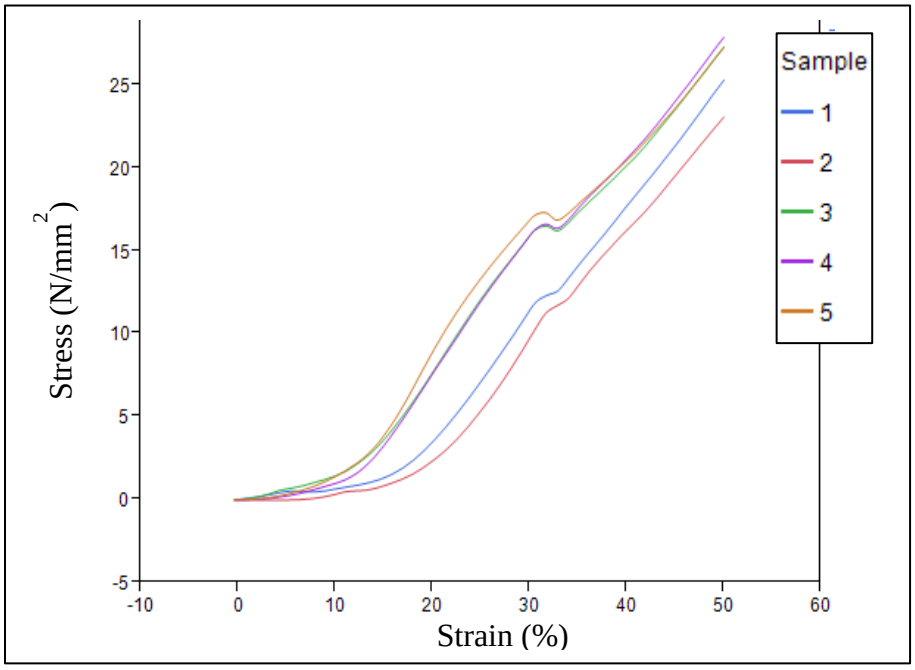

Figure 3 - 31 Stress - strain curve for scaffolds printed at 80°C with 0.4mm nozzle

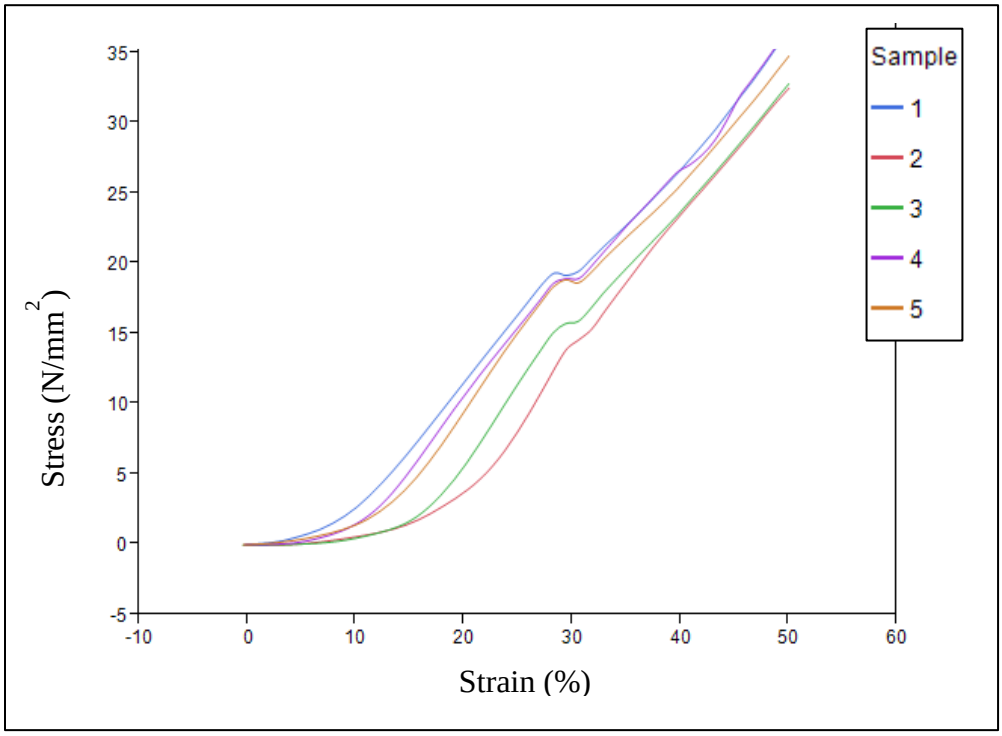

Figure 3 - 32 Stress – strain curve for scaffolds printed at 90°C with 0.4mm nozzle

Table 3 - 23 Compression testing results of scaffolds (averaged over five samples)

Nozzle diameter (mm)	Extrusion temperature (°C)	Compression modulus		Peak load	
		Mean (*10^{-2} MPa)	SD (*10^{-2} MPa)	Mean (N)	SD (N)
0.3	80	52.39	6.0399	2654.00	385.76
	90	65.95	5.2088	2674.01	302.42
	100	97.28	18.3100	5043.37	1427.24
0.4	80	59.66	6.8580	4144.67	315.42
	90	79.0	5.2162	5488.61	317.72

The results from the compression testing are represented graphically in Figure 3 - 33.

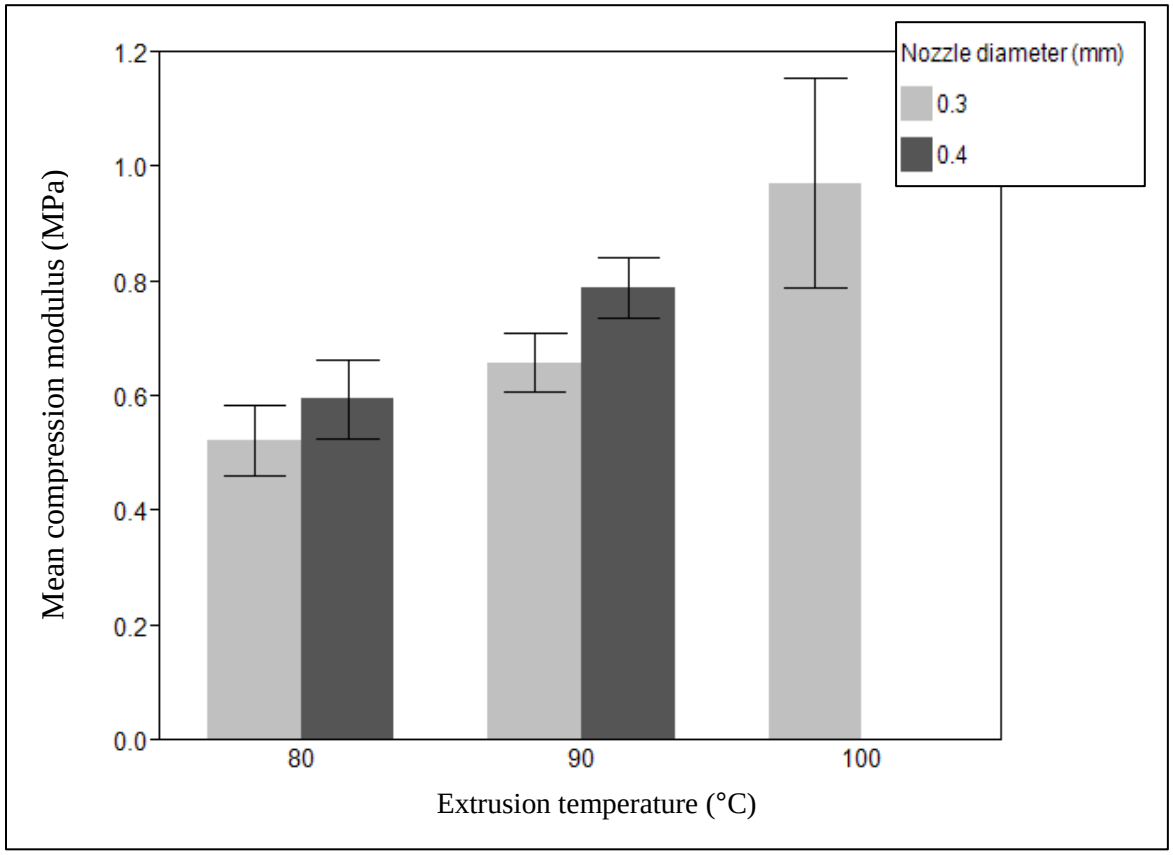

Figure 3 - 33 Bar graph of mean compression modulus of scaffolds against extrusion temperature for both nozzle diameters; error bar showing one standard deviation

3.4.5 Inferences

The discussion of the results obtained is listed below:

1. A higher variance in strand width data was observed for scaffolds fabricated at 80°C using a nozzle diameter of 0.3 mm. This can be attributed to inconsistent melting of PCL causing non-uniform strands (Figure 3 - 34).
2. The PCL was allowed to stand for 30 minutes in the high temperature head before extrusion (referred to as waiting time). The PCL melt is more consistent at 90°C and 100°C compared to 80°C for the same amount of waiting time. This inconsistent melting

can be eliminated by allowing PCL to stand for a longer period of time at 80°C to ensure uniform melting.

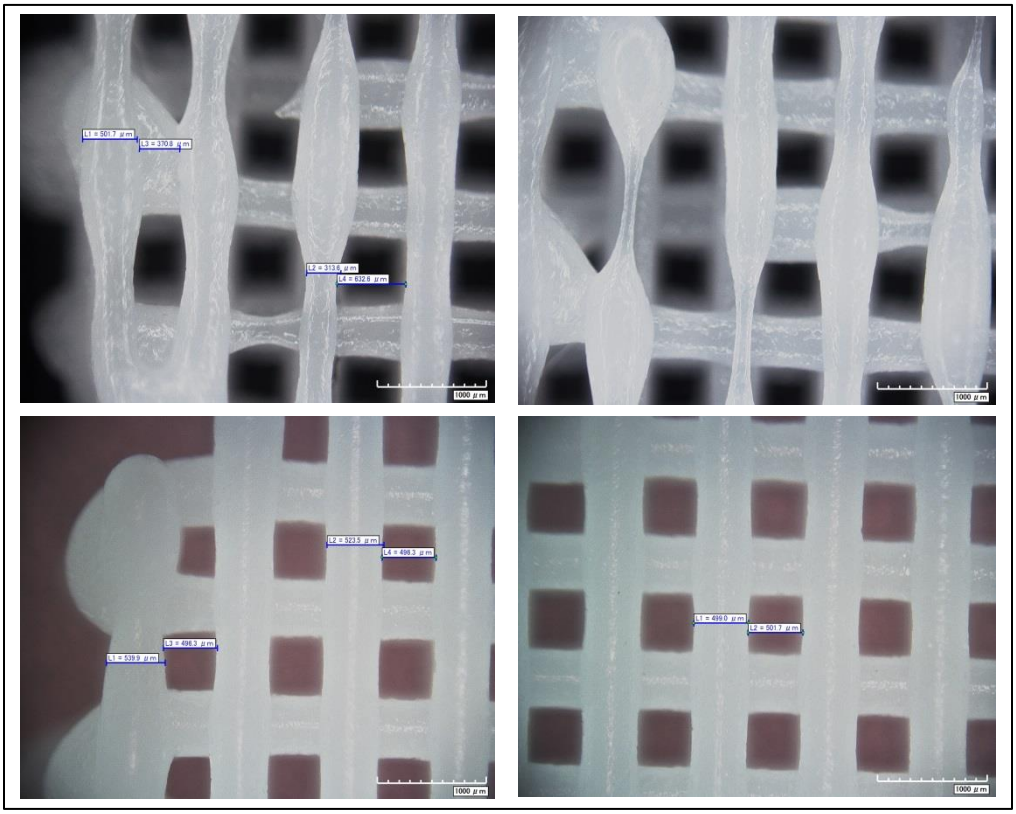

Figure 3 - 34 Non-uniform strands of PCL extruded at 80°C (top) when compared to homogenous strands extruded at 90°C (bottom)

3. The mean strand width of scaffolds fabricated was found to increase with increase in extrusion temperatures for both nozzle diameters. It can be inferred that an increase in extrusion temperature causes PCL viscosity to decrease which results in an increase in the strand width of PCL filaments. PCL viscosity at the different extrusion temperatures is investigated in Chapter 4.

4. The regression models for predicting average strand width show an increasing trend with increase in extrusion temperature and nozzle diameter with an interaction term. These models showed a high R^2 value for the given values of constant dispensing speed and extrusion pressure. This shows that the variation in strand width is explained by the two factors namely, extrusion temperature and nozzle diameter for these conditions.
5. The decrease in porosity with increase in extrusion temperature can be attributed to the increase in the strand width. The porosity calculated using the actual measurement of strand separation generated higher values compared to relative density method. Strand separation measurements are based on two dimensional (2D) data using digital microscopy images. This does not provide an accurate representation of the scaffold structure in 3D, but accounts for the higher values obtained using this technique. Scaffold porosity and pore size can be tailored to match design requirements once the mean strand width is known.
6. The peak load and compression modulus of the PCL scaffolds increased with increase in extrusion temperature and nozzle diameter. This is in agreement with previous results which showed that the strand width increased with extrusion temperature and nozzle diameter as well. This implies that the scaffold is able to bear higher loads with increasing strand width. The compression modulus and peak load for the two diameters cannot be directly compared using ANOVA because the scaffolds fabricated using the 0.4mm nozzle consist of five layers and those fabricated using 0.3mm nozzle consist of seven layers.

The scaffolds fabricated in this set of experiments used a constant dispensing speed and extrusion pressure. This can also be a cause for variation in the strand width. At higher temperatures and higher nozzle diameter combinations, such as 90°C with 0.4 mm nozzle diameter, lower pressures and higher dispensing speeds can potentially result in more homogenous data. However, this was not investigated in this study. A major factor in this variation can also be attributed to the change in PCL viscosity with extrusion temperature. A set of experiments designed to measure PCL viscosity is explained in the next chapter.

3.5 Chapter Summary

The experimental approach and procedure employed to examine scaffold fabrication using PCL on a 3D-Bioplotter™ is described in this chapter. A set of preliminary experiments were performed to determine a feasible range of the process parameters – extrusion temperature, extrusion pressure, nozzle diameter and dispensing speed. PCL scaffolds fabricated using these parameters were characterized using digital microscopy and compression testing. The effect of extrusion temperature and nozzle diameter on scaffold metrology was studied using a DOE. Additionally, the scaffold porosity and swell ratio of strands was calculated. The results to the statistical analysis and scaffold characterization was presented and discussed. The effect of extrusion temperature and nozzle diameter on scaffold strand width was found to be statistically significant at a significance level of 0.05.

CHAPTER 4: RHEOLOGICAL ANALYSIS

This chapter discusses the materials and methods used to study the rheological behavior of PCL at the extrusion temperatures used during scaffold fabrication (Chapter 3). The experimental methodology (Section 4.3) details the rheological tests carried out using PCL 767. This is followed by the results and inferences discussed in Section 4.4.

4.1 Introduction

This chapter addresses the specific aim 3 defined in Section 1.4 of Chapter 1. The main goal of this study is to establish a relationship between PCL viscosity and extrusion temperatures which can be instrumental in explaining differences in the resultant scaffold features. The effect of extrusion temperature and nozzle diameter on scaffold strand width was found to be statistically significant (p-value < 0.0001) (Chapter 3). For a chosen nozzle diameter, the difference in scaffold strand width at varying extrusion temperatures was also significant. This difference can be attributed to a change in PCL 767 viscosity for the chosen extrusion temperatures [83]. It has been observed that scaffold characteristics differ between materials of different viscosities for a given set of processing parameters [26]. This study is directed towards testing the hypothesis that the viscosity of PCL 767 significantly differs over the temperatures - 80°C, 90°C and 100°C. The viscosity of PCL 15 was also measured in one of the tests to draw a comparison of viscosity with different molecular weights.

4.2 Material

The specifications of PCL used in this study are identical to the ones used during scaffold fabrication (Table 3 - 1). PCL viscosities for both MWs were compared at extrusion temperatures – 80°C, 90°C and 100°C as a function of time. Additionally, PCL 767 was studied under increasing shear rates to assess flow parameters such as consistency index K and flow index n.

4.3 Experimental methodology

4.3.1 Viscosity measurement

The rheological properties of the PCL samples detailed in this study were measured using a Brookfield RVDV III ULTRA rheometer (Figure 4 - 1) with a small sample adapter (SSA). The rheometer consists of a spring loaded calibrated spindle which extends into the test fluid. The resistance offered by the fluid to the spindle rotation gives the viscosity of the fluid at that shear rate. The viscosity measurements are stable within a torque range of 10% to 100%.

Figure 4 - 1 Rheometer setup with the SSA and temperature control bath (TC – 150)

A temperature control bath (TC – 150) was used to maintain constant temperature in the SSA during viscosity measurements. This is critical since viscosity is a temperature-sensitive property [28]. Ethylene glycol was used as the circulating fluid in the temperature bath for the chosen temperature range (70°C to 100°C) [90] .

The SSA is designed to measure a sample volume of 7.1 mL for a given shear rate (Equation 3 -1). The SSA also has a temperature sensing probe which provides a feedback of the actual temperature inside the sample chamber. The specification of the spindle SC4 – 21 used in this study is shown in Figure 4 - 2.

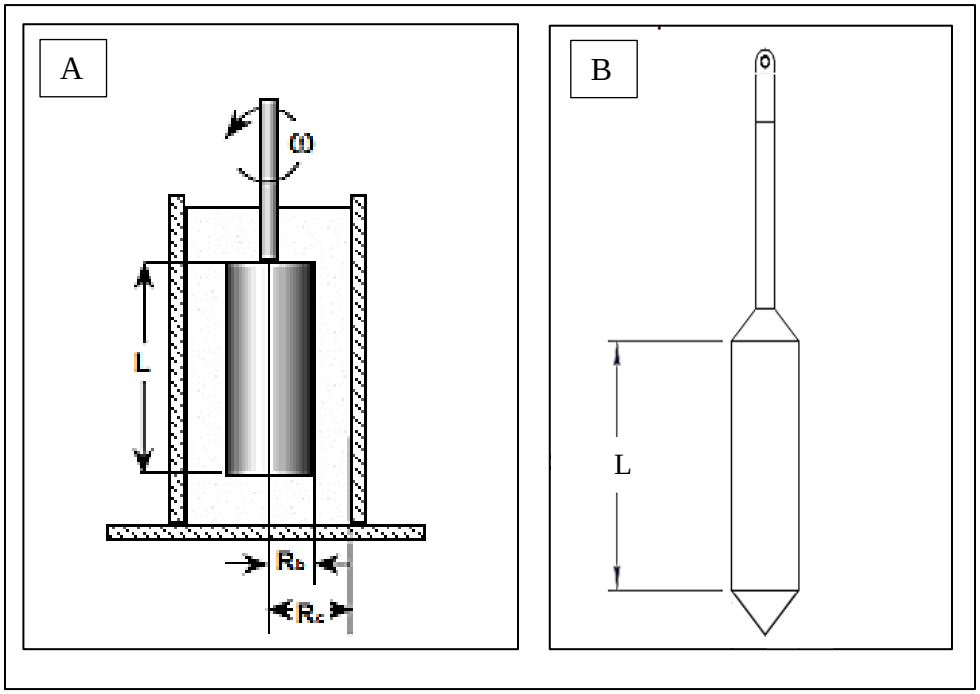

Figure 4 - 2 (A) SSA setup; (B) specifications of the SSA spindle SC-21 [91]

The rheometer output for the SSA using SC-21 is based on Equations 4 - 1 and 4 - 2. The shear rate ($\dot{\gamma}$) is given by:

$$\dot{\gamma} = \left(\frac{2Rc^2}{Rc^2 - Rb^2}\right) * \omega \qquad \text{Equation 4 - 1}$$

where,

$\dot{\gamma}$ = shear rate (s^{-1}) at the surface of spindle

R_b = radius of the spindle (= 8.385 mm) (Figure 4 - 2)

R_c = radius of the container (Figure 4 - 2)

ω = angular velocity of the spindle (rad/sec)

For SC4 – 21 used with the SSA, shear rate is given by the Equation 4 – 2 shown below.

$$\dot{\gamma} = 0.93 \times RPM \qquad \text{Equation 4 - 2}$$

Shear stress (τ) is given by,

$$\tau = \frac{M}{2\pi {R_b}^2 L} \qquad \text{Equation 4 - 3}$$

where,

τ = shear stress (dyne / cm^2)

M = torque input by the instrument (dyne - cm)

L = length of the spindle (= 31.24 mm) (Figure 4 - 2)

The material viscosity η is then given by Equation 4 - 4 represented as follows,

$$\eta = \frac{\tau}{\dot{\gamma}} \qquad \text{Equation 4 - 4}$$

4.3.2 Rheometer Calibration

The rheometer was calibrated using a standard test fluid (mineral oil) with a known viscosity of 5040 cP at 25°C. The viscosity of 7.1 mL of the standard test fluid is measured in the SSA at an increasing rpm. The allowable error range for the readings obtained is ±1% of the full scale viscosity range (FSR) (Equation 4 - 5).

$$FSR = TK * SMC * (10{,}000/RPM) \qquad \text{Equation 4 - 5}$$

where,

TK = Torque constant of the instrument (= 1 for RVDV-III Ultra)

SMC = Spindle multiplier constant (= 5 for spindle SC4 - 21)

RPM = spindle speed selected (revolutions per minute)

If the rheometer readings are beyond the allowable range, the troubleshoot procedure is available in the manual [91]. Once the calibration check was passed, the setup described above was used to assess the rheological properties of PCL. This was done to establish a relationship between the rheological properties of PCL 767 and the extrusion temperatures. PCL viscosity was measured at constant and varying shear rates over time. These studies were conducted at the feasible extrusion temperatures used during scaffold fabrication. 6.8 g of PCL, which corresponds to 7.1 mL of molten PCL, was allowed to stand for 30 minutes in the SSA at the given temperature before collecting data in both studies explained below.

4.3.3 Time sensitivity study

The main purpose of this study was to observe PCL behavior over time. This study was performed at a constant spindle rotational speed of 0.35 RPM which corresponds to a shear rate of 0.325 s^{-1} over 5 hrs. This RPM was selected since it fell within the allowable torque range for PCL 767 at all three temperatures. The time period was chosen based on the consumption rate of a full cartridge of PCL on the 3D-Bioplotter™. The rheometer was programmed to collect data every 15 minutes during this time period. This experiment was replicated thrice. This study primarily focused on the behavior of PCL 767. PCL 15 was then

studied to provide a comparison in viscosity in an attempt to explain differences in feasible processing parameters. Difference in PCL viscosity at different extrusion temperatures and molecular weights was compared using ANOVA.

4.3.4 Shear sensitivity study

The main goal was to study viscosity of PCL 767 as a function of rotational speed or shear rate. This was then used to calculate flow parameters of PCL – flow index *n* and consistency index *K*. This study considered only on PCL 767 since it was used in the scaffold fabrication experiments (Chapter 3). PCL 767 viscosity was measured over increasing shear rates at the following levels.

- RPM: 0.1 to 0.4 in steps of 0.05
- Shear rate: 0.093 s^{-1} to 0.372 s^{-1}
- Temperatures - 80°C, 90°C, 100°C
- Data collection frequency: 5 minutes
- Replicates: 2

The shear study data was modeled with the best fit power law trend line. The power law is given by Equation 4 – 6.

$$\tau = K\dot{\gamma}^{n} \qquad \text{Equation 4 - 6}$$

where,

τ = shear stress (Pa)

K = consistency index (Pa.s)

$\dot{\gamma}$ = shear rate (s^{-1})

n = flow index (which is <1 for non-Newtonian shear-thinning fluids)

The consistency index K and flow index n at each extrusion temperature were then solved from this equation for each temperature.

4.3.5 Calculation of apparent viscosity during 3D-Bioplotting

The apparent viscosity of PCL at the nozzle tip during 3D-Bioplotting was estimated to measure the sensitivity of the process to material viscosity. These calculations were based on the following assumptions:

1. The fluid is incompressible and time independent
2. There is no slip between the fluid and cylinder (cartridge) walls and the nozzle
3. The flow in the cartridge is steady, laminar and axisymmetric

The material flow rate (Q) was determined experimentally by measuring the weight and time taken to fabricate scaffolds designed for this thesis on the 3D-Bioplotter™ (Section 3.2.2). The apparent shear rate $\dot{\gamma}_a$ was then calculated using Equation 4 - 7 [28].

$$\dot{\gamma}_a = \frac{32Q}{\pi D^3} \qquad \text{Equation 4 - 7}$$

where,

Q = material flow rate (cc / min)

D = nozzle diameter (cm)

The apparent viscosity η_a at the nozzle tip was then calculated using Equation 3- 7 [83]**:**

$$\eta_a = K\dot{\gamma}_a^{\,n-1} \qquad \text{Equation 4 - 8}$$

4.4 Results and Discussion

4.4.1 Calibration test results

Figure 4 - 3 shows the calibration test results using a test fluid with a viscosity of 5040 cP. Since FSR is directly proportional to the spindle speed, the error reduces with increasing rotational speed. The calibration plot shows that the rheometer output is within the allowable limit.

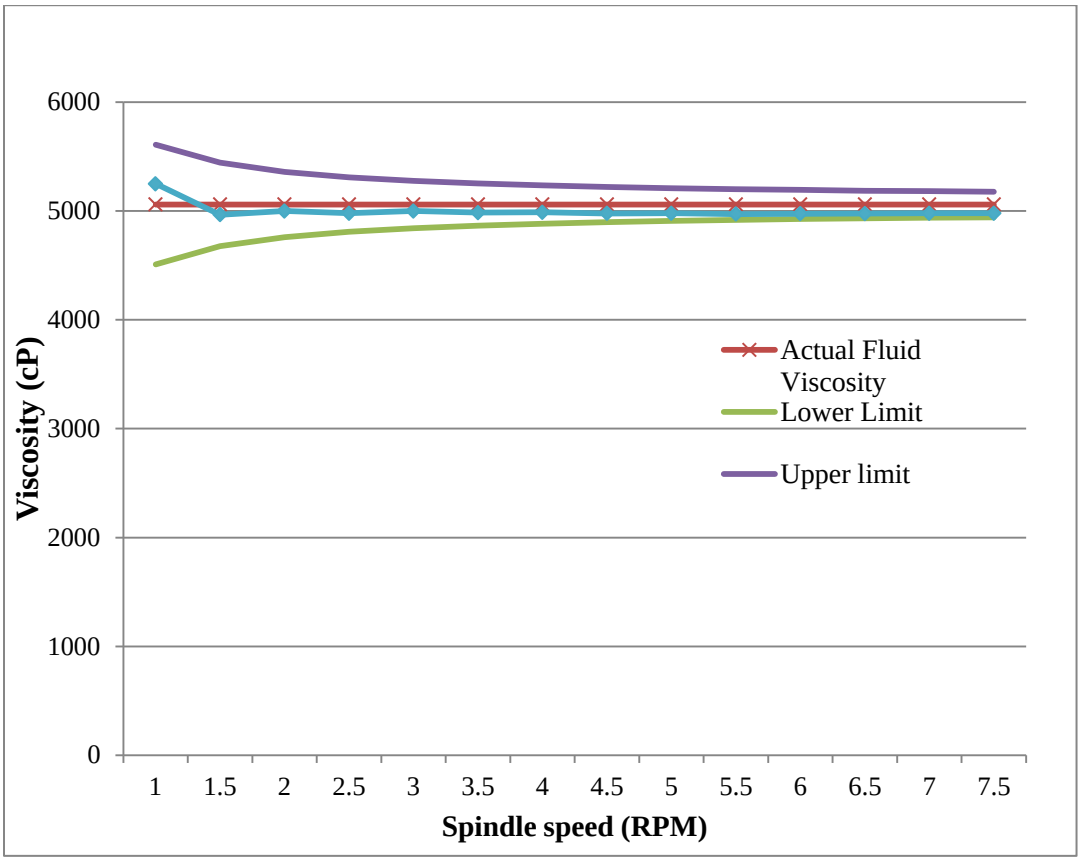

Figure 4 - 3 Calibration results of the Brookfield rheometer with small sample adapter using silicone mineral oil – 5040 cP at 25°C

4.4.2 Time sensitivity study results

Figure 4 - 4 displays an overlay plot of the viscosity of PCL 767 over time at temperatures - 80°C, 90°C and 100°C for a constant shear rate of 0.326 s^{-1}. The plot shows that the data points are approximately parallel to the X-axis implying that time has no effect on the material viscosity. In this case, for the selected time period of 5 hrs, it is observed that PCL is a time independent material. Another observation from the scatter plot is the difference in PCL viscosity with temperature. This variation in viscosity was compared using an ANOVA model followed by a Tukey HSD *post-hoc* test.

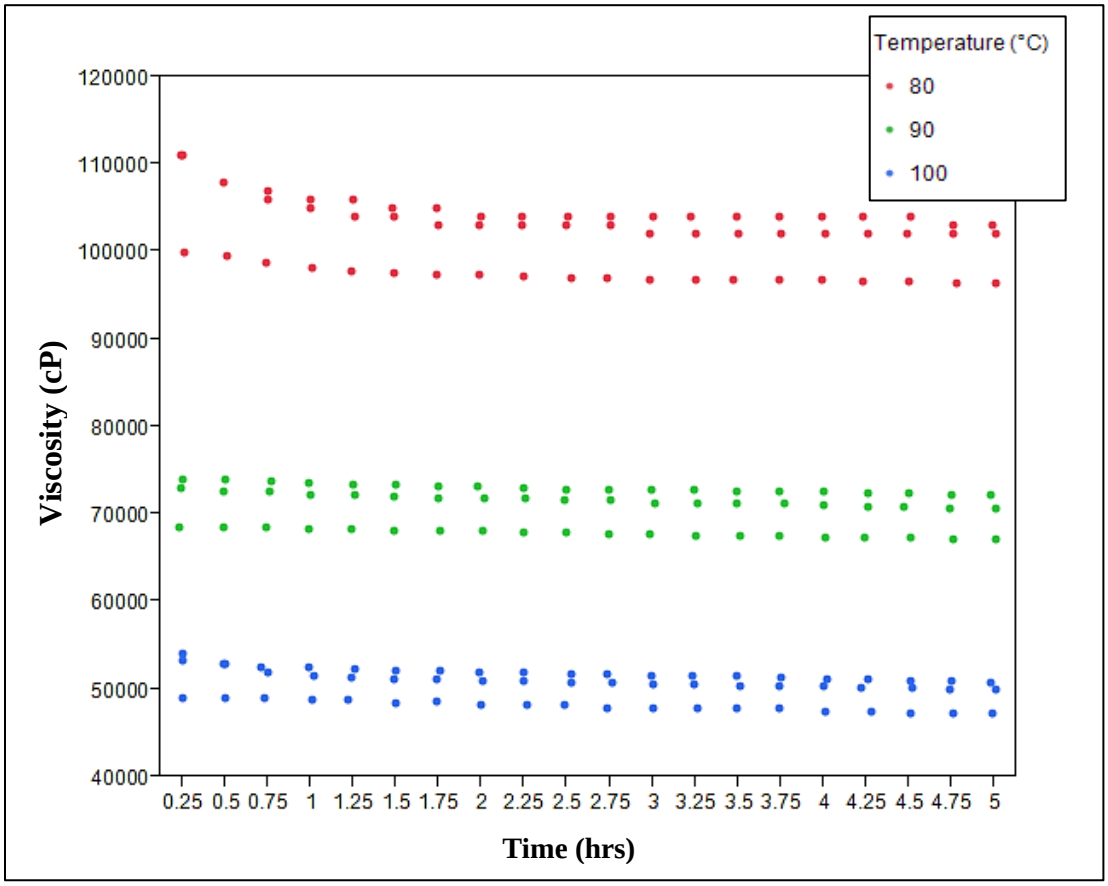

Figure 4 - 4 Overlay scatter plot of PCL 767 viscosity against time at a shear rate of 0.325s^{-1}

The statistical analysis of this data set consists of two categories: One way ANOVA to compare PCL viscosity at the different extrusion temperatures and a regression model of average strand width against PCL viscosity.

1) One-way ANOVA

The viscosity data for different extrusion temperatures was fit to the ANOVA model given by Equation 4 – 9.

$$Y_{ij} = \mu + a_i + \varepsilon_{ij} \qquad \text{Equation 4 - 9}$$

$$i = 1, 2, 3$$

$$\varepsilon_{ij} \sim iid\ N(0, \sigma^2)$$

where,

Y_{ij} = PCL viscosity (response)

μ = overall (grand) mean

α = main effect of extrusion temperature

The box plot (Figure 4 - 5) shows the distribution of mean viscosity of PCL 767 at the three chosen extrusion temperatures.The one-way ANOVA tests the null hypothesis that the mean viscosity at different extrusion temperatures is equal versus the alternative that at least one of them is not equal. The null hypothesis H_0 is represented by:

$$H_0: \mu_{80} = \mu_{90} = \mu_{100}$$

where,

μ_{80} = Mean viscosity at extrusion temperature of 80°C

μ_{90} = Mean viscosity at extrusion temperature of 90°C

μ_{100} = Mean viscosity at extrusion temperature of 100°C

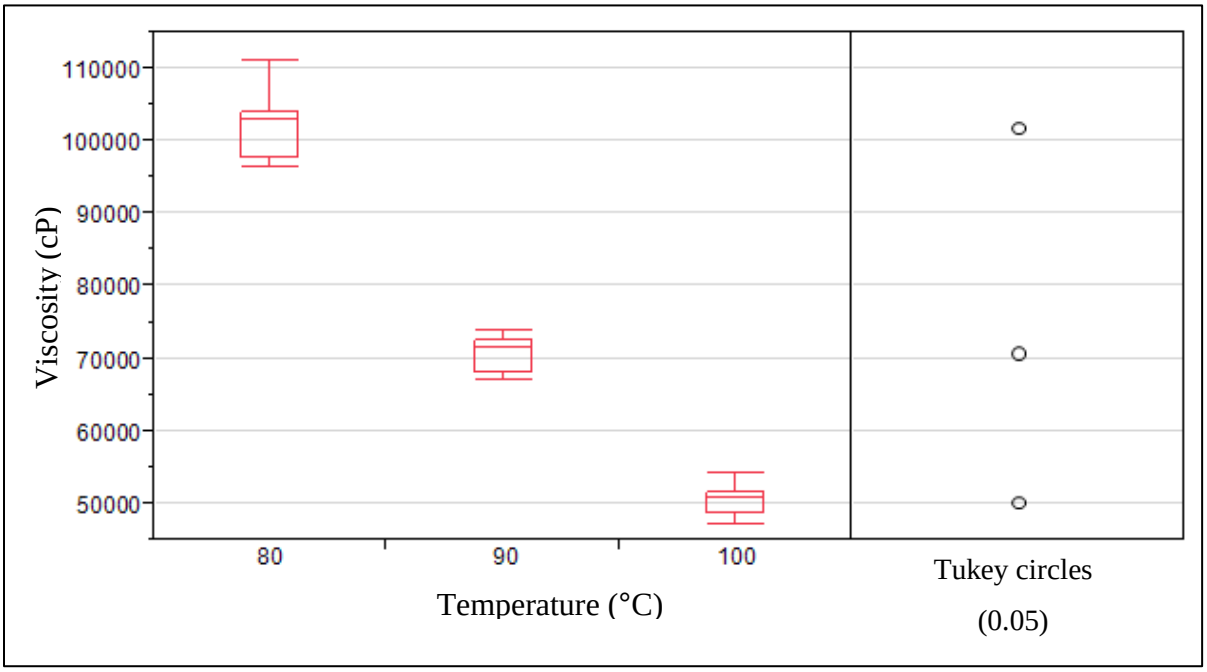

Figure 4 - 5 Box plot of PCL viscosity against temperature

The plot shows that the variance of viscosity is higher at 80°C than at 90°C and 100°C. A p-value of < 0.0001 obtained in this analysis indicates a strong evidence that the mean viscosity of PCL at different extrusion temperatures are not equal (Table 4 - 1). These results were further examined by computing the mean viscosity at each temperature level along with a 95% CI (Table 4 - 2). The mean viscosity of PCL 767 at different temperatures was compared using a Tukey's test. The results show that the mean viscosity at different extrusion temperatures is significantly different (p-value ≤ 0.0001). The output of this test represents significantly different pairs by different alphabets (Table 4 - 3)

Table 4 - 1 ANOVA output for the effect of extrusion temperature on PCL viscosity

Source	DF	Sum of squares	Mean square	*F* Ratio	*p*-value
Temperature (°C)	2	8.1184×10^{10}	4.05×10^{10}	5386.804	<.0001*
Error	177	0.1333×10^{10}	7.5354×10^{7}		
Total	179	8.2518×10^{10}			

Table 4 - 2 Mean and standard deviation of PCL viscosity with a 95% CI

Level (°C)	Mean viscosity (cP)	SD (cP)	Lower 95% CI	Upper 95% CI
80	101940.47	3773.28	100966	102915
90	70795.23	2270.05	70209	71382
100	50283.33	1793.25	49820	50747

Table 4 - 3 Tukey HSD output comparing mean PCL viscosity at all extrusion temperatures

Level (°C)	Grouping			Mean viscosity (cP)
80	A			101940.47
90		B		70795.23
100			C	50283.33

2) Regression model for average strand width:

The strand width data was fit to a least square regression against extrusion temperature previously (Chapter 3). Extrusion temperature was replaced with average PCL viscosity given by the expression in Equation 4 -1. This was done to develop a model which is dependent on the material property (viscosity) rather than extrusion temperature during fabrication.

$$(y) = \beta_0 + \beta_1 * Average\ Viscosity + \varepsilon_i \qquad \text{Equation 4 – 1}$$

where,

β_0 = intercept

β_1 = slope of the regression line

ε_i = error term

The parameter estimates obtained from the least square regression is shown in Table 4 - 4. Here the intercept (β_0) is equal to the strand width at zero viscosity of PCL. This value loses its meaning in this context. The slope of the line (β_1) represents the increase in strand width per unit (cP) increase in the average viscosity of PCL. This value being negative indicates a negative relation between strand width and average viscosity. The summary of fit (Table 4 – 6) and the regression plot (Figure 4 - 6) indicate that this model accounts for the variation in the data set since the R^2 value is close to 1.

Table 4 - 4 Parameter estimates for regression of strand width against mean PCL viscosity (Nozzle diameter = 0.3 mm)

Term	Estimate	Std. error	*t*-ratio	*p*-value
Intercept (β_0)	753.9626	12.2465	61.57	<.0001
Average Viscosity (β_1)	-0.00322	0.0001	-21.14	<.0001

Table 4 - 5 Summary of fit for regression plot

Parameter	Value
R^2	0.8994
Adjusted R^2	0.8974
Root Mean Square Error	22.8191

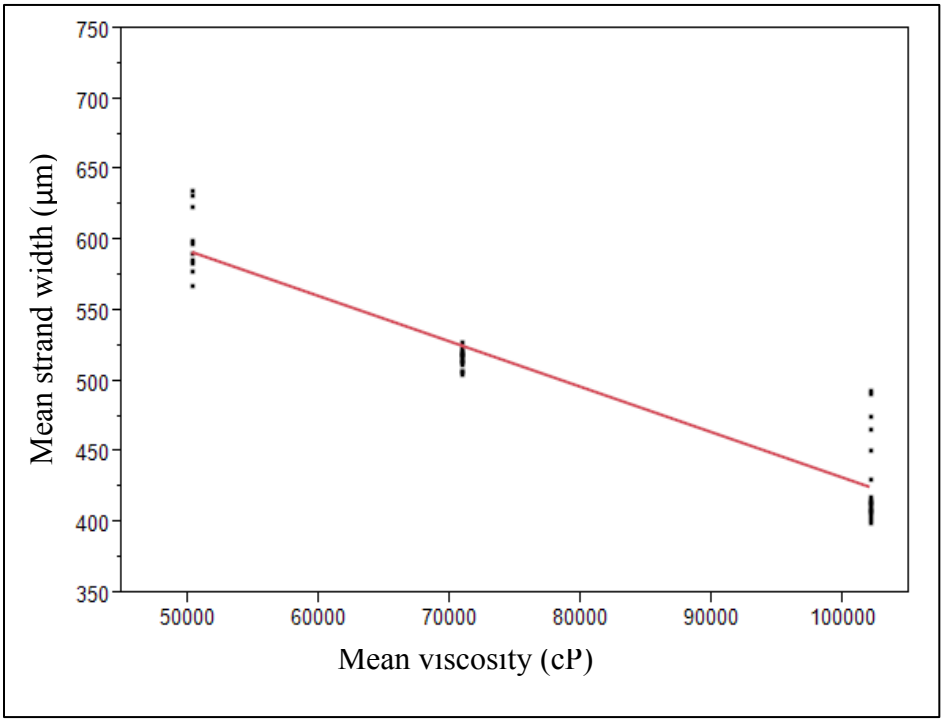

Figure 4 - 6 Regression plot for strand width against average viscosity of PCL for a nozzle diameter of 0.3 mm

The prediction expression for average strand width can be represented by Equation 4 – 2. This model is valid under the constant extrusion pressure and dispensing speed used in these experiments.

$$(y) = 753.9626 - 0.00322 \ * Average\ viscosity + \varepsilon_i \qquad \text{Equation 4 – 2}$$

- Time sensitivity study for PCL 15

An identical time sensitivity study was repeated for PCL 15. Due to torque constraints of the rheometer these tests were done at a different RPM for each temperature (Table 4 - 6). The main objective was to compare PCL viscosity for the two molecular weights. PCL 767 was also measured over the new chosen RPMs – 0.35, 0.5 and 0.7 for 80°C, 90°C and 100°C respectively. The plot of viscosity against time of the two types of PCL is shown in Figure 4 - 7.

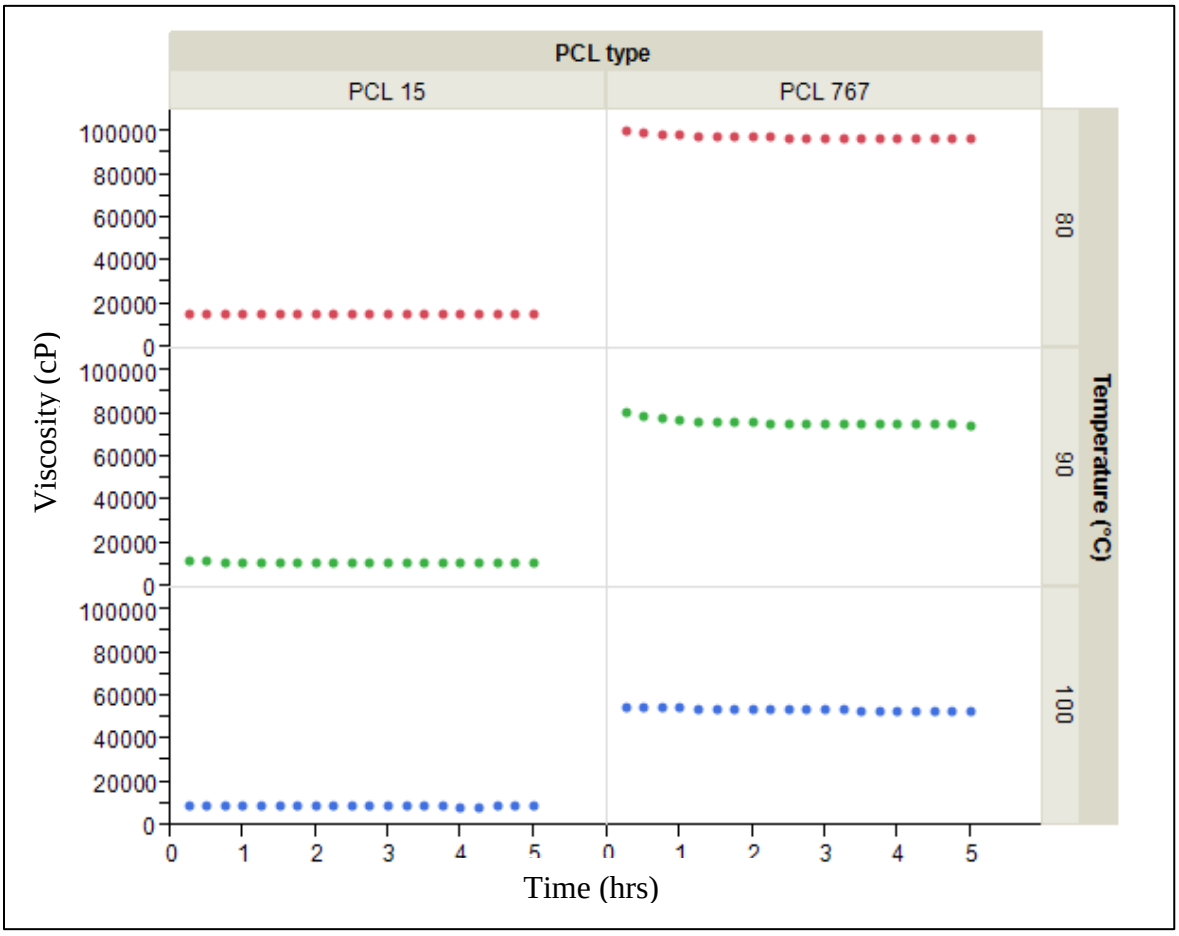

Figure 4 - 7 Viscosity of PCL 767 and PCL 15 against time for different temperatures

The plot shows a distinct difference in average PCL viscosity of the two MWs over the 5 hr time period. This difference in viscosity was compared using ANOVA individually for each extrusion temperature. The results from these tests indicate a significant difference in PCL viscosity for the two molecular weights (p-value < 0.0001) at a given temperature. The mean and SD computed for the two types of PCL along with the p- value obtained from the ANOVA is shown in Table 4 - 6.

Table 4 - 6 Mean and SD viscosity of PCL 767 and PCL 15

Temperature (°C)	RPM	Viscosity (cP)				*p* - value
		PCL 15		PCL 767		
		Mean	SD	Mean	SD	
80	0.35	15429	0	101940	3773.28	0.0001
90	0.5	11110	30.77	75885	1529.11	0.0001
100	0.7	8514.2	43.70	53550.05	590.88	0.0001

4.4.3 Shear sensitivity tests

Viscosity of PCL 767 is presented as a function of RPM (Figure 4 - 8). The plot shows that the viscosity is not affected by the increasing RPM. This implies that the range of measurement is still within the linear visco-elastic region of the polymer melt which can be attributed to the low rotational speeds (0.1 to 0.4 RPM). Hence, a plot of shear stress v/s shear strain for each extrusion temperature was generated (Figure 4 - 8). The shear data was modeled with a power law trend line since the power law has been shown to closely model pseudoplastic behavior [77] [91]. The average power law constant K and the flow index n were calculated from these plots. The high R-squared value for the data indicates a good fit to the chosen math model Table 4 - 7. The shear stress – shear rate plot shows a shear-thinning or pseudoplastic behavior of the polymer [91]. The flow index solved using this plot ranged from 0.69 to 0.71 which is a characteristic of a shear-thinning fluid, since $n < 1$.

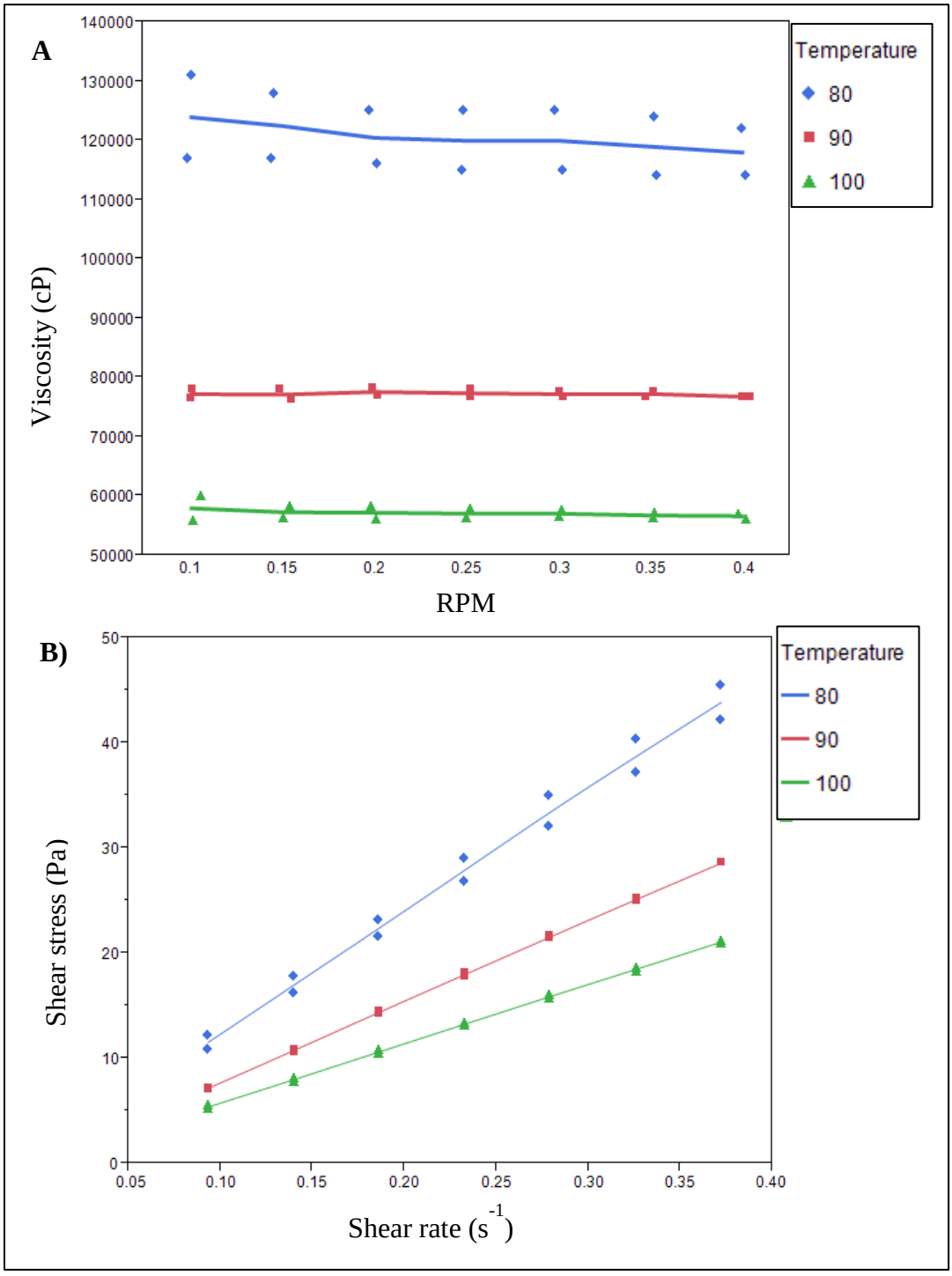

Figure 4 - 8 (A) PCL 767 viscosity against RPM for the three extrusion temperatures; (B) Shear sensitivity test for PCL 767 at three extrusion temperatures (replicates = 2)

Table 4 - 7 Shear sensitivity test results for PCL 767 – Consistency and flow index values

Temperature (°C)	Consistency index *K* (Pa.s)	Flow index *n*	R^2 value
80	10.955	0.6925	0.9948
90	6.8325	0.7155	0.9949
100	5.1185	0.70635	0.9943

4.4.4 Calculation of apparent viscosity during 3D-Bioplotting

The flow parameters determined for PCL 767 are summarized in Table 4 - 8. The extrusion temperature – nozzle diameter combination of 100°C – 0.4 mm was excluded since it was previously not used in the scaffold fabrication DOE (Section 3.4.3).

Table 4 - 8 PCL flow properties during 3D-Bioplotting

Nozzle diameter (mm)	Extrusion temperature (°C)	Material flow rate (* 10^{-3} cc/min)	Apparent viscosity (cP)	Apparent shear rate (s^{-1})
0.3	80	9.1396	3152.0076	57.4687
	90	12.6579	1967.2786	79.5382
	100	14.7896	1352.4038	92.9936
0.4	80	13.9358	2768.9381	87.5863
	90	17.6489	1789.4466	110.9699

Figure 4 - 9 shows the distribution of apparent viscosity of PCL 767. The apparent viscosity of PCL 767 at the nozzle tip reduces steeply with increase in temperatures (Figure 4 - 9). This trend is observed for both nozzle diameters – 0.3 mm and 0.4 mm. The viscosity calculated for a nozzle diameter of 0.4 mm is lower than that at 0.3 mm.

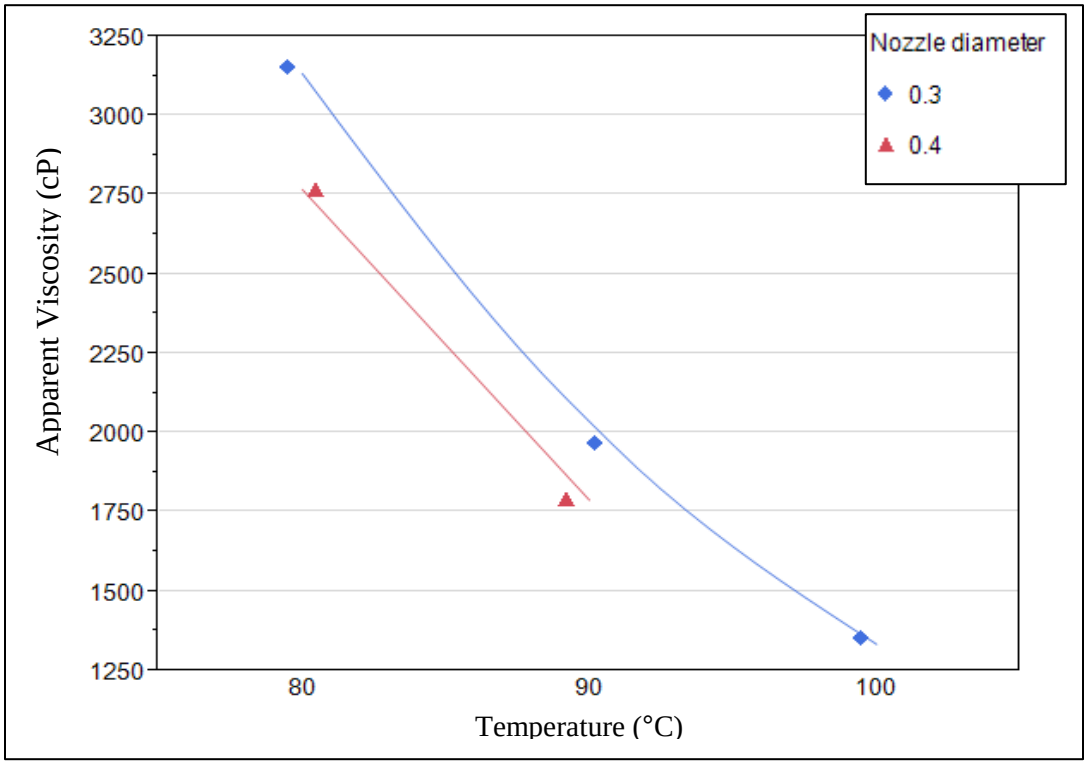

Figure 4 - 9 Distribution of apparent viscosity of PCL during 3D-Bioplotting

4.4.5 Inferences

1. The viscosity of PCL 767 is significantly different at the three extrusion temperatures for a given shear rate. This implies that processing PCL 767 at these temperatures would result in varied flow behavior. This is in agreement with the results obtained in the previous chapter for scaffold strand width measurement analysis which differed with each extrusion temperature – nozzle diameter combination.
2. The variance of the viscosity of PCL 767 was much higher at 80°C when compared to the other two extrusion temperatures. This is consistent with previous results which showed inconsistent melts in strands of scaffolds fabricated at 80°C (Section 3.3.5).
3. The regression model for average strand width against average PCL viscosity shows a negative relationship between the two parameters for a nozzle diameter of 0.3 mm. This

model replaces extrusion temperature and shows dependency of scaffold geometry on material property. Since viscosity is a temperature dependent property, this prediction expression can be used when a material possesses a comparable viscosity but at a different temperature.

4. The difference in viscosity for the two molecular weights of PCL was found to be statistically significant. This would explain the difference in the feasible range of processing parameters for the two types of PCL on the 3D-Bioplotter™. PCL 15, which has a much lower viscosity, could be processed at lower pressures and higher dispensing speeds.
5. The shear tests in this study were useful in estimating the flow index *n* and the consistency index *K* which determines PCL flow behavior. The flow index determined for PCL 767 was < 1 indicating that PCL is pseudoplastic in nature and exhibits shear-thinning [83]. However the actual shear rates during extrusion based processes such as 3D-Bioplotting are generally much higher than the ones used in this study.
6. The apparent viscosity calculated at the nozzle tip varies with each temperature-nozzle diameter combination. This demonstrates the sensitivity of the process to material viscosity. These results are in conjunction with previous research in extrusion based scaffold fabrication techniques [74]. The significant interaction between the two experimental factors in the statistical analysis can be due to this difference in material viscosity.
7. The material flow rate (*Q*) increased with increasing temperature and increasing nozzle diameter for a constant dispensing speed and extrusion pressure. Since this is a measure of volume of fluid flow per minute, it indicates that scaffolds fabricated at higher temperatures possess greater volume compared to those fabricated at lower temperatures. This is in agreement with the results from compression testing of the scaffolds which showed increased strength with higher extrusion temperature and nozzle diameter.

4.5 Chapter Summary

The methodology and the experimentation of the rheological assessment of PCL have been discussed in this chapter. PCL viscosity was studied under conditions of constant and increasing shear rates over time (i.e. time sensitivity and shear sensitivity studies). Time sensitivity study results indicated that viscosity of PCL 767 remained fairly constant over a time period of five hours at each chosen temperature. Further, the results of these studies indicated that the chosen extrusion temperatures had a significant influence on PCL viscosity ($p < 0.0001$). The shear sensitivity study was used to calculate the flow index n and consistency index K of PCL 767. This was further used to estimate the apparent viscosity at the nozzle tip during 3D-Bioplotting which was also reported in this chapter.

CHAPTER 5: CONCLUSIONS AND FUTURE WORK

This chapter presents the conclusions from this study, discussing potential implications and directions for future research.

5.1 Conclusions

The primary contribution of this thesis is the set of feasible process parameters determined for 3D-Bioplotting PCL scaffolds. The corresponding scaffold characteristics – geometry and strength - using these parameters was also determined. The results indicate a relationship between process parameters, PCL viscosity and scaffold characteristics (Table 5 - 1).

Table 5 - 1 Summary of findings

Nozzle diameter (mm)	Extrusion temperature (°C)	Viscosity (cP) (at 0.325 s^{-1})		Apparent viscosity (cP)	Strand width (µm)		Compression modulus (*10-2 MPa)	
		Mean	SD		Mean	SD	Mean	SD
0.3	80	101940.5	3773.28	3152.01	428.81	30.04	52.39	6.03
	90	70795.23	2270.05	1967.28	517.17	6.05	65.95	5.20
	100	50283.33	1793.25	1352.40	599.62	21.99	97.28	18.31
0.4	80	101940.5	3773.28	2768.94	790.76	9.91	59.66	6.85
	90	70795.23	2270.05	1789.45	1042.37	25.84	79	5.21

By the use of statistically designed experiments, it has been shown that scaffold fabrication using 3D-Bioplotting is dependent on extrusion temperatures, extrusion pressure, nozzle diameter and dispensing speed. 3D-Bioplotting with an extrusion temperature of 90°C with a nozzle diameter of 0.3 mm resulted in scaffolds with an average strand width of 517.17 µm with a standard deviation of 6.05 µm. These scaffolds showed the least variance compared to

scaffolds fabricated at 80°C (μ = 428.81 µm, σ = 30.04 µm.) and 100°C (μ = 599.62 µm, σ = 21.99 µm). The results from the statistical analysis indicate that extrusion temperature, nozzle diameter and the combination of the two have a significant effect on the scaffold strand width, fabricated at a constant dispensing speed and extrusion pressure. Scaffold features such as scaffold porosity and swell ratio of extruded strands also depend on these process parameters since they are correlated to strand width. The strength of these scaffolds under compression for each extrusion temperature – nozzle diameter combination was also measured. A direct implication of these results would be that the scaffold strand width (and related properties - scaffold porosity and strength) can be controlled by varying process parameters. A least square regression model of the dependence of average strand width of bioplotted scaffolds on extrusion temperature and nozzle diameter showed a good fit. These results show that similar predictive models can be effectively used in minimizing scaffold fabrication cycle time and therefore assist in consistent production of application specific TE scaffolds.

This mapping of process parameters and scaffold characteristics can significantly reduce the cycle time of scaffold fabrication to suit TE applications. Designing PCL scaffolds for fabrication on a 3D-Bioplotter or a similar system can be based on these results. Scaffold design requirements for engineering different tissues are often listed in terms of porosity and mechanical properties. Hence, process characterization studies similar to the one presented in this thesis would be relevant in optimizing and automating scaffold fabrication.

PCL viscosity showed a significant variation at the different extrusion temperatures which was validated using ANOVA. Average PCL viscosity at 80°C, 90°C and 100°C measured over a constant shear rate was found to be 10.1×10^4 cP, 7.07×10^4cP and 5.02×10^4cP respectively. This decrease in viscosity at higher temperatures can explain the increase in the scaffold strand width measured at these temperatures, due to improved flow properties. This also depends on the material flow parameters - flow index *n* and consistency index *K* which were determined experimentally in this study. These results show that the impact of polymer

viscosity on the process output (i.e. scaffold characteristics) is significant. The direct inference of these results is that scaffold specifications (porosity and strength) can be tailored for a given application by measuring the material flow behavior. The regression model showing the dependence of PCL viscosity on scaffold strand width also showed a good fit. These results can be useful while working with different scaffold materials or blends which may have a similar viscosity range.

Overall, a model which connects process parameters and scaffold features for a material of a known viscosity can be a useful tool to researchers in the field of scaffold based TE. Such models have the potential to simplify the logistics involved in these complex processes by offering manufacturing control and reliability.

5.2 Future Work

The experiments and analyses conducted in this thesis were primarily centered on the scaffold fabrication of PCL with a molecular weight of 43 – 50 kDa. The effect of 3D-Bioplotting process parameters and material rheology on TE scaffold characteristics was investigated. However, there is room for deeper characterization studies. Some future directions emerging from this study are listed below.

1. Inclusion of more factors in the statistical DOE

The results show that the scaffold architecture and strength are influenced by extrusion temperatures and nozzle diameters for a constant dispensing speed and extrusion pressure. Varying these factors and including them in the statistical design of experiments can be part of another study. This study was designed around PCL with a molecular weight of 43 – 50 kDa. Preliminary experiments using PCL with a lower molecular weight of 15 kDa on the 3D-Bioplotter showed lower feasible extrusion pressures and temperatures. This was coupled with a higher dispensing speed compared to that of PCL with molecular weight of 45 – 50 kDa. This can be attributed to the difference in polymer viscosity which was measured and reported in Section 4.4 of Chapter 4. The inclusion of molecular weight as an experimental

factor in the statistical design can also be a part of a future study. The inclusion of more factors in the process characterization study will be helpful in refining the model.

2. Compression testing in simulated physiological conditions

ASTM standards for the compression testing of TEMPs recommend a height to diameter (L / D) ratio of 2 for the TEMP samples [92]. The samples tested in this study possess a low L / D ratio as they were designed with the idea of performing cell culture experiments in 24 well plates. These standards also recommend the simulation of *in vivo* environment while performing the testing. Hence, compression testing of samples with a higher L / D ratio will be necessary. These samples can be tested in compression while submerged in a saline environment of phosphate buffered saline solution (PBS) at 37°C in a closed compression chamber. The samples are to be submerged for a minimum of 1hr before the testing is done. The results of testing under ambient conditions and aqueous conditions can be compared. Similar tests can be conducted after keeping the samples submerged for a period of 3 weeks in the PBS. These tests can be valuable in understanding the mechanical properties of the scaffolds under *in situ* loading. The degradation mechanical properties can also be understood via these tests. It might also be interesting to test different molecular weights of a polymer under these conditions to draw a comparison.

3. Testing approach for different materials

The approach to characterize the process of 3D-Bioplotting was limited to PCL with a molecular weight of 43 – 50 kDa. This analysis can be repeated using PLA and hydrogels such as sodium alginate. The validity of this approach to different materials can be tested along with the characterization of a new material for the process of 3D-Bioplotting. It would be interesting to observe the difference in viscosity, process parameters and scaffold characteristics for different materials that are used as scaffold materials.

4. Cell culture study

The cell culture on the PCL scaffolds designed to fit a 24 Well plate can be an interesting future study to pursue. The PCL scaffolds fabricated in this study can be evaluated using

osteosarcoma MG 63 cells which are osteoblast-like cells. The culture medium generally used for these cells consists of Dulbecco's Modified Eagle's Medium supplemented with 10% fetal bovine serum and 1% penicillin/ streptomycin at 37^{o}C in a humidified atmosphere of 5% CO_2 [93]. The scaffolds are seeded with an approximate cell density of 1 x 10^6 cells / scaffold decided based on scaffold volume. This value may require modification based on cell adhesion observed subsequently. Cell proliferation within these scaffolds can be assessed using a colorimetric assay such as an MTT assay that determines the mitochondrial activity of cells. Differentiation of these cells on the scaffolds can be assessed by measuring the expression of alkaline phosphatase (ALP) using an ALP assay kit.

5. Viscosity measurements at higher shear rates

The viscosity measurements in this study were limited to lower shear rates due to torque constraints of the rheometer used. The actual shear rates during extrusion based processes can reach a maximum of 100 s^{-1}. Measurements at these shear rates is possible with the use of instruments designed to measure viscosity at higher shear rates such as a capillary rheometer. This would provide a direct correlation between viscosity measurements made and the viscosity during 3D-Bioplotting.

REFERENCES

[1] D. Varghese, M. Deshpande, and T. Xu, "Advances in tissue engineering: cell printing," *J. Thorac. Cardiovasc. Surg.*, vol. 129, no. 2, pp. 470–472, Feb. 2005.

[2] B. Palsson and S. N. Bhatia, *Tissue Engineering*. Prentice Hall, 2003.

[3] R. Langer and J. P. Vacanti, "Tissue Engineering," *Science (80-.).*, vol. 260, no. 5110, pp. 920–926, 1993.

[4] "Optn/srtr 2012 annual report Available from: www.ustransplant.org." .

[5] T. Billiet and M. Vandenhaute, "A review of trends and limitations in hydrogel-rapid prototyping for tissue engineering," *Biomaterials*, vol. 33, no. 26, pp. 6020–41, Sep. 2012.

[6] R. K. Malcolm, S. D. McCullagh, a D. Woolfson, S. P. Gorman, D. S. Jones, and J. Cuddy, "Controlled release of a model antibacterial drug from a novel self-lubricating silicone biomaterial.," *J. Control. Release*, vol. 97, no. 2, pp. 313–20, Jun. 2004.

[7] N. E. Fedorovich, J. Alblas, W. E. Hennink, F. C. Oner, and W. J. a Dhert, "Organ printing: the future of bone regeneration?," *Trends Biotechnol.*, vol. 29, no. 12, pp. 601–6, Dec. 2011.

[8] J. Lee, M. J. Cuddihy, and N. a Kotov, "Three-dimensional cell culture matrices: state of the art.," *Tissue Eng. Part B. Rev.*, vol. 14, no. 1, pp. 61–86, Mar. 2008.

[9] L. E. Freed and F. Guilak, "Eleven Engineering Functional Tissues," in in *Principles of Tissue Engineering*, 3rd ed., R. Langer, J. Vacanti, and R. Lanza, Eds. Academic Press, 2007, pp. 137 – 153.

[10] E. Carletti, A. Motta, and C. Migliaresi, “Scaffolds for Tissue Engineering and 3D Cell Culture,” in in *3D Cell Culture: Methods and Protocols*, vol. 695, no. 2, J. W. Haycock, Ed. Totowa, NJ: Humana Press, 2011.

[11] R. Langer, “Perspectives and challenges in tissue engineering and regenerative medicine.,” *Adv. Mater.*, vol. 21, no. 32–33, pp. 3235–6, Sep. 2009.

[12] F. Berthiaume, T. J. Maguire, and M. L. Yarmush, “Tissue engineering and regenerative medicine: history, progress, and challenges.,” *Annu. Rev. Chem. Biomol. Eng.*, vol. 2, pp. 403–30, Jan. 2011.

[13] “Standard Guide for Assessing Microstructure of Polymeric Scaffolds for Use in Tissue-Engineered Medical Products,” *ASTM Des. f2450-10*, pp. 1–10, 2013.

[14] B. C. Isenberg and J. Y. Wong, “Building structure into We describe the importance of structural organization on tissue function,” vol. 9, no. 12, pp. 54–60, 2006.

[15] F. R. A. J. Rose and R. O. C. Oreffo, “Bone tissue engineering: hope vs hype.,” *Biochem. Biophys. Res. Commun.*, vol. 292, no. 1, pp. 1–7, Mar. 2002.

[16] Y. Luo, G. Engelmayr, D. T. Auguste, S. Ferreira, and J. M. Karp, “Three-Dimensional Scaffolds,” in in *Principles of Tissue Engineering*, 3rd ed., R. Langer, J. Vacanti, and R. Lanza, Eds. Academic Press, 2007, pp. 359–373.

[17] L. Freed, F. Guilak, and X. Guo, “Advanced tools for tissue engineering: scaffolds, bioreactors, and signaling,” *Tissue Eng.*, vol. 12, no. 12, 2006.

[18] M. Murphy and A. Mikos, “Polymer Scaffold Fabrication,” in in *Principles of Tissue Engineering*, 3rd ed., J. Langer, R, Lanza, R, Vacanti, Ed. Academic Press, 2007, pp. 309 – 321.

[19] S. Yang, K. Leong, Z. Du, and C. Chua, “The design of scaffolds for use in tissue engineering. Part I. Traditional factors,” *Tissue Eng.*, vol. 7, no. 6, pp. 679–689, 2001.

[20] S. Yang, K. Leong, Z. Du, and C. Chua, “The design of scaffolds for use in tissue engineering. Part II. Rapid prototyping techniques,” *Tissue Eng.*, vol. 8, no. 1, pp. 1–11, 2002.

[21] “Reprinted with permission from TISSUE ENGINEERING (2008), published by Mary Ann Liebert, Inc., New Rochelle, NY.”

[22] O. A. Abdelaal and S. M. Darwish, “Fabrication of Tissue Engineering Scaffolds Using Rapid Prototyping Techniques,” pp. 577–585, 2011.

[23] Y. Kinoshita and H. Maeda, “Recent developments of functional scaffolds for craniomaxillofacial bone tissue engineering applications.,” *ScientificWorldJournal.*, vol. 2013, p. 863157, Jan. 2013.

[24] B. Stevens, Y. Yang, A. Mohandas, B. Stucker, and K. T. Nguyen, “A review of materials, fabrication methods, and strategies used to enhance bone regeneration in engineered bone tissues.,” *J. Biomed. Mater. Res. B. Appl. Biomater.*, vol. 85, no. 2, pp. 573–82, May 2008.

[25] W. Yeong and C. Chua, “Rapid prototyping in tissue engineering: challenges and potential,” *TRENDS ...*, vol. 22, no. 12, pp. 643–652, Dec. 2004.

[26] H. Ke and X. Chen, “Modeling of the scaffold fabrication process for tissue engineering applications,” *Electr. Comput. Eng. 2005. ...*, no. May, pp. 1255–1261, 2005.

[27] G. Vozzi and A. Previti, “Microsyringe-based deposition of two-dimensional and three-dimensional polymer scaffolds with a well-defined geometry for application to tissue engineering,” ... *Eng.*, vol. 8, no. 6, 2002.

[28] J. Liang, “Characteristics of melt shear viscosity during extrusion of polymers,” *Polym. Test.*, vol. 21, pp. 307–311, 2002.

[29] T. Bronshtein and G. Au-Yeung, “A Mathematical Model for Analyzing the Elasticity, Viscosity, and Failure of Soft Tissue: Comparison of Native and Decellularized Porcine Cardiac Extracellular Matrix,” *Tissue Eng. ...*, vol. 19, no. 8, pp. 620–630, 2013.

[30] “OpenStax College. Connections between Cells and Cellular Activities, Connexions Web site.” [Online]. Available: http://cnx.org/content/m44413/1.7/.

[31] S. CHUNG, “Fibrous Scaffolds for Tissue Engineering Applications,” North Carolina State University, 2010.

[32] J. Hubbell, “Biomaterials in tissue engineering,” *Nat. Biotechnol.*, 1995.

[33] J. Pachence, “Biodegradable polymers,” in in *Principles of Tissue Engineering*, 3rd ed., J. Langer, R, Lanza, R, Vacanti, Ed. Academic Press, 2007, pp. 323–339.

[34] D. Hutmacher, “Scaffold design and fabrication technologies for engineering tissues—state of the art and future perspectives,” *J. Biomater. Sci. Polym. Ed.*, vol. 12, no. 1, pp. 107–124, 2001.

[35] C. Liu and J. Czernuszka, “Development of biodegradable scaffolds for tissue engineering: a perspective on emerging technology,” *Mater. Sci. Technol.*, vol. 23, no. 4, pp. 379–391, Apr. 2007.

[36] E. Eisenbarth, “Biomaterials for Tissue Engineering,” *Adv. Eng. Mater.*, vol. 9, no. 12, pp. 1051–1060, Dec. 2007.

[37] G. P. Duffy, T. M. McFadden, E. M. Byrne, S.-L. Gill, E. Farrell, and F. J. O’Brien, “Towards in vitro vascularisation of collagen-GAG scaffolds.,” *Eur. Cell. Mater.*, vol. 21, no. 01, pp. 15–30, Jan. 2011.

[38] M. Woodruff and D. Hutmacher, “The return of a forgotten polymer—polycaprolactone in the 21st century,” *Prog. Polym. Sci.*, vol. 35, no. 10, pp. 1217–1256, Oct. 2010.

[39] P. Fabbri, V. Cannillo, and A. Sola, “Highly porous polycaprolactone-45S5 Bioglass® scaffolds for bone tissue engineering,” *Compos. Sci. Technol.*, vol. 70, no. 13, pp. 1869–1878, Nov. 2010.

[40] T. S. Karande, J. L. Ong, and C. M. Agrawal, “Diffusion in musculoskeletal tissue engineering scaffolds: design issues related to porosity, permeability, architecture, and nutrient mixing.,” *Ann. Biomed. Eng.*, vol. 32, no. 12, pp. 1728–43, Dec. 2004.

[41] A. Rosengren and L. M. Bjursten, “Pore size in implanted polypropylene filters is critical for tissue organization.,” *J. Biomed. Mater. Res. A*, vol. 67, no. 3, pp. 918–26, Dec. 2003.

[42] J. H. Brauker, V. E. Carr-Brendel, L. a Martinson, J. Crudele, W. D. Johnston, and R. C. Johnson, “Neovascularization of synthetic membranes directed by membrane microarchitecture.,” *J. Biomed. Mater. Res.*, vol. 29, no. 12, pp. 1517–24, Dec. 1995.

[43] W. Saltzman, “Cell interactions with polymers,” *Princ. tissue Eng.*, 2000.

[44] R. Landers, A. Pfister, and U. Hübner, “Fabrication of soft tissue engineering scaffolds by means of rapid prototyping techniques,” *J. Mater. …*, vol. 7, pp. 3107–3116, 2002.

[45] J. Daoud, K. Asami, L. Rosenberg, and M. Tabrizian, “Dielectric spectroscopy for non-invasive monitoring of epithelial cell differentiation within three-dimensional scaffolds,” *Physics in Medicine and Biology*, vol. 57. pp. 5097–5112, 2012.

[46] B. P. Chan and K. W. Leong, “Scaffolding in tissue engineering: general approaches and tissue-specific considerations.,” *Eur. Spine J.*, vol. 17 Suppl 4, pp. 467–79, Dec. 2008.

[47] J. D. Kiang, J. H. Wen, J. C. Del Álamo, and A. J. Engler, “Dynamic and reversible surface topography influences cell morphology.,” *J. Biomed. Mater. Res. A*, pp. 2313–2321, Jan. 2013.

[48] L. Yin, H. Bien, and E. Entcheva, “Scaffold topography alters intracellular calcium dynamics in cultured cardiomyocyte networks.,” *Am. J. Physiol. Heart Circ. Physiol.*, vol. 287, no. 3, pp. H1276–85, Sep. 2004.

[49] D. L. Butler, S. a Goldstein, and F. Guilak, “Functional tissue engineering: the role of biomechanics.,” *J. Biomech. Eng.*, vol. 122, no. 6, pp. 570–5, Dec. 2000.

[50] X. Wang, J. S. Nyman, X. Dong, H. Leng, and M. Reyes, *Fundamental Biomechanics in Bone Tissue Engineering*, vol. 2, no. 1. 2010, pp. 1–225.

[51] P. Thurner, B. Erikson, and Z. Schriock, “High-speed photography of human trabecular bone during compression,” *MRS ...*, vol. 874, pp. 1–6, 2005.

[52] S. Masood, J. Singh, and Y. Morsi, “The design and manufacturing of porous scaffolds for tissue engineering using rapid prototyping,” *... J. Adv. Manuf. ...*, vol. 27, no. 3–4, pp. 415–420, Jan. 2005.

[53] C. J. Bettinger, J. T. Borenstein, R. Langer, and I. Introduction, “Twenty-Four Micro- and Nanofabricated Scaffolds,” in in *Principles of Tissue Engineering*, 3rd ed., R. Langer, J. Vacanti, and R. Lanza, Eds. 2007, pp. 341 – 358.

[54] P. Grant, C. Vaz, and P. Tomlins, “Physical characterisation of a polycaprolactone tissue scaffold,” *Surf. Chem. Biomed. Environ. Sci.*, pp. 215–228, 2006.

[55] W.-J. Li and R. S. Tuan, “Fabrication and application of nanofibrous scaffolds in tissue engineering.,” *Curr. Protoc. Cell Biol.*, vol. Chapter 25, p. Unit 25.2, 2009.

[56] M. Truscott, G. Booysen, and D. De Beer, “Rapid prototyping and manufacturing in medical product development,” vol. 21, no. 1, pp. 1573–1575, 2009.

[57] N. E. Fedorovich, J. Alblas, J. R. de Wijn, W. E. Hennink, A. J. Verbout, and W. J. a Dhert, “Hydrogels as extracellular matrices for skeletal tissue engineering: state-of-the-art and novel application in organ printing.,” *Tissue Eng.*, vol. 13, no. 8, pp. 1905–25, Aug. 2007.

[58] N. E. Fedorovich, J. R. De Wijn, A. J. Verbout, J. Alblas, and W. J. a Dhert, “Three-dimensional fiber deposition of cell-laden, viable, patterned constructs for bone tissue printing.,” *Tissue Eng. Part A*, vol. 14, no. 1, pp. 127–33, Jan. 2008.

[59] N. Fedorovich, “Distinct tissue formation by heterogeneous printing of osteo-and endothelial progenitor cells,” *Tissue Eng. Part A*, vol. 17, 2011.

[60] D. Hutmacher, M. Sittinger, and M. Risbud, “Scaffold-based tissue engineering: rationale for computer-aided design and solid free-form fabrication systems,” *Trends Biotechnol.*, vol. 22, no. 7, pp. 354–362, Jul. 2004.

[61] C. Norotte, F. Marga, L. Niklason, and G. Forgacs, “Scaffold-free vascular tissue engineering using bioprinting,” *Biomaterials*, vol. 30, no. 30, pp. 5910–5917, Oct. 2009.

[62] G. Chen, T. Ushida, and T. Tateishi, “Scaffold design for tissue engineering,” *Macromol. Biosci.*, vol. 2, no. 2, pp. 67–77, 2002.

[63] R. Sodian, S. Weber, M. Markert, D. Rassoulian, I. Kaczmarek, T. C. Lueth, B. Reichart, and S. Daebritz, “Stereolithographic models for surgical planning in congenital heart surgery.,” *Ann. Thorac. Surg.*, vol. 83, no. 5, pp. 1854–7, May 2007.

[64] K. Kim and A. Yeatts, “Stereolithographic bone scaffold design parameters: osteogenic differentiation and signal expression,” *Tissue Eng. Part B …*, vol. 16, no. 5, 2010.

[65] “Reprinted with permission from TISSUE ENGINEERING (2010), published by Mary Ann Liebert, Inc., New Rochelle, NY.”

[66] R. A. Levy, T. M. Chu, J. W. Halloran, S. E. Feinberg, and S. Hollister, “CT-generated porous hydroxyapatite orbital floor prosthesis as a prototype bioimplant.,” *AJNR. Am. J. Neuroradiol.*, vol. 18, no. 8, pp. 1522–5, Sep. 1997.

[67] J. T. Rimell and P. M. Marquis, “Selective laser sintering of ultra high molecular weight polyethylene for clinical applications.,” *J. Biomed. Mater. Res.*, vol. 53, no. 4, pp. 414–20, Jan. 2000.

[68] I. Gibson, M. Savalani, and C. Lam, “Towards a medium/high load-bearing scaffold fabrication system,” *Tsinghua Sci. Technol.*, vol. 14, no. June, pp. 13–19, 2009.

[69] H. Chim, D. Hutmacher, and A. Chou, “A comparative analysis of scaffold material modifications for load-bearing applications in bone tissue engineering,” *Int. J. Oral Maxillofac. Surg.*, vol. 35, no. 10, pp. 928–934, Oct. 2006.

[70] M. Domingos, F. Chiellini, A. Gloria, L. Ambrosio, P. Bartolo, and E. Chiellini, “Effect of process parameters on the morphological and mechanical properties of 3D Bioextruded poly(ε-caprolactone) scaffolds,” *Rapid Prototyp. J.*, vol. 18, no. 1, pp. 56–67, 2012.

[71] P. Maher and R. Keatch, “Construction of 3D biological matrices using rapid prototyping technology,” *Rapid Prototyp. J.*, vol. 15, no. 3, pp. 204–210, 2009.

[72] J. Cheng, F. Lin, H. Liu, Y. Yan, and X. Wang, “Rheological properties of cell-hydrogel composites extruding through small-diameter tips,” *J. Manuf. Sci. Eng.*, vol. 130, no. 2, p. 021014, 2008.

[73] Q. Hamid, J. Snyder, and C. Wang, “Fabrication of three-dimensional scaffolds using precision extrusion deposition with an assisted cooling device,” …, vol. 3, no. 3, p. 034109, Sep. 2011.

[74] M. Hoque, Y. Chuan, and I. Pashby, “Extrusion based rapid prototyping technique: An advanced platform for tissue engineering scaffold fabrication,” *Biopolymers*, vol. 97, no. 2, pp. 83–93, Feb. 2012.

[75] J. Lee, S. Park, K. Park, J. Kim, and K. Kim, “Fabrication and characterization of 3D scaffold using 3D plotting system,” *Chinese Sci. ...*, vol. 55, no. 1, pp. 94–98, Jan. 2010.

[76] A. Sood, R. Ohdar, and S. Mahapatra, “Parametric appraisal of mechanical property of fused deposition modelling processed parts,” *Mater. Des.*, vol. 31, no. 1, pp. 287–295, Jan. 2010.

[77] I. Zein, D. Hutmacher, K. Tan, and S. Teoh, “Fused deposition modeling of novel scaffold architectures for tissue engineering applications,” *Biomaterials*, vol. 23, no. 4, pp. 1169–1185, 2002.

[78] R. Anitha, S. Arunachalam, and P. Radhakrishnan, “Critical parameters influencing the quality of prototypes in fused deposition modelling,” *J. Mater. Process. Technol.*, vol. 118, pp. 2–5, 2001.

[79] K. Ang and K. Leong, “Investigation of the mechanical properties and porosity relationships in fused deposition modelling-fabricated porous structures,” *Rapid Prototyp. J.*, vol. 12, no. 2, pp. 100–105, 2006.

[80] D. Hutmacher and T. Schantz, “Mechanical properties and cell cultural response of polycaprolactone scaffolds designed and fabricated via fused deposition modeling,” *J. …*, vol. 55, no. 2, pp. 203–216, 2001.

[81] “Reprinted with permission from TISSUE ENGINEERING (2001), published by Mary Ann Liebert, Inc., New Rochelle, NY.”

[82] W. Jiang, J. Shi, W. Li, and K. Sun, “Morphology, wettability, and mechanical properties of polycaprolactone/hydroxyapatite composite scaffolds with interconnected pore structures fabricated by a mini-,” *Polym. Eng. Sci.*, 2012.

[83] H. S. Ramanath, C. K. Chua, K. F. Leong, and K. D. Shah, “Melt flow behaviour of poly-epsilon-caprolactone in fused deposition modelling.,” *J. Mater. Sci. Mater. Med.*, vol. 19, no. 7, pp. 2541–50, Jul. 2008.

[84] D. Ramkumar and M. Bhattacharya, “Steady shear and dynamic properties of biodegradable polyesters,” *Polym. Eng. ...*, vol. 3, no. 9, pp. 1426–1435, 1998.

[85] “Tone Polymers, Union Carbide, PCL specifications.” [Online]. Available: http://www.biodeg.net/bioplastic.html.

[86] “Sigma-Aldrich, PCL 15kDa specifications.” [Online]. Available: http://www.sigmaaldrich.com/catalog/product/aldrich/440752?lang=en&region=US.

[87] Envisiontec., “Instruction Manual for the 3D-Bioplotter.”

[88] C. M. Ghajar, X. Chen, J. W. Harris, V. Suresh, C. C. W. Hughes, N. L. Jeon, A. J. Putnam, and S. C. George, “The effect of matrix density on the regulation of 3-D capillary morphogenesis.,” *Biophys. J.*, vol. 94, no. 5, pp. 1930–41, Mar. 2008.

[89] “HIROX KH-7700 Digital Microscope specifications.” [Online]. Available: http://www.hirox-usa.com/products/microscope/index7700.html.

[90] “Brookfield Engineering, Temperature Control bath TC-150.” [Online]. Available: http://www.brookfieldengineering.com/products/accessories/temp-bath-accessories.asp#accessories.

[91] “Brookfield Engineering, More solutions to sticky problems,” 2006.

[92] M. Slivka, “In vitro compression testing of fiber-reinforced, bioabsorbable, porous implants,” *Synth. Bioabsorbable Polym. Implant.*, pp. 124–135, 1999.

[93] S. A. Park, S. H. Lee, and W. D. Kim, “Fabrication of porous polycaprolactone/hydroxyapatite (PCL/HA) blend scaffolds using a 3D plotting system for bone tissue engineering.,” *Bioprocess Biosyst. Eng.*, vol. 34, no. 4, pp. 505–13, May 2011.